Cooperative Research Centre for Coastal Zone, Estuary & Waterway Management

Technical Report 64

Improving our knowledge of Australia's near-pristine estuaries

Geomorphic habitat mapping and related applications

John Creasey, Ashwin Dyall.
Catherine Ticehurst, Ben Rodgers,
Alan Marks, Lynda Radke,
Brendan Brooke, David Ryan,
Andrew Heap, Emma Murray,
Arnold Dekker

June, 2006

CSIRO

Australian Government
Geoscience Australia

CRC for Coastal Zone
Estuary & Waterway Management

Improving our knowledge of Australia's near-pristine estuaries

Geomorphic habitat mapping and related applications

Final report

John Creasey, Ashwin Dyall, Catherine Ticehurst, Ben Rodgers, Alan Marks, Lynda Radke, Brendan Brooke, David Ryan, Andrew Heap, Emma Murray and Arnold Dekker

June 2006

CRC for Coastal Zone Estuary & Waterway Management

Improving our knowledge of Australia's near-pristine estuaries: Geomorphic habitat mapping and related applications – Final report

Written by:

John Creasey
Ashwin Dyall
Catherine Ticehurst
Ben Rodgers
Alan Marks
Lynda Radke
Brendan Brooke
David Ryan
Andrew Heap
Emma Murray
Arnold Dekker

Published by the Cooperative Research Centre for Coastal Zone, Estuary and Waterway Management (Coastal CRC)

Indooroopilly Sciences Centre
80 Meiers Road
Indooroopilly Qld 4068
Australia

www.coastal.crc.org.au

National Library of Australia Cataloguing-in-Publication data
Improving our knowledge of Australia's near-pristine estuaries: Geomorphic habitat mapping and related applications – Final report

QNRM06285

ISBN 1 921017 36 8 (print)

ISBN 1 921017 37 6 (online)

Acknowledgments

The work described in this report was funded by the Cooperative Research Centre for Coastal Zone, Estuary and Waterway Management (Coastal CRC) and relied on extensive inputs of data and ideas from CRC members. In particular, we thank Regina Souter and Rachel Mackenzie for their critical reviews of an earlier draft off this work. We also acknowledge and thank the following other people for their various contributions to this work:

The following people from state and territory organisations are thanked for kindly providing aerial photos: Andrew Moss and Alan McDonaugh from the Queensland Environmental Protection Agency; Ray Murphy and Eric Brain from the Tasmanian Department of Primary Industries, Water and Environment; David Miller and Dave Rissik from the New South Wales Department of Infrastructure, Planning and Natural Resources; Dianne Rose from the Victorian Environment Protection Authority; Simon Townsend from the Northern Territory Department of Natural Resources, Environment and the Arts; and Malcolm Robb and Suzanne Thompson from the Western Australian Department of Environment.

The report was written by John Creasey, Ashwin Dyall, Catherine Ticehurst, Ben Rodgers, Alan Marks, Lynda Radke, Brendan Brooke, David Ryan, Andrew Heap, Emma Murray and Arnold Dekker. Ashwin Dyall wrote Chapter 2, with input from John Creasey, Andrew Heap, Emma Murray, Brendan Brooke, David Ryan and Lynda Radke. Catherine Ticehurst and Arnold Dekker wrote Chapter 3, and Ben Rodgers wrote Chapter 4. The executive summary and introduction were written by Lynda Radke with help from Catherine Ticehurst and Emma Murray. The report was compiled by Lynda Radke, Emma Murray, Helen Bostock and Jodie Smith.

Table of contents

List of figures

List of tables

Acronyms and abbreviations

(see also Glossary, p. 44)

.aat	Arc attribute table file extension
ACRES	Australian Centre for Remote Sensing
AML	Arc Macro Language (script)
API	Aerial photo interpretation
AVHRR	Advanced very high resolution radiometer
CASI	Compact airborne spectrographic imager
CDOM	Coloured dissolved organic matter
DEM	Digital elevation model
dgn	(Microstation) design file
dpi	Dots per inch
DSM	Digital surface model
ETM	Enhanced thematic mapper
GDA	Geocentric datum of Australia
HRVIR	High resolution visible infrared (wavelengths)
jpeg	Joint Photographic Experts Group (image file format and file extension)
MLC	Maximum likelihood classification
MSS	Multi-spectral scanner
NDVI	Normalised difference vegetation index
NLWRA	National Land and Water Resources Audit
nm	Nanometres
NOAA	(US) National Oceanic and Atmospheric Administration
.pat	Polygon attribute table file extension
PCA	Principal component analysis
RGB	Red/green/blue (Landsat imagery)
ROI	Region of interest
SAM	Spectral angle mapper
SAR	Synthetic aperture radar
SPOT	*System Probatoire pour l'Observation de la Terre*
SRTM	Shuttle Radar Topography Mission (data source)
SWIR	Shortwave infrared (wavelengths)
Tic points	GIS control points representing known locations on the earth's surface
tif	Tagged image file (extension); part of Tiff (Tagged image file format)
TM	Thematic mapper
TSS	Total suspended sediment
.txt	Text file extension

Executive summary

Aims and context of the geomorphic habitat mapping

The central aim of the Comparative Geomorphology of Estuaries Project of the Coastal CRC was to improve our understanding of Australia's near-pristine estuaries. As the title implies, the project had a geomorphic focus in that a major output was mapping of geomorphic habitats of a representative selection of near-pristine estuaries from around Australia. In the coastal context, geomorphic habitats are landforms ('geo' = land, 'morph' = shape) such as saltmarshes and intertidal flats whose shape and position in the landscape are strongly governed by the effect of physical and biological forces on sediments. The mapping follows on from similar work undertaken during the National Land and Water Resources Audit (NLWRA 2002), when the geomorphic habitats of 540 of Australia's estuaries were mapped. However, near-pristine estuaries were poorly represented in the NLWRA (2002) process because the NLWRA intention was to target estuaries requiring management rather than conservation. Consequently, only 41 near-pristine estuaries were mapped.

In addition to the generation of new information on near-pristine estuaries in the form of maps and measured habitat areas, we also highlight remote sensing techniques (satellite-based or airborne sensors) and related applications (eCognition^{TM}) for their potential in monitoring and gathering more detailed information on the habitats and water quality of near-pristine estuaries.

This project produced a total of four technical reports. These are:

- A summary report of the project (Radke *et al.* 2006a)
- A literature review of the current knowledge and management of Australia's near-pristine estuaries (Murray *et al.* 2006)
- A report describing the mapping of near-pristine estuaries (Creasey *et al.* 2006; this report)
- A report investigating the potential of the mapped habitat areas as indicators for assessing catchment disturbance (Radke *et al.* 2006b).

Report highlights

Geomorphic habitat mapping

The geomorphic habitats of 158 near-pristine estuaries were mapped in the Comparative Geomorphology of Estuaries Project by methods outlined in the Chapter 2. The maps comprise industry-standard ArcGIS files consisting of a base map of the estuary boundary, and vector layers showing the extent of sub-aerial, tidal and sub-tidal habitats. The maps are available for download in the OzEstuaries database (<www.ozestuaries.org> where they exist alongside the maps of near-pristine and modified estuaries generated during the NLWRA (2002).

The near-pristine estuaries that were mapped in this project were chosen to reflect, as far as possible, the full range of geomorphic variability in Australia: A statistically significant number of the different types of estuaries (between 16 and 26) were chosen, and these were spread as far as practicable around the Australian coastline. These estuaries are located in all the coastal geomorphic regions of Australia (Harris *et al.* 2002). Within this context, state government preferences and the availability of suitable images and photographs were also taken into account. By 'estuary types', we refer to the major kinds of coastal waterways (i.e. wave- and tide-dominated estuaries and deltas, tidal creeks, strandplains and embayments) which experience differing amounts of wave, tide and river energy (Heap *et al.* 2001). By 'coastal geomorphic regions' (Harris *et al.* 2002) we refer to the North-west Coast, Gulf of Carpentaria, North-east Coast, South-east Coast and South-west Coast.

Near-pristine estuaries from Queensland and the Northern Territory comprised by far the largest proportion of the estuaries mapped during the project, accounting for 46% and 30% respectively. Significantly fewer estuaries were mapped in Western Australia (11%), Tasmania (9%), New South Wales (2%) and Victoria (<1%) and none was mapped in South Australia. This was mainly because there are far fewer near-pristine estuaries in these (mostly) southern states, and many of them had already been mapped during the NLWRA. Some important observations were made about the estuaries during the mapping process that might have a bearing on the established coastal geomorphic regionalisation. For example, it was suggested that the North-west Region should be divided into two regions to recognise the unique bedrock-controlled coastal waterways of the Kimberley. Near-pristine estuaries in the south and west Gulf of Carpentaria were also found to be distinct from those of the east Gulf of Carpentaria, where habitats extended further inland and there is a greater abundance of mangroves and saltflats.

The national set of habitat maps in OzEstuaries now includes near-pristine examples of Australia's diverse estuaries and coastal waterways.

Remote sensing techniques and applications to near-pristine estuaries

As mentioned previously, near-pristine estuaries tend to be located along the most remote and inaccessible parts of the coastline, making them difficult to study. This is why remote sensing techniques (satellite-based or airborne sensors) and related applications (eCognition™) were scoped for their potential use in monitoring and gathering further information on the habitats and water quality of near-pristine estuaries. Remote sensing involves the collection of information about the earth's surface, using sensors mounted on satellites or aeroplanes. The result of remote sensing is an image from which the spatial distribution of different landscape characteristics *(e.g.* mangrove forests and seagrass beds) can be mapped.

Remote sensing has been used for many years to map the coastal zone both for research and for management purposes. One relevant example was the use of aerial photography to map Australia's coastal geomorphic habitats during the NLWRA. However, it is underscored in the remote sensing methods and applications portions of this report that more advanced satellite and /or airborne remote sensing instruments are now available, and these can be even more cost-effective and objective than aerial photo interpretation. This is because the imagery can be collected at larger spatial scales (regional) and because computer software is now available that can help automate the process by which maps are made from the images. For example, the eCognition™ software package is designed to produce maps from remote sensing images by grouping similar adjacent features (e.g. water body or forest patches) in the landscape. We present a case study from the near-pristine Wildman River in the Northern Territory (see Chapter 4) in which we demonstrate that maps made from remotely sensed images using eCognition™ are comparable to or better than maps made using manual digitising.

The level of detail and number of physical properties that can be mapped using remote sensing imagery depend largely on the characteristics and availability of the remote sensing instruments. In a second case study on near-pristine estuaries in tropical northern Queensland (see Chapter 3), different types of imagery were investigated for their ability to differentiate between the dominant vegetation types in an estuarine environment. An automated mapping routine was then developed and applied to widely available satellite data (Landsat ETM) to

produce maps of the Daintree River, Cooper Creek and Noah Creek. These maps were then compared to aerial photo interpretations. Although slightly different land-cover types were used, the results were comparable for the common vegetation classes. The advantage in using Landsat ETM (Enhanced Thematic Mapper) data in an automatic mapping routine over manual interpretation of aerial photographs is that it is fast and can cover large regions. The disadvantage is that user knowledge and experience cannot be applied at the same level of detail.

It can be summarised that remote sensing used in combination with eCognition™ (or like-programs) can reduce the time and effort required for routine monitoring and mapping of Australia's near-pristine estuaries, and allow environmental managers and researchers to regularly update habitat maps to monitor changes through time.

1. Introduction

Background

Roughly half of Australia's estuaries[1] were classified as near-pristine during the National Land and Water Resources Audit (NLWRA; NLWRA 2002). In the NLWRA framework, the physical and ecological processes of near-pristine estuaries were considered essentially unaltered by humans, and the catchments of these estuaries retained >90% of their natural vegetation cover (Table 1.1). Little is known about Australia's near-pristine estuaries. This is partly because managers have tended to focus on the more disturbed systems that are subject to public scrutiny and in need of direct management, and partly because near-pristine estuaries tend to be located along the remotest parts of the coastline (Figure 1.1). However, it is important that we learn more about near-pristine estuaries from the perspectives of both science and management. Scientifically, near-pristine estuaries can be important reference systems for assessing natural variability in physical and biological processes. Such benchmark information is also useful for monitoring and management because it is often difficult to distinguish between changes caused by human activity and changes associated with natural cycles of disturbance and change. Near-pristine estuaries are also valuable in their own right as undisturbed habitat for native plants and animals, and for biodiversity conservation, tourism and fisheries.

The central aim of the Comparative Geomorphology of Estuaries Project (also known as the Near-Pristine Estuaries Project) of the Cooperative Research Centre for Coastal Zone, Estuary and Waterway Management (Coastal CRC) was to improve our understanding of Australia's near-pristine coastal waterways. Three of the major outputs in the project were: (1) the mapping of geomorphic habitats of a representative selection of near-pristine estuaries from around Australia using aerial photographs and satellite imagery (this report); (2) an analysis of these datasets to assess the indicator potential of the mapped habitat areas for assessing catchment disturbance (Radke *et al.* 2006b); and (3) a comprehensive literature review of the current knowledge and management of Australia's near-pristine estuaries (Murray *et al.* 2006). For the first output, the geomorphic habitats of 158 near-pristine estuaries were mapped using methods similar to those used during the NLWRA. These maps are currently available on the OzEstuaries website (<www.ozestuaries.org>) and greatly enhance the

[1] For the purposes of this report, the term 'estuary' is also often used interchangeably with 'coastal waterway', of which there are several different types.

national information set. For the second output, a preliminary scoping of geomorphic indicators was undertaken, and was based on the measured habitat areas (new and previous) of both wave- and tide-dominated coastal waterways (Radke *et al.* 2006).

This report constitutes the final mapping report in the Comparative Geomorphology of Estuaries project. The report provides a detailed account of the mapping method and, as such, may serve as a companion document for the habitat maps now available in OzEstuaries. Detailed reviews of remote sensing methods and related applications are also provided, and are illustrated with case-specific studies on near-pristine estuaries. It is shown that remote sensing and related applications (eCognition^{TM}) can potentially reduce the time and effort of routine monitoring and mapping, and allow environmental managers and researchers to regularly update habitat maps.

Table 1.1. The NLWRA (2002) criteria for a near-pristine estuary

Physical characteristic	**Condition**
Catchment natural cover	>90%
Land use	Limited roads and disturbance to natural conditions and processes
Catchment hydrology	No dams or impoundments, virtually nil abstraction
Tidal regime	No impediments to tidal flow, changes from natural morphology (e.g. training walls, barrages, bridges and causeways)
Floodplain	Wetlands intact in vegetation and hydrology, no alterations to flood pattern
Estuary use	Extractive activities limited to Indigenous or limited and sustainable commercial and recreational fishing, no aquaculture
Pests and weeds	Minimal impact on estuary from catchment weeds and limited pests and weeds within estuary
Estuarine ecology	Ecological systems and processes intact (e.g. benthic flora and fauna)

Figure 1.1. The locations of Australia's near-pristine estuaries

Report outline

A detailed account of the geomorphic mapping and observations undertaken in the current project is provided in Chapter 2. The chapter includes the criteria that were used to select the estuaries for mapping, an outline of the mapping process and some interesting observations on the regional characteristics of near-pristine estuaries that were made during the mapping process.

The remote sensing review (Chapter 3) looks at a range of remote sensing technologies that have been used for estuary mapping and monitoring, starting with aerial photography and commonly used satellite instruments, followed by less commonly used instruments. It also reports on a range of mapping methods and applications including: the use of remote sensing for detecting changes in the landscape; the combining of data from different remote sensing instruments to improve the map quality; and the challenges faced when using remote sensing for estuary mapping. A case study is presented on near-pristine estuaries in tropical northern Queensland, in which different types of imagery were investigated for

their ability to differentiate between the dominant vegetation types in an estuarine environment.

The capacity of eCognition™ software to use spatial information to intelligently group similar adjacent features in the landscape is the subject of Chapter 4, and is illustrated through a case study example on a near-pristine estuary (Wildman River, Northern Territory).

The current mapping of near-pristine estuaries complements the previous audit mapping (NLWRA 2002) and serves as a definitive baseline for future audit style mapping at national scales. Such mapping could also take advantage of integrating new remote sensing datasets and incorporating semi-automated classification and feature extraction processes to provide a more rapid mapping process.

Conclusions are provided at the end of each chapter so that they can be viewed in the appropriate context.

2. Mapping the geomorphic habitats of Australia's near-pristine estuaries: procedures and observations

Near-pristine estuary selection

The project aimed to capture a representative selection of near-pristine estuaries, incorporating, as far as practicable, the full range of natural variability.
A statistically significant number of near-pristine estuaries (between 16 and 26; Table 2.1) were chosen for each geomorphic classification outlined in Ryan *et al.* (2003) (Figure 2.1, spread across the geomorphic regions of Harris *et al.* (2002) (Figure 2.2 Table 2.1). The geomorphic classifications are based on the relative strength of wave, tide, and river energy, which in turn shape the geomorphic habitats and character of the estuary. The geomorphic regions of Harris *et al.* (2002) divide the coastline into areas with similar tide, wave, and river energy. Very broadly, the northern half of Australia is tide-dominated, whereas the southern half is mainly wave-dominated (Ryan *et al.* 2003).

State and territory government natural resource managers were also asked to select estuaries of interest to them within the above parameters. Table 2.1 shows the final number of near-pristine estuaries mapped for each geomorphic class within each state/territory and geomorphic region. This set of habitat maps, combined with that produced during the NLWRA, now includes all of Australia's wave-dominated estuaries, wave-dominated deltas, and embayments, as well as a significant proportion of the other estuary types (see Figure 2.1).

Near-pristine estuaries from Queensland and the Northern Territory (the North-east, North-west, and the Gulf of Carpentaria regions) comprised by far the largest proportion of the estuaries mapped during the project, accounting for 46% and 30% respectively. Significantly fewer estuaries were mapped in Western Australia (11%), Tasmania (9%), New South Wales (2%), and Victoria (<1%). This was mainly because there are far fewer near-pristine estuaries in these (mostly) southern states and many of them were already mapped during the NLWRA (**Figure 2.3**).

Table 2.1. The number of near-pristine estuaries mapped for each different geomorphic type in each state/territory and geomorphic region

State	QLD		NT		WA	TAS	NSW	VIC	TOTAL
Geomorphic region	**(NE)**	**(Carp)**		**(NW)**			**(SE)**		
Wave-dominated estuary	0	2	0	2	0	10	1	1	16
Wave-dominated delta	10	7	2	4	0	0	1	0	24
Strandplain/coastal lagoon	3	4	5	3	1	4	1	0	21
Tide-dominated estuary	8	6	0	7	5	0	0	0	26
Tide-dominated delta	7	8	1	10	0	0	0	0	26
Tidal creek	9	7	2	4	3	0	0	0	25
Embayment	2	0	0	8	9	1	0	0	20
TOTAL	39	34	10	38	18	15	3	1	158
TOTAL (state)	73		48		18	15	3	1	158
TOTAL (geomorphic region)	39	44		56		19			158

(NE) North-east Coast, (Carp) Gulf of Carpentaria, (NW) North-west Coast, (SE) South-east Coast. Note that Tasmania, New South Wales and Victoria are all incorporated within the South-east Coast geomorphic region, whereas Queensland, the Northern Territory and Western Australia are all divided between two geomorphic regions. There are no unmapped near-pristine estuaries within the South-west Coast region.

Figure 2.1. Ternary classification of coastal systems showing the seven different geomorphic classes (after Dalrymple *et al.* 1992 and Boyd *et al*. 1992)

The position of each coastal waterway type depends on the relative influence of waves, tides and rivers. Embayments and drowned river valleys are omitted from the diagram as they represent 'immature' coastal waterways (or coastal waterways which are not significantly filled with sediment). WDD = wave-dominated deltas, and TDD = tide-dominated deltas.

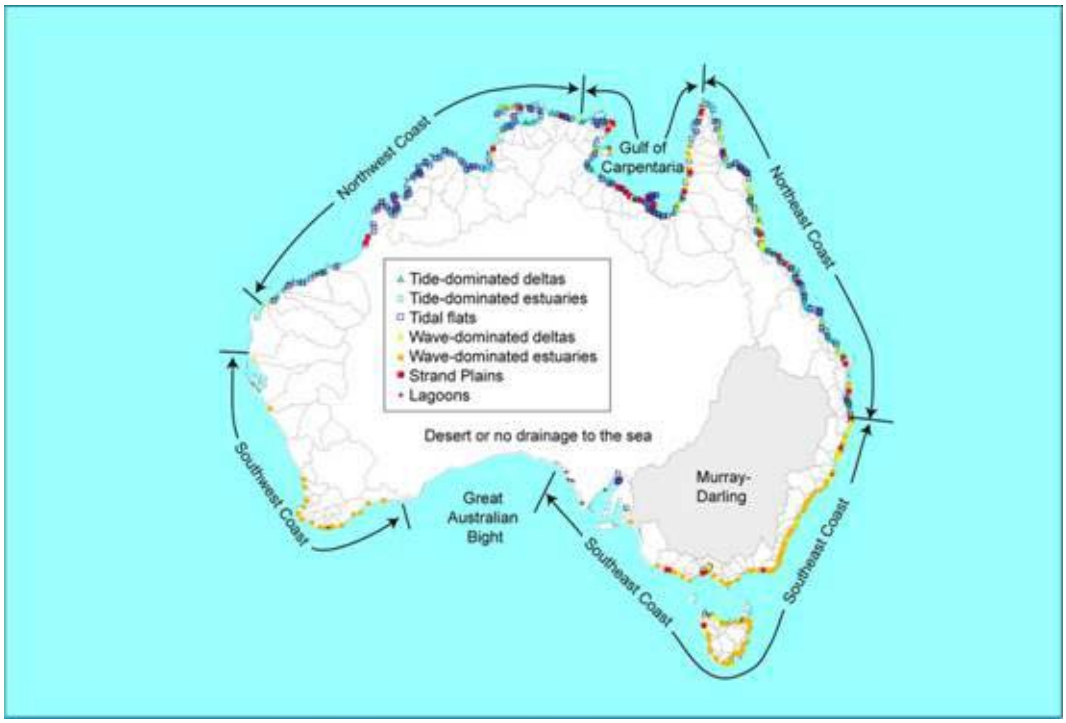

Figure 2.2. The geomorphic regions according to Harris *et al.* (2002)

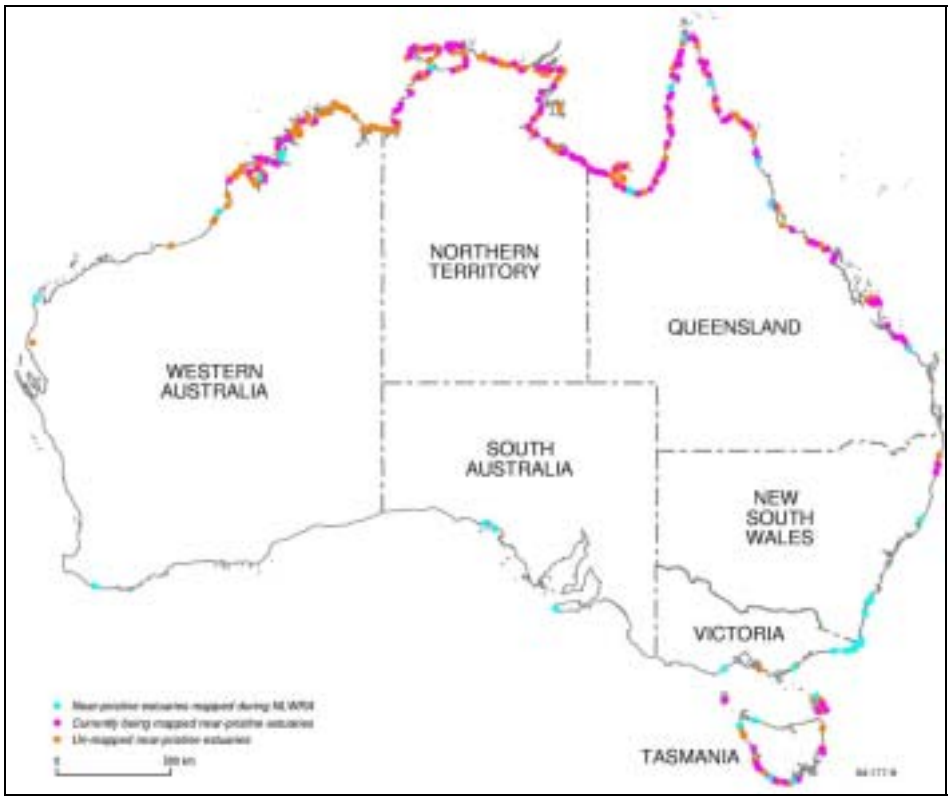

Figure 2.3. The location of near-pristine estuaries mapped during the NLWRA (2002) and this project, and estuaries that remain unmapped

The mapping process

The project made several improvements to the 'heads up' digitising procedure used by the NLWRA. For the NLWRA mapping, Landsat TM (Thematic Mapper) images were geo-rectified using ER Mapper and 10–15 ground control points from appropriate 1:250 000 topographical map sheets (Heap *et al.* 2001). Individual estuaries were then identified within a scene and saved as algorithms. The resultant algorithms were printed to create a 'base map' at scales ranging from 1:15 000 to 1:40 000. The estuary was first drawn or interpreted onto film which was attached to the Landsat image base map. The facies interpretation was then digitised on-screen over the Landsat image using ER Mapper while referring to the hardcopy map. After careful assessment of this procedure it was found that facies interpretation was duplicated (hardcopy and digitised version) which made the whole process time-consuming and labour-intensive. ER Mapper's strengths are in image processing, not data capture or line editing, hence digitising in ER Mapper was not deemed to be user friendly. In addition, 'heads up' digitising requires a well trained and experienced operator to produce an accurate map in minimal time (Figure 2.4).

For the current project, the decision was made to devise a procedure which streamlined the NLWRA process and delivered more accurate maps but at the same time was consistent with the previous NLWRA maps to allow for habitat area comparisons. Consequently, the following process of mapping near-pristine estuaries was devised (see also Figure 2.5):

- Acquisition of aerial photos and Landsat TM processing
- Facies interpretation
- Reviewing and checking
- Scanning, vectorising, and creating ArcInfo coverages
- Editing and attributing ArcInfo coverages
- Creation of frequency tables and quantification of facies relationships
- Preparing shapefiles and metadata for online download
- Archiving of interpretation maps and data.

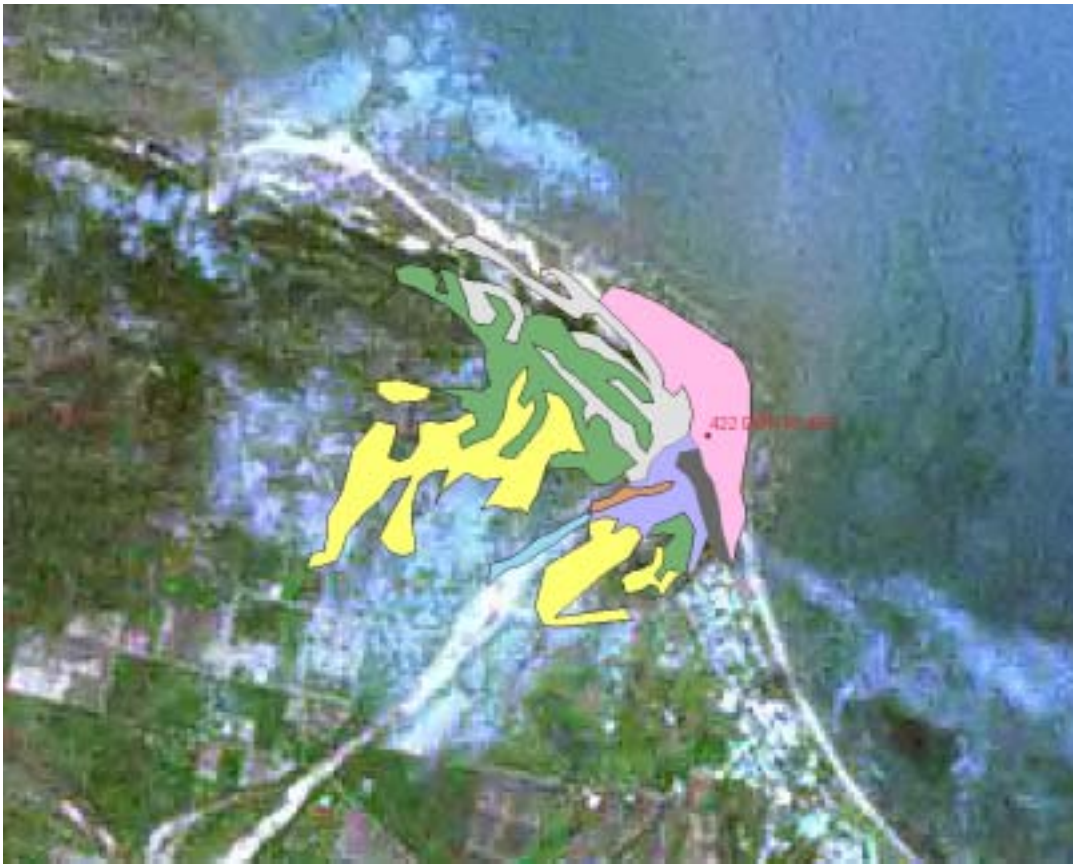

Figure 2.4. Geomorphic habitat map of the Don River estuary, near Bowen in central Queensland, produced during the NLWRA. Habitat boundaries are jagged and not realistic, demonstrating that digitising requires an experienced operator

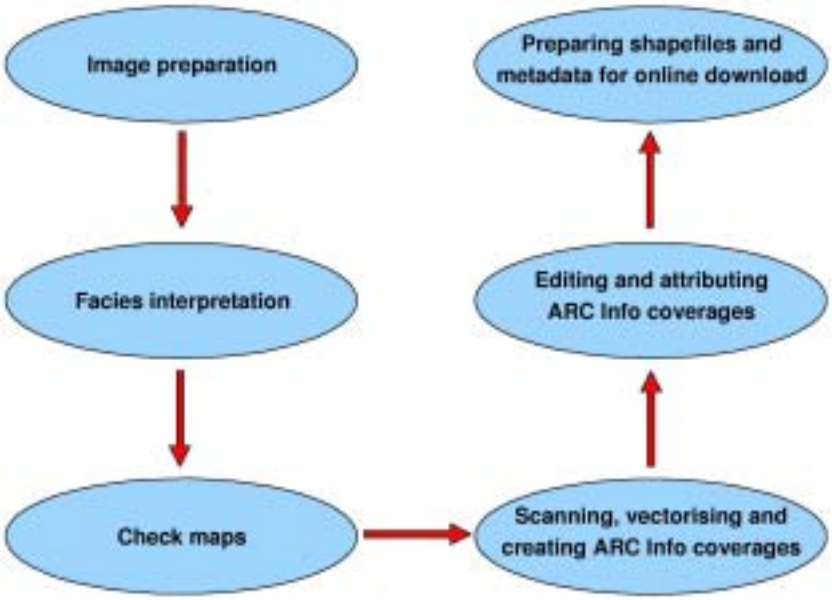

Figure 2.5. Flowchart of the main steps used to map the habitats of Australia's near-pristine estuaries

The process of scanning and vectorising using Microstation™ produced maps which were not only visually pleasing, but had the following benefits:

- The estuary was interpreted only once then scanned, which eliminated the need to re-digitise, therefore saving time.
- Saving time allowed productivity to increase and was less labour-intensive.
- Line work was much more accurate as vectorising identifies the centre pixel of each scanned line and maintains the line curvatures from the hand-drawn maps.
- The outcome was greater consistency in line work when compared to other estuaries and throughout the estuary itself.
- Consistency in line work means consistent results when calculating statistics such areas of habitats.

The maps were more detailed and accurate when overlaid onto Landsat ETM7+ for visual purposes or when analysis maps were overlain onto a Landsat ETM7+ image (Figures 2.6 and 2.7).

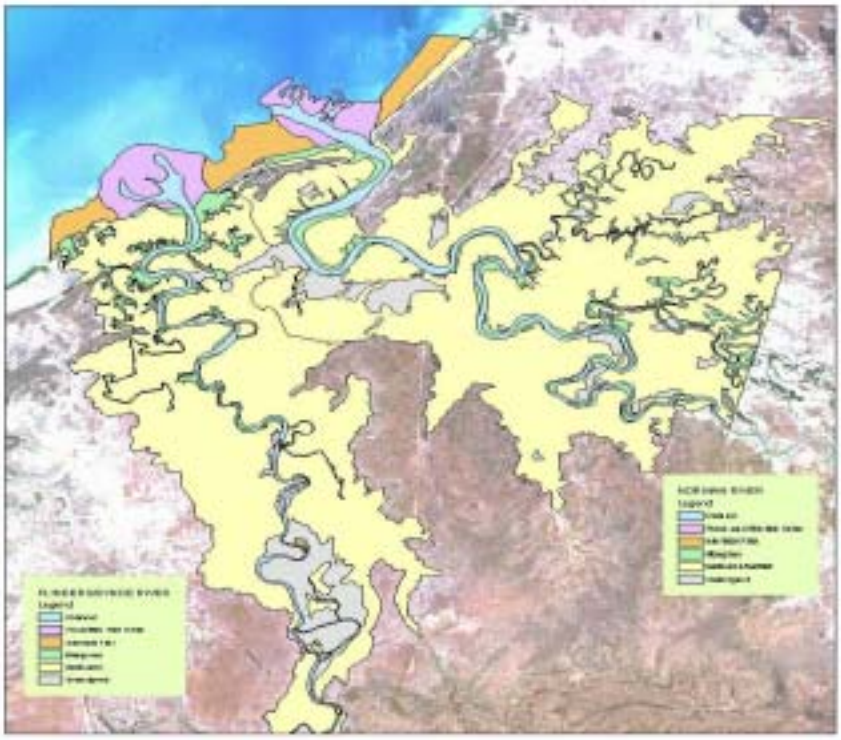

Figure 2.6. The newly mapped Flinders River (on the left) is compared to its neighbour (Norman River) which was mapped for the NLWRA

At this scale, a difference in the quality of line work cannot be discerned. The maps are overlain onto a Landsat ETM7+ image.

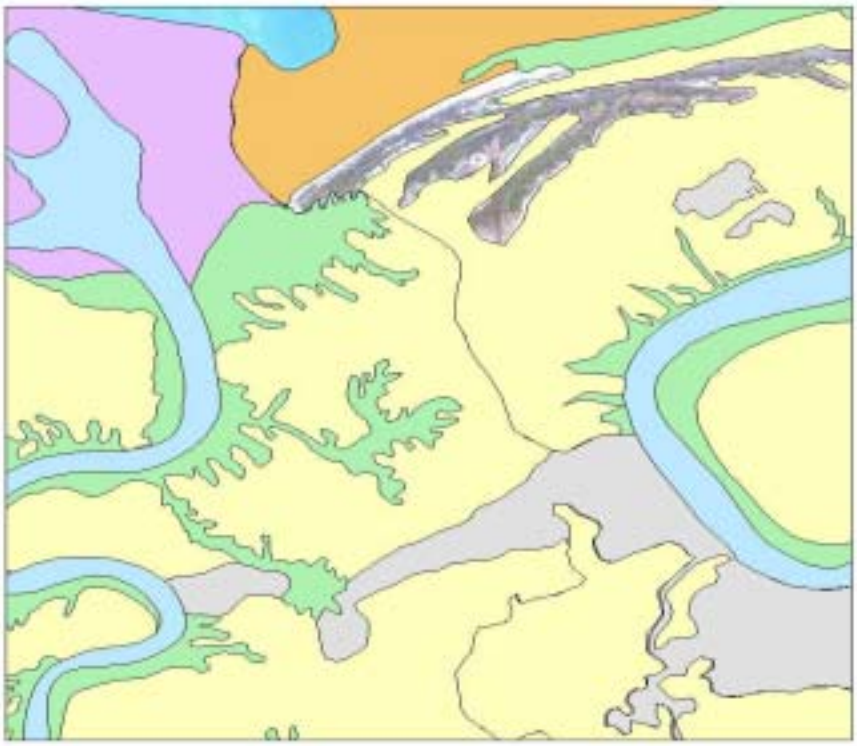

Figure 2.7. Enlarged portion of Figure 2.6: The Flinders River (left of the boundary) possesses much more accurate, clear and detailed line work

Aerial photos and satellite image processing

Air photos were gathered from a number of state government agencies. They ranged in scale from 1:5 000 to 1:40 000 and were no more than ten years old. In most cases air photos were only available along the coastline and did not cover the full extent of the estuary. Some air photos were obtained from the archives of Geoscience Australia; these were at 1:80 000 scale and dated back to 1969. They proved to be very useful, though in some cases allowances were made for vegetation growth and tidal variations.

Prints of selected aerial photos were sent via mail from relevant state agencies which included:

- Queensland Environmental Protection Agency
- Tasmanian Department of Primary Industries, Water, and Environment
- New South Wales Department of Infrastructure, Planning and Natural Resources
- Victorian Environment Protection Authority
- Northern Territory Department of Natural Resources, Environment and the Arts
- Western Australian Department of Environment.

Once received, the photo prints were scanned as JPEG graphic file format onto CD, and then returned to the state agencies.

The aerial photographs were used in addition to the Landsat ETM7+ imagery, which proved to be a very useful combination for identifying estuarine habitats. Although the air photos were a secondary resource to the Landsat ETM7+ imagery, their higher resolution was beneficial for:

- distinguishing between vegetation types;
- identifying habitats for tidal creeks not clearly visible on Landsat imagery at 1:20 000 scale;
- determining the extent of tidal sand banks, flood/ebb tide deltas and intertidal flats; and
- identifying estuaries where cloud cover hindered Landsat imagery and generally any areas not clearly visible on the Landsat images.

Coastline Landsat ETM7+ scenes were selected by the Australian Centre for Remote Sensing (ACRES) from January 2002 to June 2003. For each estuary, three images were created using ERMapper™:

- A band 8 panchromatic image (Figure 2.8)
- A multispectral ratio image of bands 3/2, 4/3 and 4/5 displayed in red, green and blue respectively, to differentiate spectral properties of habitat types (Figure 2.9)
- A false colour composite image of bands 7, 4 and 1 displayed in red, green and blue respectively (Figure 2.10).

All images were geocoded to geographic projection and GDA 94 datum. The panchromatic image was annotated with latitude and longitude coordinates grid and a scale bar, then printed at various scales ranging from 1:20 000 to 1:40 000 depending on the size of the estuary to be mapped.

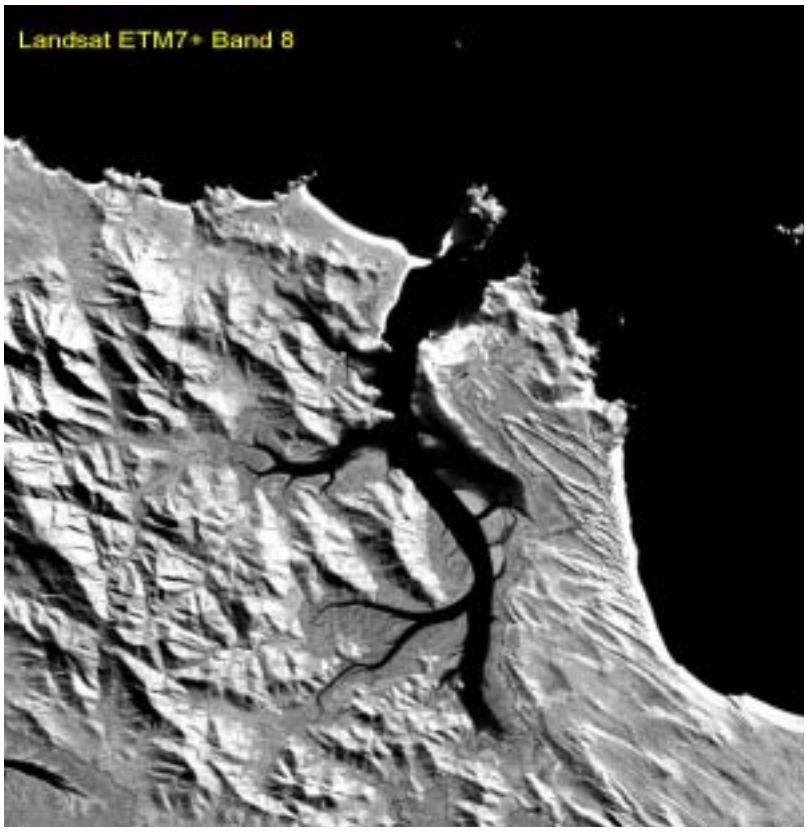

Figure 2.8. Panchromatic Landsat ETM7+ band 8 scene

This scene is printed and used as the base map for facies interpretation due to its 12.5 m resolution. The estuary shown here and in Figures 2.10 to 2.17 is Island Head Creek located on the east coast of Queensland, about 250 km south of Mackay.

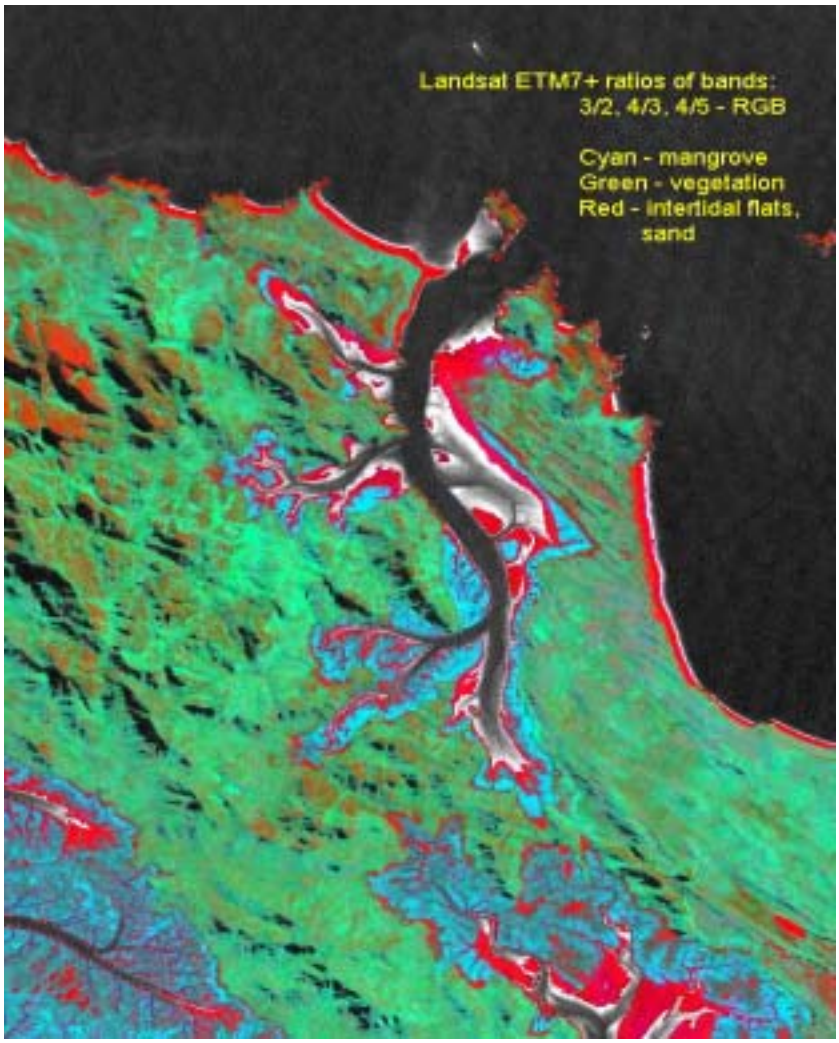

Figure 2.9. Multispectral Landsat ETM7+ image using ratios of bands 3/2, 4/3 and 4/5 RGB. Cyan colour shows mangrove habitats, greens show other vegetation, and reds display sands and intertidal flats.

Figure 2.10. Example of a real colour composite Landsat ETM7+ image using bands 7, 4, 1 RGB. This scene shows the extent of vegetation but does not distinguish between vegetation types.

Facies interpretation

Identification of estuarine facies was undertaken by interpreting the Landsat ETM7+ panchromatic image with assistance from the following:

- conceptual models (from Heap *et al.* 2001)
- Landsat ETM7+ multispectral ratio image
- Landsat ETM7+ false colour composite 7, 4, 1 band combination image
- 1:250 000 topographic maps
- relevant aerial photos.

The facies boundaries were hand drawn and labelled onto an overlay/transparency over the panchromatic Landsat print (Figures 2.11 and 2.12). A minimum of four tic points were registered onto the overlay, covering the extent of the interpretation. The scale at which each estuary was drawn was no greater than 1:20 000.

Figure 2.11. A black and white (panchromatic) Landsat ETM7+ image with the facies interpretation overlaid onto it. The print also shows a scale bar, latitude/longitude grid and name of the estuary.

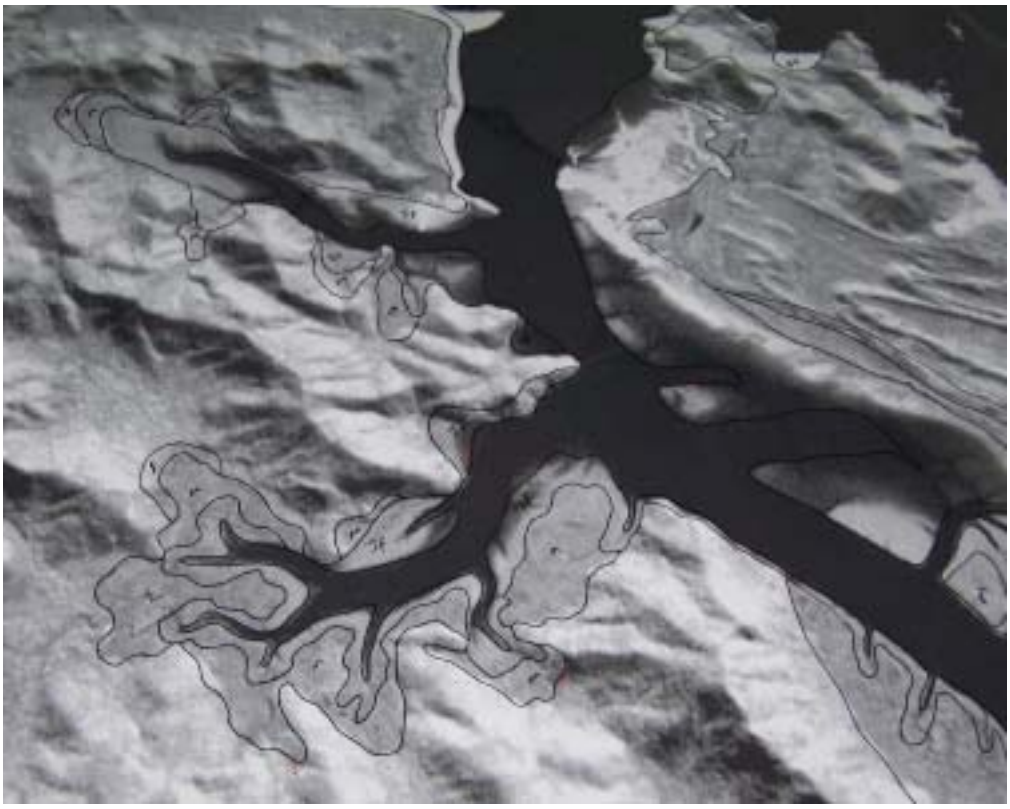

Figure 2.12. An enlarged view of the facies interpretation

Notice the hand-drawn lines which trace the boundaries of the habitats on the Landsat ETM7+ image**.**

Reviewing and checking

At the completion of a series of maps categorised by Australian state, approximately 25% of the facies interpretations were visually inspected for consistency and correctness by experienced colleagues. Notes were hand-written onto the overlays, so the edits required would be identified and carried out. This process ensured consistency with previous NLWRA mapping interpretations.

Scanning, editing, and attributing

When interpretations were completed, the overlays were removed from the base image map and scanned at 400 dots per inch (dpi), and binary tif files produced. The tif files were then georeferenced to a grid created in Microstation™ using the tics registered on the overlay (Figure 2.13).

Figure 2.13. Overlay removed from the base map

The overlay was scanned at 400 dpi, creating a tif file. Notice the registered tic points at each corner of the overlay which was used to georeference the tif file.

Using the Provec™ module within Microstation™ the georeferenced tif image was vectorised, producing a Microstation™ Design (dgn) file (Figure 2.14). The dgn file was edited and cleaned until dangles, undershoots and other errors in the line work were eliminated. Polygon labels were also placed (Figure 2.15) and the dgn file was converted into an ArcInfo™ coverage. An AML script was used to add a 'GH_SYMB' item and populate it with the relevant habitat type.

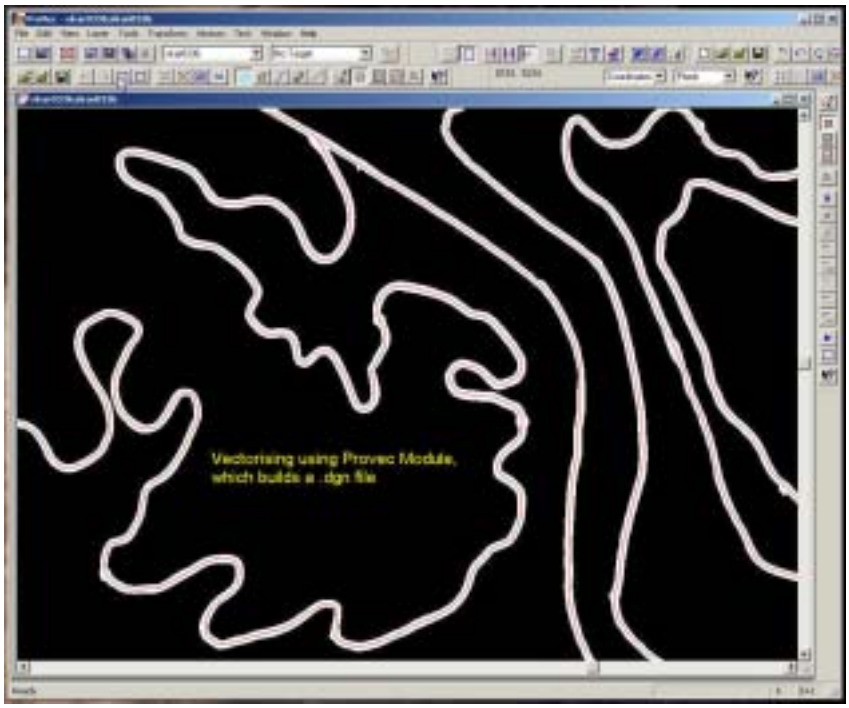

Figure 2.14. Provec™ module interface within Microstation™

The georeferenced tif is vectorised with literally just a press of a button, which builds a dgn file.

Figure 2.15. The dgn file is brought back into Microstation™ for editing/cleaning and placement of polygon labels which are displayed in red

Editing and attributing ArcInfo coverages

Once a desired ArcInfo coverage was produced it was loaded into ArcMap™ and the habitats were displayed in appropriate colours over a Landsat ETM7+ image (Figure 2.16) to identify whether the habitats were spatially and geomorphologically correct and that boundaries did not separate homogeneous polygons.

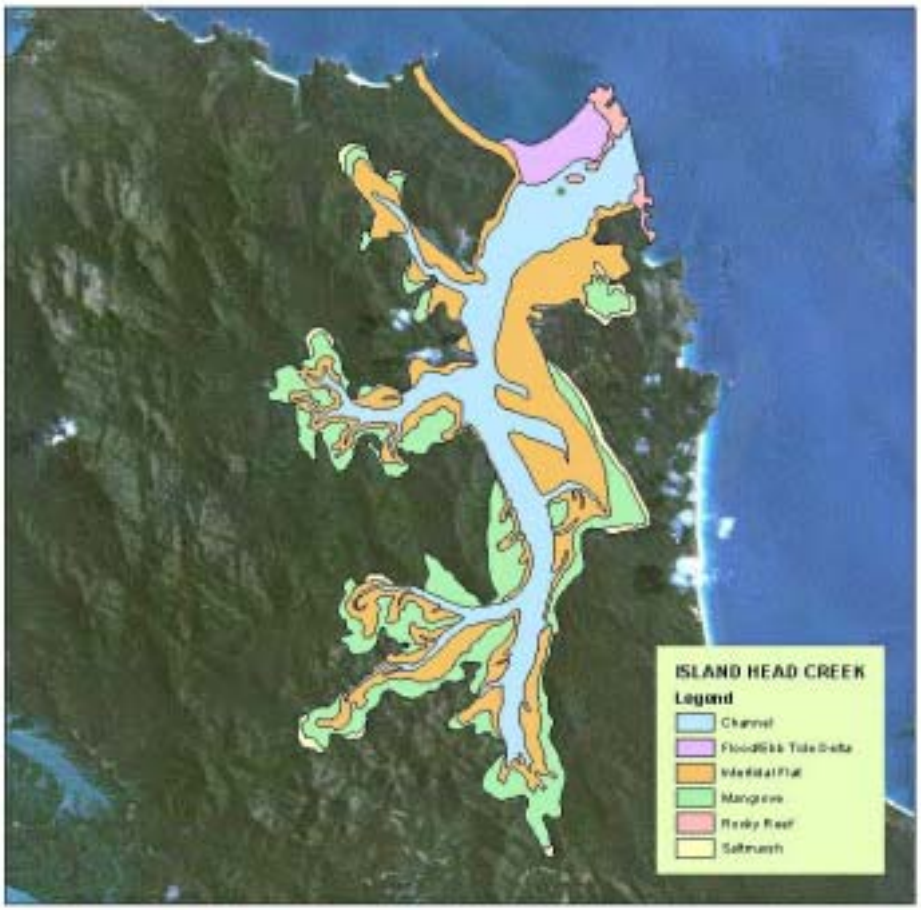

Figure 2.16. The ArcInfo cover created from the dgn file is loaded into ArcGIS for a visual inspection. The habitats are displayed in appropriate colours over a Landsat ETM7+ image

If boundaries separating homogeneous polygons were present, then the 'dissolve' command was used in workstation ArcInfo to delete the boundary. This command also deletes the label point accordingly. In the situation where polygons require further editing, workstation ArcInfo was used to display and edit an ArcInfo coverage over the Landsat ETM7+ multispectral image in order to accurately make updates to the line work.

When all the covers were checked and compiled for the whole state, a series of AML scripts was used to attribute the ARC attribute tables (.aat), polygon attribute tables (.pat) according to the Geoscience Australia Data Dictionary. The AML scripts also checked for topology and attribute errors.

Creation of frequency tables and quantification of facies relationships

After the ArcInfo covers were completed, frequency tables and associated .aat and .pat files were created using AML scripts that quantified several aspects of each cover. These were as follows:

- Channel boundary/contacts relationships
- Length of bedrock-channel/interface boundaries
- Frequency and area of each facies type present within the coverage
- Frequency of specific polygon relationships to assist in determining estuarine classification (i.e. wave, tide or river).

This data was then collated and stored in spreadsheet form for further analysis.

Preparing the data for online download

For online delivery of the data, an ESRI shapefile was compiled for each state. To create a shapefile, the ArcInfo covers were merged using the geoprocessing wizard in ArcMap. The ArcInfo-generated columns were deleted and the projection/datum was defined using ArcCatalog. As part of Geoscience Australia's standard for delivering data online, the following text (.txt) files were created to describe the shapefile:

- Descriptions.txt—provides a description of the habitats
- OSDM Licence.txt—copyright and licence agreement
- Mapping_definitions.txt—describes the criteria used for mapping each habitat
- Metadata.txt—describes the data as per ANZLIC metadata standards
- Quality.txt—describes the quality of the data
- Readme.txt—lists the data fields in the shapefile and associated metadata.

After further quality control/quality assurance procedures were carried out, the shapefile and associated metadata were then delivered together as a zip file to the OzEstuaries website's 'downloads' section.

Archiving of interpretation maps and data

Interpretation maps, copies of Landsat imagery on CD and hardcopy documents have been catalogued and stored in the Geoscience Australia archives. Digital ArcInfo coverages and frequency files were archived in appropriately labelled directories.

Near-pristine estuary mapping observations

The distribution and abundance of geomorphic environments in the near-pristine estuaries mapped as part of this project differ around Australia. These differences are ascribed to the influences of waves, tides and rivers along the coast which have produced different coastal geomorphic regions (Harris *et al.* 2002) (Figure 2.2). Observations seen in the near-pristine estuaries are described in the context of these different coastal geomorphic regions. Further differentiation of two of these geomorphic regions could be recognised based on the mapping of the near-pristine estuaries.

The North-west Coast region was divided into two separate regions that recognised the significant difference between near-pristine estuaries in the Kimberley region, which are bounded by bedrock valleys, and those along the rest of the coast. The Gulf of Carpentaria region was divided into two regions that reflected differences in the influence of waves and tides at the coast and thus the extent that the geomorphic units extended into the catchment. As a result, a total of six geomorphic regions were defined. Table 2.2 summarises the key factors that define these regions.

Table 2.2. Summary of the key factors that define the six geomorphic regions

Geomorphic region	Key factors
North-east Coast	Definite habitat boundaries Matured and well formed habitats. Definite sequence of intertidal flats/mangrove/saltmarsh Abundant mangrove along channel and deep into catchment Estuaries can have a large intertidal zone at entrance and along channel Saltflats border mangroves
South-east Coast	No mangroves Basic systems Lack habitat formation or habitats in general Minimal saltmarsh or none exist
North-west Coast	Similar to estuaries along south and west of the Gulf Non-mangrove vegetation is very prominent Transitional habitats are evident Some have well formed habitats Similar to North-east region Saltflats extend deep into catchment Mangrove branching more evident
Kimberley Coast	Not as extensive due to bedrock Wide entrances and large channels Very similar to North-east region estuaries Well developed habitats Sequence of intertidal flats/mangrove/saltmarsh is definite Saltflats border mangroves
East Gulf of Carpentaria Coast	Generally basic to complex systems Transitional (new to relic) habitats Mangroves not always present The Gulf has a continuous strandplain running along the coast
South and West Gulf of Carpentaria Coast	Strandplains dominated by salt or sand Saltflats are continuous along south and west coast and extend deep into the catchment Non-mangrove type of vegetation is introduced Fringing mangroves at entrance Mangrove branching

North-east Coast

The distribution and abundance of geomorphic environments in near-pristine estuaries in the North-east Coast region are relatively simple compared with the other regions. The boundaries between the environments are distinct, as shown in Landsat ETM7+ scenes (Figure 2.17). Figure 2.17 shows the typical characteristics of the near-pristine estuaries in this region. A principal trait of these systems is the sequence of intertidal flat, followed by mangroves, and then saltmarsh/saltflats that borders the main channels. Specifically, mangroves are abundant along the channels and extend relatively far inland into the catchment. Also, the near-pristine estuaries are characterised by relatively large intertidal flat areas, particularly near the entrance and along the main channels. In nearly all cases mangroves border the channels and separate the intertidal flat areas from the saltflats.

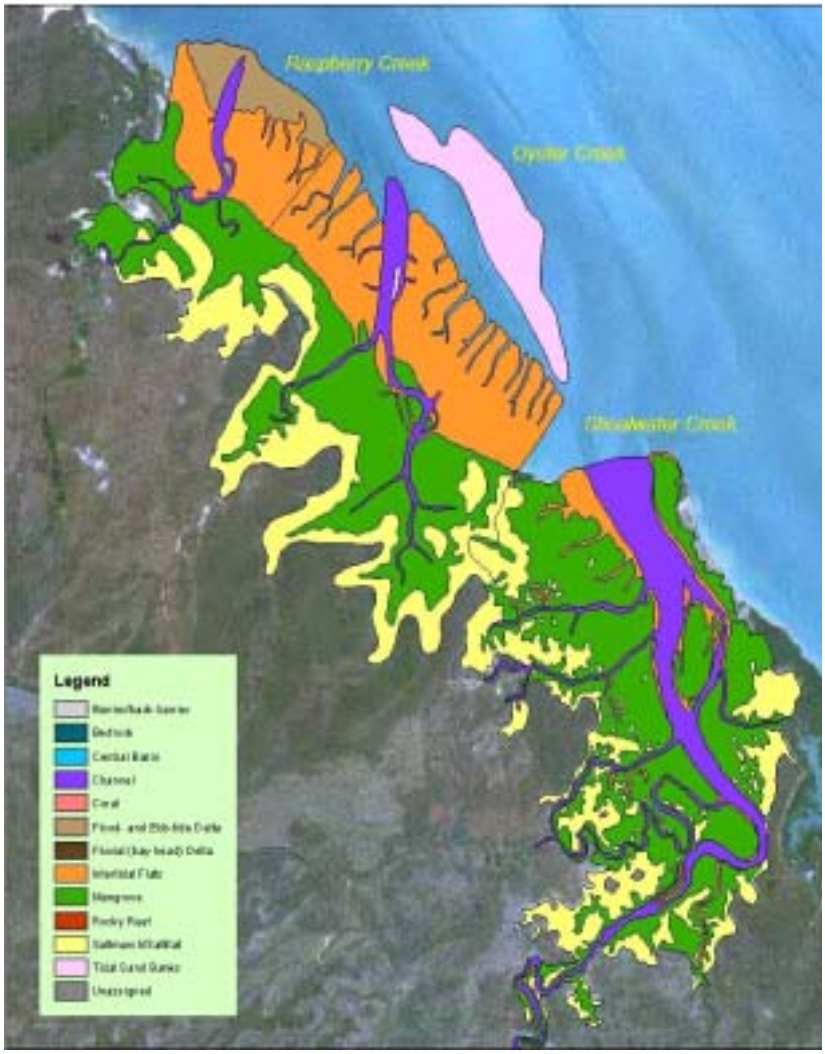

Figure 2.17. Landsat ETM7+ image with the facies maps of Raspberry Creek, Oyster Creek and Shoalwater Creek overlaid

The maps show the sequence of intertidal flat, mangrove, saltmarsh/ saltflat, and the large intertidal zone at the entrance.

South-east Coast

Most near-pristine estuaries mapped in the South-east Coast region were located in Tasmania and the observations for this region reflect only those seen the Tasmanian estuaries. Overall, the near-pristine estuaries in this region are relatively small compared with the other regions. Geomorphic environments are generally poorly developed, with sparse areas of marginal marine vegetation and patchy distributions of saltmarsh. Specifically, near-pristine estuaries in the South-east Coast region have very restricted areas of melaleuca mangroves. Typically, these systems contain relatively large areas of intertidal environments surrounding a well-developed central basin. Cloudy Bay Lagoon (Figure 2.18) is an example of one of the more well-developed systems from this region.

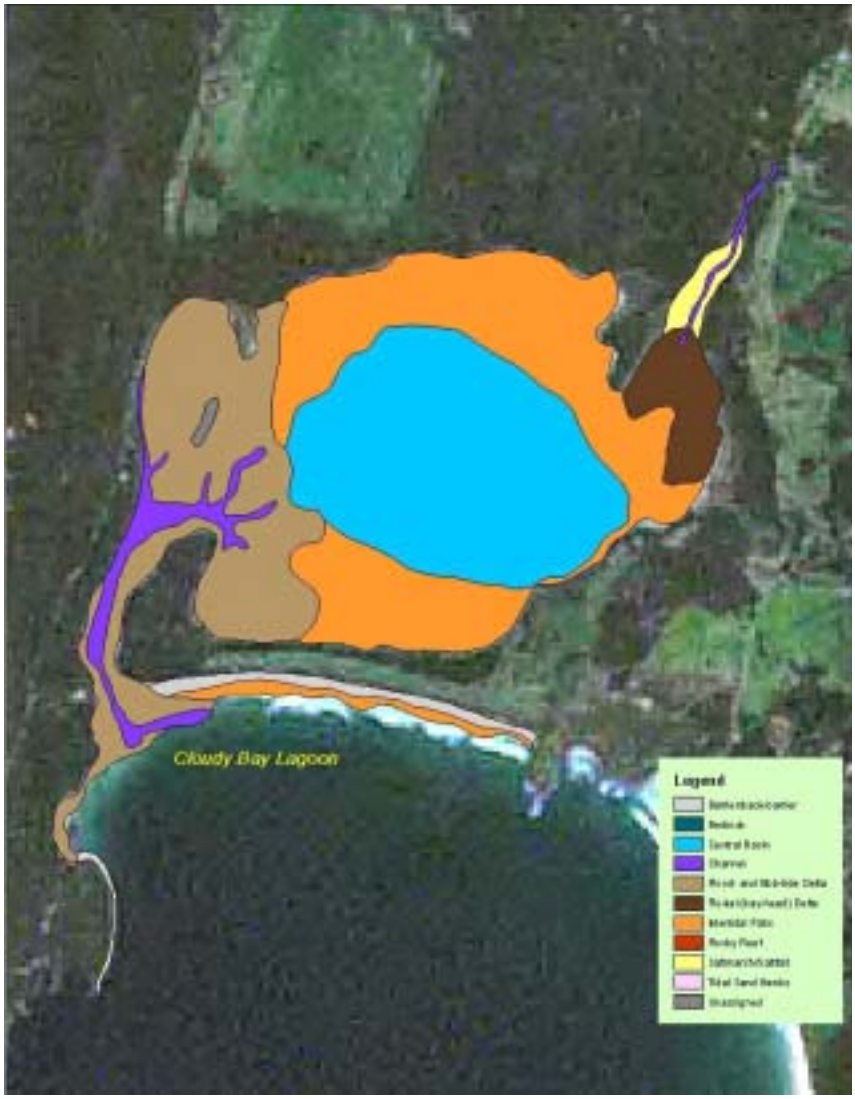

Figure 2.18. Map of Cloudy Bay Lagoon (wave-dominated estuary), located on the south-east coast of Tasmania. The estuary has no mangrove vegetation and minimal saltmarsh.

North-west Coast

The diagnostic feature of the systems in this region is the well-developed marginal marine vegetation that abuts the extensive saltflat areas (Figure 2.19). These features make these systems very similar in their geomorphology to those contained in the south and west Gulf of Carpentaria Coast region (see below). A distinctive feature of the near-pristine estuaries in this region is the branching pattern of marginal marine vegetation caused by the strongly dendritic morphology of the estuarine channels (Figure 2.20). In the analysis of systems in this region, the marginal marine vegetation cover did not produce the characteristic cyan colour from the multispectral Landsat images of mangroves. It is thus unclear whether the near-pristine estuaries in the North-west Coast region contain only mangroves; it is more likely that they contain a mixture of vegetation.

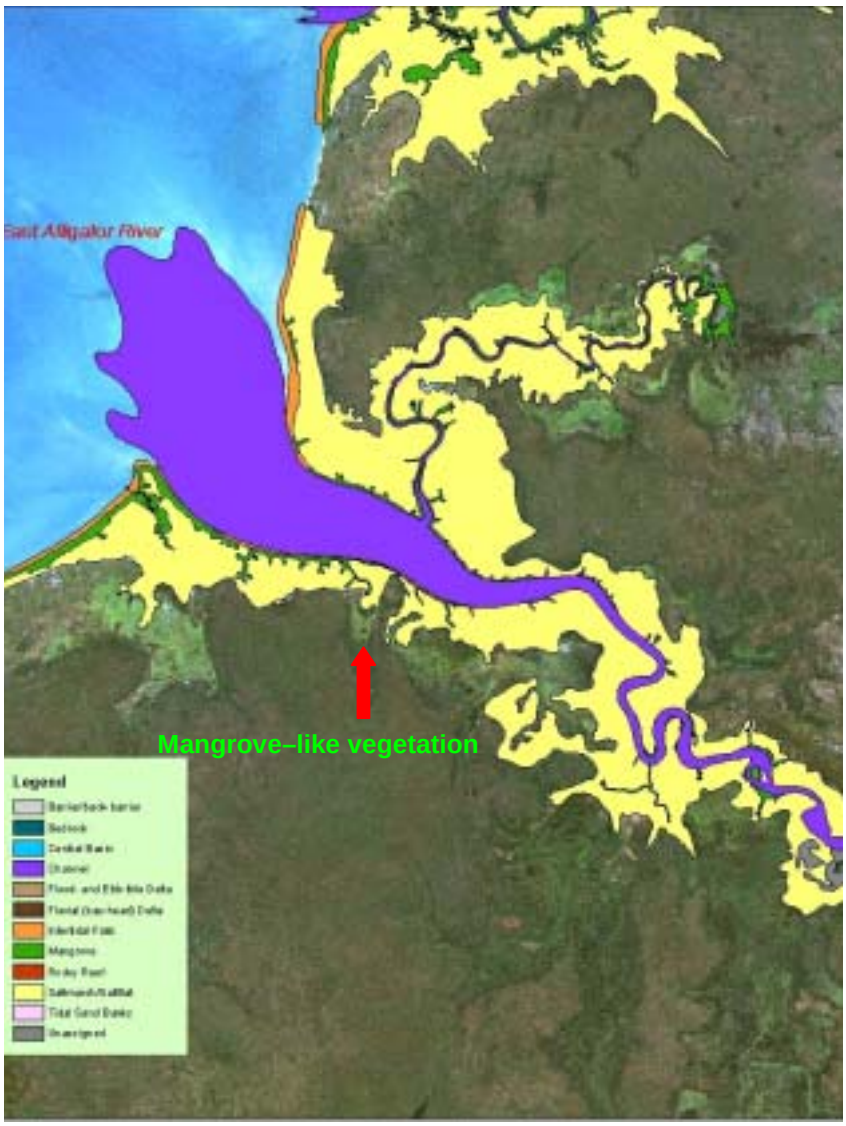

Figure 2.19 Map of East Alligator River showing the 'mangrove-like' vegetation and the way habitats are generally distributed in the North-west region

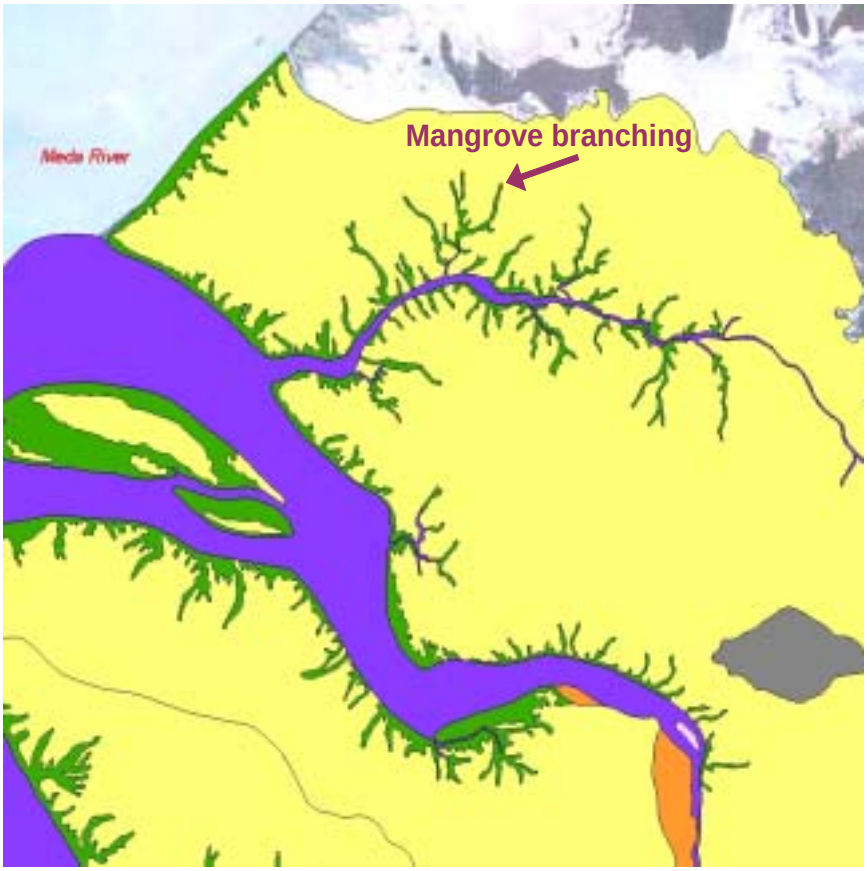

Figure 2.20. Map of the Meda River estuary, located in northern Western Australia showing an example of 'mangrove branching'

Kimberley Coast

Near-pristine estuaries in the Kimberley Coast region are distinguished by the prominent influence that the surrounding bedrock valleys play in shaping the geomorphic environments. Generally, the geomorphic environments are restricted and relatively poorly developed (Figure 2.21). The spatial distribution of geomorphic environments is similar to near-pristine estuaries in the North-east Coast region (see above), and characteristically the sequence of intertidal flat, mangrove, saltmarsh/saltflat is a dominant feature of systems of the Kimberley Coast (Figure 2.21). However, due to the bedrock control, near-pristine estuaries in this region tend to display a much simpler morphology characterised by a single dominant channel bordered by of intertidal flat, mangrove, saltmarsh/ saltflat environments, with a large and deep entrance.

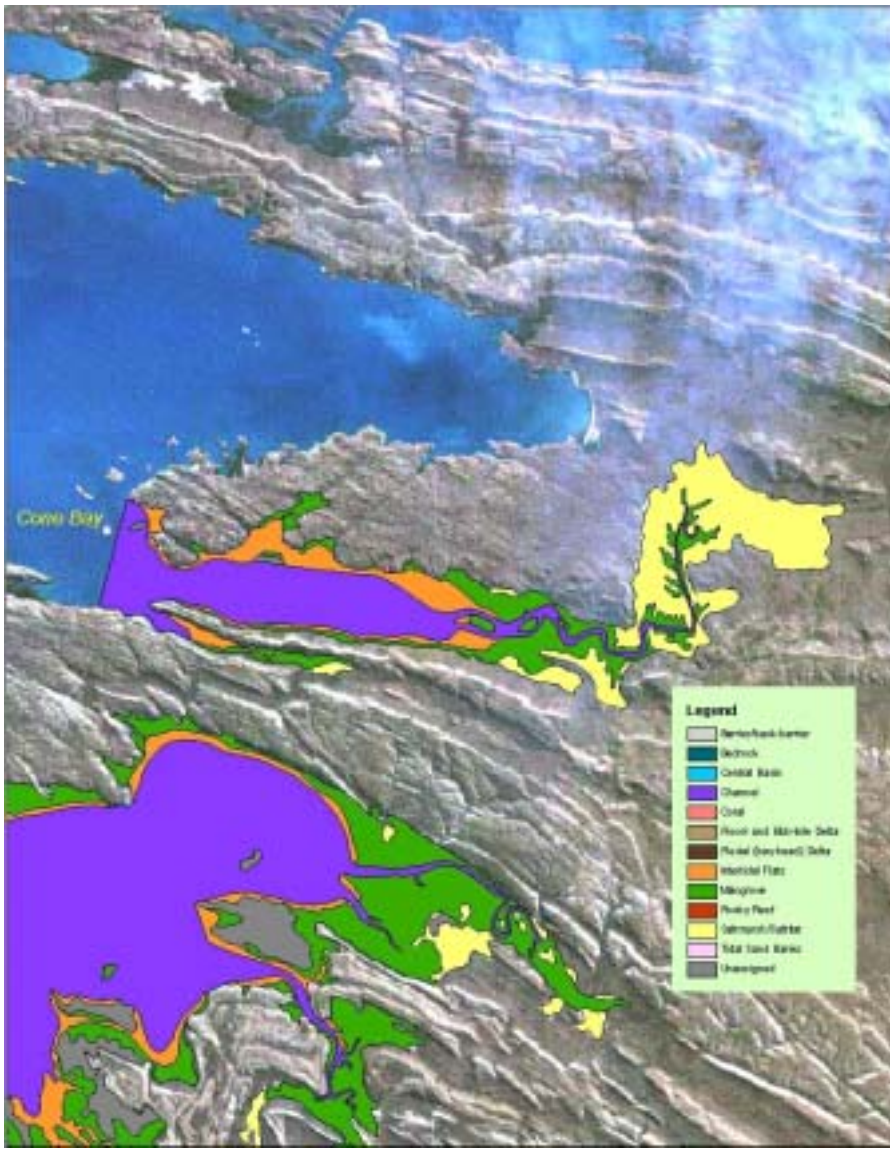

Figure 2.21. Facies map of Cone bay showing the typical geomorphic environments of estuaries in the Kimberley region

Generally, geomorphic environments show a sequence of intertidal flat, mangrove, saltmarsh/saltflat but are restricted due to the influence of surrounding bedrock valleys.

East Gulf of Carpentaria Coast

Significant variation in the distribution and abundance of geomorphic environments occurs in the near-pristine estuaries of the east Gulf of Carpentaria coast. A characteristic feature of these systems is the extensive areas of older (probably Pleistocene) and higher-elevation material that border the present systems (Figure 2.22). This material has had an influence on the morphology and distribution of estuarine geomorphic environments in this region.

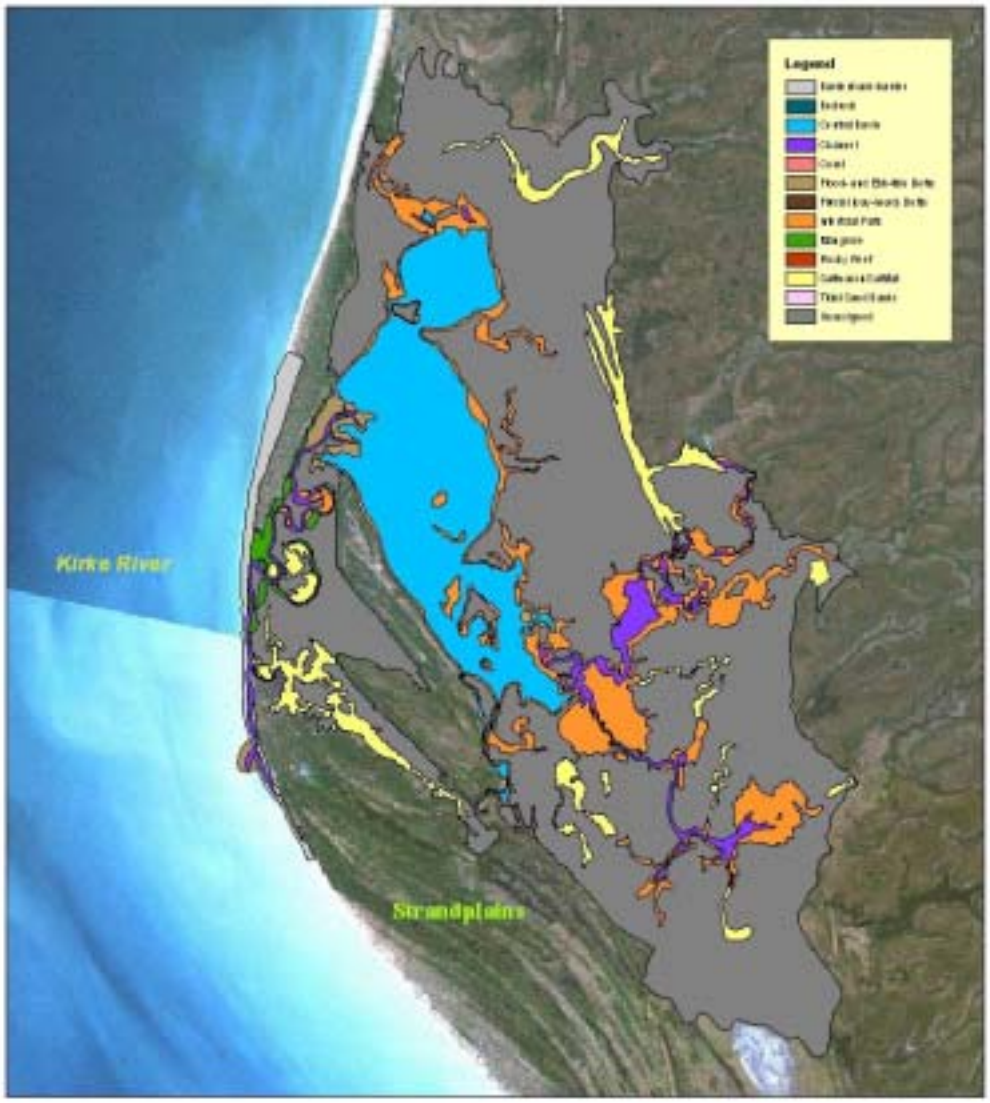

Figure 2.22. Facies map of the Kirke River estuary

Key features include large dunes of saltflat/saltmarsh and extratidal environments (unassigned); poorly developed intertidal flat and mangroves; and a central basin. These features have come about because the systems occur in a wide, low-gradient coastal landscape, bordered by a well-developed strandplain.

Significantly, near-pristine estuaries of the east coast of the Gulf of Carpentaria occupy an extensive, low-gradient coastal plain (Figure 2.22). This means that they are characterised by well developed areas of saltflats and higher extratidal environments (shown in Figure 2.2 as unassigned). A key feature is that these systems occur landward of a well developed strandplain comprising multiple beach ridges and barriers as part of the coastal plain. In many cases, the near-pristine estuaries contain poorly-developed intertidal flat and mangrove environments, with an extensive low-energy central basin (Figure 2.22). Also, the barrier tends to be very well developed in many systems. These features indicate that waves have a significant influence on the overall morphology of near-pristine estuaries on the east coast of the Gulf of Carpentaria.

South and west Gulf of Carpentaria Coast

Near-pristine estuaries in the coastal plain become more connected along the south and west Gulf of Carpentaria coast (Figure 2.23). As such, these systems are increasingly channelised and there is a greater abundance of mangrove environments associated with the extensive branching and multiple channels. Coupled with this is the greater abundance of saltflat environments that inter-digitate with the mangrove environments. Overall, the marginal marine environments extend further inland for near-pristine estuaries along the south and west Gulf of Carpentaria coast than those on the east coast.

Figure 2.23. Landsat image of Limmen Bight River (tide-dominated estuary)

The image shows the saltflats extending deep into the catchment and along the coastline. Mangroves fringe the river and the coastline and the mangrove 'branching' formation is evident throughout the catchment.

3. Using remote sensing for mapping and monitoring near-pristine estuaries

Review of remote sensing methods applicable to mapping estuarine geomorphology

Remote sensing has been used for many years for mapping and monitoring the coastal zone, at both research and operational levels, using a range of technologies. Remote sensing has the advantage of being rapid and cost-effective, and can be accurate, although this depends on the sensor resolution and capability of the classification procedure used (Green *et al.* 1998a). Aerial photography interpretation has been traditionally and successfully used for many coastal applications. However, the use of advanced satellite and/or airborne remote sensing technology now provides an opportunity for more cost-effective and objective monitoring.

Environmental indicators that are able to be mapped through remote sensing offer a spatial and temporal advantage over traditional field observations for monitoring the status of coastal ecosystems. For example, mangroves are often an integral component of many parts of the coastal zone, and mapping their distribution and change with respect to surrounding vegetation and estuary position provides a potential indicator for estuary dynamics and health (Blasco *et al.* 1996). Mangrove mapping with remote sensing technologies, including the discrimination of mangroves from non-mangrove coastal vegetation, has been commonly explored in the literature. There is also a need to map and monitor seagrass—which is strongly influenced by water quality—and associated macroalgae, microphytobenthos and physical substrata, over a range of spatial and temporal scales, for assessing the status of coastal systems (Dekker *et al.* 2004). With respect to water, remote sensing can be used to measure many environmental properties including sea surface temperature, chlorophyll *a*, suspended sediment concentration and algal blooms (Mumby *et al.* 2003).

This review looks at a range of remote sensing technologies that have been used for estuary mapping and monitoring, starting with aerial photography, high-resolution satellite sensors and commonly used optical sensors and followed by less commonly used sensors. It also reports on the various methods and applications including the use of multi-temporal remote sensing and the integration of different sensors, as well as the challenges faced when using remote sensing for estuary mapping.

Aerial photography

Aerial photography has been commonly used and is a successful medium for estuary mapping. This is partly due to its high resolution as well as its historical and current availability (Verheyden *et al.* 2002). Studies of mangrove/estuary change have used aerial photography from the 1940s, which is well before other remote sensing imagery was available. Historically, seagrass distribution mapping and assessment has relied on aerial photography interpretation and direct field mapping (Dekker *et al.* 2004). Even though earlier images were of poorer resolution and in black and white compared to more recent images (e.g. Lucas *et al.* 2002), they have been the only source of early imagery available and have still proven to be successful in assessing change in the estuarine environment.

Many studies have been done using aerial photography to assess change for periods up to around 40 years. Such changes include land cover surrounding coastal lagoons (Jayatissa *et al.* 2002), mangrove and saltmarsh distribution around Jervis Bay, Australia (Saintilan & Wilton 2001), and the reduction in native vegetation due to shrimp farming practices in Sri Lanka (Dahdouh-Guebas *et al.* 2002). The level of detail available may help in assessing the dynamics of vegetation structure (Dahdouh-Guebas *et al.* 2000), which can be useful not only in examining past changes but also for predicting future changes (Dahdouh-Guebas 2002). When used in stereoscopic form, tree height and relative position have also been used for distinguishing mangroves, as well as mapping their distribution and density information for looking at mangrove productivity (Kairo *et al.* 2002). With multi-temporal imagery, stereoscopic aerial photography can be used for assessing change in height and distribution; however, the poorer quality of the early aerial photographs does lead to a poor quality digital elevation model (Lucas *et al.* 2002).

Aerial photo interpretation usually relies on texture, tone and structural information for identifying features in the image (Jayatissa *et al.* 2002), and often requires experienced user interpretation, rather than an automated approach, which can be time-consuming. Caution must be applied since descriptive information such as texture and colour is subjective and hence not always repeatable by other users (Dahdouh-Guebas 2002). To help overcome the discrepancies, Wilton and Saintilan (2000) recommend some protocols for mangrove and saltmarsh mapping.

Satellite high resolution imagery

The recent availability of high resolution satellite imagery (such as IKONOS, launched in 1999, and QuickBird, launched in 2001) increases the accessibility of high resolution data without the expense of airborne campaigns. The quality of publicly available spaceborne imagery is now at the stage where it can compete with airborne imagery (Dahdouh-Guebas 2002). This could challenge the use of aerial photography for present and future analysis, but not for the past (Verheyden *et al.* 2002). High resolution satellite imagery now offers sub-metre pixel size in panchromatic mode (i.e. a black and white image responding to all visible light) and as small as 2.4 metres in multispectral mode with bands in the visible and infrared. Various techniques are available for integrating the high resolution of the panchromatic band with the multispectral bands to improve the interpretability (e.g. Welch & Ahlers 1987; Vrabel 1996). Although their spectral resolution is limited compared to other more commonly used remote sensing technologies, such as Landsat or hyperspectral sensors, they have a high spatial and radiometric resolution which may prove useful for spatial analysis of the marine environment (Malthus & Karpouzli 2003).

In one study, IKONOS was found to be more accurate for aquatic mapping when using texture and spectral information (with accuracies of 89%, 72% and 60% for seagrass, sand and macroalgae habitats, respectively), than using only the spectral differences due to the limited number of broad bands (Mumby & Edwards 2002). Mumby and Edwards (2002) also found that the airborne Compact Airborne Spectrographic Imager (CASI) was more accurate than IKONOS, and Landsat Thematic Mapper (TM) was more cost-effective, but concluded that IKONOS may be a cost-effective option when investigating small-scale habitats with sufficient field data. Wang *et al.* (2004) compared IKONOS with QuickBird for mapping mangrove species and found the IKONOS to perform better than QuickBird for spectral as well as textural discrimination, although both high-resolution sensors showed promising results.

Multispectral and hyperspectral imagery

Optical instruments such as Landsat and SPOT (Systeme Probatoire pour l'Observation de la Terre) have been one of the most commonly used forms of satellite remote sensing for environmental monitoring. Operating since 1972 (Landsat) and 1986 (SPOT), they also allow for regional-scale, historical change analysis at an affordable cost. Both instruments have been evolving, resulting in improved spatial and spectral quality. From 1984, Landsat-5 TM provided broadband environmental data with a spatial resolution of 30 m, and was soon followed by SPOT imagery with 20 m pixels. Although similar sensors became

available over the next 16 years, they never reached the global accessibility of Landsat and SPOT (Dekker *et al.* 2004). Landsat TM has been used extensively for coastal studies, as well as playing an important role in the United States National Oceanic and Atmospheric Administration (NOAA) Coastal Change Analysis Program (Davis *et al.* 2004).

For mangrove analysis, aerial photography has been commonly used in preference to sensors such as Landsat and SPOT. This was mainly due to their lower spatial resolution creating difficulties in identifying species or genus, as well as the longer historical archive of aerial photographs allowing for more extensive change detection analysis (Verheyden *et al.* 2002). Even so, these medium resolution sensors have proved to be beneficial.

Sulong *et al.* (2002) used aerial photography and Landsat TM imagery for discriminating different mangrove types, and found black and white aerial photographs were more accurate and detailed and could discriminate more classes than the Landsat TM, although the Landsat TM was useful and faster to classify since it was not done manually and particularly since it covered a larger area. De Vries *et al.* (2002) were able to classify the wetlands of Queensland using Landsat, validated by field visits and aerial photography, to an accuracy of 90%. After the terrestrial land features were masked out manually, the wetlands were classified into broad mangrove and saltmarsh classes, using an unsupervised classification. The availability of infrared bands has proven to be beneficial. The short wave infrared (SWIR) region was considered useful for mapping mangroves when SPOT HRVIR (High Resolution Visible and Infrared) and Landsat TM were compared (Green *et al.* 1998a), and for species/community discrimination (Lucas *et al.* 2004). The infrared wavelengths can also be of use for distinguishing between vegetation and agricultural regions (Dahdouh-Guebas 2002).

For the discrimination of benthic vegetation, Landsat TM and SPOT have suitable radiometric resolutions (i.e. brightness levels) (Lubin *et al.* 2001), which are much better than the Landsat MSS (Multispectral Scanner) (Ackleson & Klemas 1987; Mumby *et al.* 1997). However, for this purpose, the spectral resolution and signal-to-noise ratio of the Landsat TM is better than the multispectral SPOT XS instrument (Dekker *et al.* 2004). Even so, their spectral resolutions are adequate for the simple discrimination between the vegetated and non-vegetated benthic surface (Mumby *et al.* 1998). Based on applications within their capabilities, the Landsat TM and SPOT XS sensors have been successfully used for mapping benthic vegetation (e.g. Dekker *et al.* 2004; Ackleson & Klemas 1987; Zainal *et al.* 1993; Liceaga-Correa & Euan-Avila 2002).

Higher spatial and spectral resolution sensors are also available, such as the airborne CASI. Its high resolution (up to 60 cm) as well as many spectral channels (up to 18) makes it a useful sensor for mangrove discrimination and for more detailed mangrove assessment (Lucas *et al.* 2004; Green *et al.* 1998b). The higher spatial resolution sensors can utilise texture to allow for more detail to be extracted (e.g. Levesque & King 2003). The higher spectral resolution enables information about plant health and its growth processes to be derived through correlations with their narrow bands and the use of vegetation indices. For example, subtle changes in leaf canopy colour or nitrogen content that are indicative of plant health can be detected in CASI data using green, red or near-infrared reflectance values or the ratios between them (e.g. Boegh *et al.* 2002; Coops *et al.* 2004). This is particularly applicable when monitoring pristine estuaries which have more subtle changes over time, compared to outright land-cover changes. High resolution imagery can also be used for individual crown delineation, manual or automatic (e.g. Leckie *et al.* 2003; Ticehurst *et al.* 2001) which can be useful for density mapping, although difficulties are often encountered for understorey trees, and canopy shadow (Lucas *et al.* 2004). Although only an experimental satellite, the HYPERION sensor, launched in 2000, offers high spectral resolution in the visible and infrared with 220 bands at 30 m pixels, enabling the acquisition of hyperspectral imagery from space.

A range of sensors and classification methodologies have been compared for mangrove mapping, with varying conclusions. Green *et al.* (1998a) compared SPOT XS, Landsat TM and CASI for mapping mangrove communities as well as discriminating mangrove from non-mangroves. They found SPOT XS wasn't able to separate mangroves from non-mangroves and performed poorly compared to Landsat and CASI, also that visual interpretation and vegetation indices had the lowest overall classification accuracies. While CASI was no better than Landsat TM for separating mangrove and non-mangrove, it was superior when discriminating between nine different mangrove classes, with an accuracy of 85% using relationships between the different spectral bands. Although CASI is more expensive and covers a much smaller region than satellite sensors, Green *et al.* (1998b) found it to outperform SPOT and Landsat when discriminating a broad range of mangrove and non-mangrove categories, as well as Normalised Difference Vegetation Index (NDVI) relationships with leaf area index and canopy closure. According to Green *et al.* (1998a) most researchers were successful in discriminating between mangrove and non-mangrove; however, one case reported confusion between rainforest and mangroves, and another between inland vegetation and mangroves.

Investigating the spread of Rhizophora mangle on Molokai, Hawaii, D'Iorio (2003) compared the results from ASTER (multispectral, 15–30 m), AVIRIS (hyperspectral, 17–20 m) and colour aerial photography (0.5 m), and found that the processing method had a greater influence on the accuracy than the type of remote sensing used, with visual interpretation performing best. Rasolofoharinoro *et al.* (1998) also found visual interpretation to be more effective than supervised classification techniques. Saito *et al.* (2003) found the higher resolution and greater number of bands of TERRA ASTER to be no better than the SPOT-4 data when mapping a coastal ecosystem, and also found discrimination difficult between vegetation classes when ground cover was less than 50%.

Concentrations of organic and inorganic material in the water column are used as a measure of water quality in coastal, estuarine and riverine areas (Phinn *et al.* 2004). Remote sensing has been used for mapping the concentration of organic and inorganic materials in lakes and riverine environments (Dekker *et al.* 2001). Water parameters that can be successfully mapped using remote sensing include chlorophyll concentration, turbidity, secchi depth, photosynthetically active radiation and substrate types, as demonstrated in Moreton Bay, Queensland (Phinn *et al.* 2004). Hyperspectral data have been used for mapping water quality parameters such as total suspended sediment (TSS) and coloured dissolved organic matter (CDOM) concentrations as well as mangroves, rock platform vegetation and saltflats (Dekker *et al.* 2001; Brando & Dekker 2003). Brando and Dekker (2003) developed a method for retrieving concentrations of chlorophyll, CDOM and tripton in coastal waters using three spectral bands from the HYPERION spaceborne hyperspectral sensor, which was then adapted to multispectral imagery (Brando *et al.* 2004).

Parameters such as chlorophyll *a* concentration and suspended sediment concentration can be measured with airborne hyperspectral (e.g. CASI), satellite hyperspectral (e.g. Hyperion), multispectral high-resolution (e.g. IKONOS), medium-resolution (e.g. Landsat) and low-resolution instruments (e.g. MODIS). Algal blooms can also be detected using the same instruments with the exception of high-resolution multispectral sensors (Mumby *et al.* 2003). While the simultaneous mapping of water quality parameters and substrate is presently not possible, semi-analytic models are being investigated to allow this to happen (Phinn *et al.* 2004). Hyperspectral image data may be required to achieve this, as it is unknown whether multispectral sensors, such as Landsat, will be sufficient (Phinn *et al.* 2004).

Other instruments

Due to its ability to acquire imagery in cloudy environments, Synthetic Aperture Radar (SAR) offers great potential for the mapping of coastal environments. For water bodies, SAR's relationship to surface roughness allows it to provide qualitative information about coastal currents, bathymetry and wind fields (Davis *et al.* 2004). Compared to optical sensors over the land, radar's longer wavelength (C-band ~ 6 cm, L-band ~ 24 cm, P-band ~ 60 cm) means its response is more related to vegetation structure and moisture conditions rather than colour and chemistry. SAR's relationship to vegetation structure can be used to investigate the different mangrove canopy structures (Proisy *et al.* 2002) and potentially biomass (Lucas *et al.* 2005). Good relationships between vegetation height, tree diameter at breast height and biomass can be achieved, particularly with the longer radar wavelengths (Mougin *et al.* 1999). Radar may also be able to assist in separating pioneer from mature forest due to there being more double bounce scattering when ground is visible to the radar, and more volume scattering in dense forests (Lucas *et al.* 2005). This difference is accentuated for flooded vegetation, where double bounce interaction between the water and trunks is strong (e.g. Mougin *et al.* 1999; Simard *et al.* 2002).

Perez *et al.* 2002 used both historical aerial photography and Radarsat data to monitor the growth and changes in a delta due to variation in water flow rate as it drained into the lagoon, over a greater than 30 year period. Aschbacher *et al.* (1995) found that single band radar was insufficient for discriminating between mangrove and non-mangrove vegetation, however combining radar bands has been shown to improve results. A tropical coastal region of Gabon was able to be mapped using texture and backscatter information from JERS-1 (L-band) and ERS-1 (C-band) SAR in a decision tree classifier (Simard *et al.* 2002). The combined dataset improved the classification results by 18% to give 84% accuracy compared to classifications using a single band. Radar's structural information and double-bounce effects between trees and the ground allowed for discrimination between high and low mangroves by using flood extent.

Radar interferometry is a relatively new technology that allows for the generation of digital surface models. Since recent and current instruments (e.g. SRTM and ERS-1 and 2) operate at relatively short wavelengths, these models usually represent the height close to the top of the vegetation canopy. For vegetated flat coastal regions, these digital surface models approximate vegetation height (Lucas *et al.* 2004; Held *et al.* 2003).

LIDAR technology has also been useful for mapping structural information about forests (e.g. Drake *et al.* 2002; Lim *et al.* 2003). However, the disadvantage of

using laser is that it is expensive and can be difficult to interpret (Lucas *et al.* 2004) if it is not captured with aerial photography or other imagery. For bathymetric studies, LIDAR also offers a high density of data (Malthus & Mumby 2003), and fluorescence induced from active lasers can be used for mapping ocean chlorophyll, bathymetry, macroalgae and seagrass and potentially subtidal benthic habitat mapping (Mumby *et al.* 2003).

Although optical instruments are often used for benthic mapping, acoustic systems are also useful when light penetration is low due to high turbidity (Malthus & Mumby 2003). Acoustic systems may be point data or image swaths of the sea floor (Foster-Smith & Sotheran 2003). Although point data has its limitations, it does provide data where it may otherwise be unavailable (Foster-Smith and Sotheran 2003). Active sonar sensors are used to measure water depth and surface roughness, and have some advantages over optical methods in that they can penetrate deeper into the water and are independent of optical water properties. However, since they are usually towed behind a boat, they cannot be used in very shallow water, so interpolation must be used to generate maps of spatial distribution, and they do not provide colour information about the benthos (Mumby *et al.* 2003), as optical instruments do.

Multi-temporal analysis

The use of satellite sensors for repeated temporal coverage is a valuable monitoring technique. Multi-temporal satellite remote sensing is a repeatable and cost-effective method for detecting large changes in seagrass distribution over time (Ward *et al.* 1997; Macleod & Congalton 1998) although some changes may be indistinguishable from map error (Dekker *et al.* 2004). Even so, Dekker *et al.* (2004) were able to use Landsat retrospectively to map changes in benthic material in a shallow estuarine lake over a 14-year period (1988, 1991, 1995, 2002) and Jensen *et al.* (1995) was able to assess changes in cat's tail and seagrass species in the Everglades using multi-date Landsat MSS and SPOT scenes.

The accessibility of freely available, relatively frequent temporal data such as MODIS and AVHRR has allowed for regional to global scale analysis of both seasonal and singular events. These datasets are acquired daily, and often composted (i.e. integrated into a single image) into weekly or fortnightly scenes to reduce cloud effects. Although their resolution is coarse (250 m to 8 km), initial scenes date from the early 1980s (AVHRR) providing a detailed historical record. Temporally frequent instruments such as MODIS and MERIS were not designed to work in turbid waters or in shallow coastal regions where the sea floor is visible, which complicates the calculation of chlorophyll and sediments (Mumby *et al.*

2003). However, these multi-temporal instruments do have potential in mapping the movement and spatial distribution of flooding events into the ocean (e.g. Hardman-Mountford & McGlade 2003), or change in coastal vegetation cover (e.g. Keith *et al.* 2002).

Combining different technologies

Combinations of remote sensing data types may be used to improve results. Using a range of remote sensing data, mangrove species and communities can be better discriminated, although there appears to be an emphasis on the use of optical imagery by itself (Lucas *et al.* 2004). Blasco *et al.* (1998) recommend combining optical and microwave data to improve the discrimination of coastal vegetation, as has been demonstrated in the literature. However, the benefits in combining optical and SAR do depend partly on the data combination used as well as specific land cover (Davis *et al.* 2004).

Combining CASI with AIRSAR improved discrimination between different mangrove and surrounding vegetation types, and mangrove zonations (Held *et al.* 2003). Similarly Aschbacher *et al.* (1995) used SAR to establish more mangrove classes than could be identified with SPOT XS alone, and found the visual interpretation improved. Souza Filho and Paradella (2002) integrated Landsat TM with Radarsat-1 using intensity hue saturation techniques and found the combined Landsat/radar image improved the interpretability of coastal features. Distinguishing between intertidal and supratidal mangroves were also improved in the combined dataset due to their different density and size of trees as well as the change in amount of visible background. Although no measure of accuracy is provided, Souza Filho and Paradella (2002) mapped 19 different coastal land-cover types, including sand dunes, marshes, mangroves (including degraded and regenerated), urban and water.

Lucas *et al.* (2004) conclude that SAR and optical combined is optimal for looking at species/community composition, vegetation structure and biomass, as well as growth stage. For benthic mapping, there is also the possibility of combining spectral information from optical sensors with acoustic datasets (Mumby *et al.* 2003).

The challenges of using remote sensing

While the mapping and monitoring of coastal regions using remote sensing has been tested on numerous sites using a variety of sensors, and with quite successful results, no standard procedure has been adopted. According to Davis *et al.* (2004) remote sensing has not become operational since no satellite system has been designed specifically for coastal mapping (i.e. a relatively high

resolution and temporal frequency) and there are no established algorithms for producing the products. Remote sensing from satellite sensors and from airborne sensors has long been considered a potentially valuable tool for monitoring changes to seagrass but operational mapping procedures (apart from aerial photography) have not yet been established. For the mapping of mangrove ecosystems, the methods are operational at a local scale, but not for permanent monitoring, or at regional scales (Blasco *et al.* 1998). This is further highlighted given the range of remote sensing technologies used synergistically to improve results. Malthus *et al.* (2003) concluded that for the remote sensing of the coastal zone, areas which need further research are the combined use of different datasets, change detection analysis and better classifications through a knowledge-based approach.

For temporal analysis which uses images from different times over the same area, the early and later scenes must be calibrated. Depending on the data available, this calibration is either for the same sensor type, or it could be for different remote sensing technologies (Dahdouh-Guebas 2002). As noted for aerial photo interpretation, the same species may appear different (e.g. for canopy colour) in different geographic units (Verheyden *et al.* 2002), so care must be taken when extrapolating information from a local site to an extended region. Soil type and moisture, as well as tide levels may also lead to difficulties when extrapolating, especially when the vegetation is sparse (Rasolofoharinoro *et al.* 1998). Mangroves are able to be distinguished from non-mangrove when they border mudflats or saline environments free of vegetation; however, difficulties have been found in separating them from rainforests (Lucas *et al.* 2005) or inland vegetation (Green *et al.* 1998a). According to Green *et al.* (1998a) this difficulty in separation appears to be site-specific, and discrimination should be possible when the appropriate sensors and processing techniques are used.

There is a restriction on the pixel size acceptable for vegetation mapping especially when investigating coastal and estuary environments because the vegetation classes tend to exist in narrow strips due to their particular soil and water requirements, particularly within the tidal zone. For mangrove mapping it was noted by Lucas *et al.* (2004) that coarse resolution imagery (>100 m pixel resolution) is only really effective in mapping large regions of mangroves, and for the more narrow strips only the presence or absence of mangroves can be detected. Furthermore, the large pixel size results in mixed pixels which are more difficult to analyse. For these reasons, high-resolution imagery is optimal, however they are also more expensive to acquire (Lucas *et al.* 2004). At scales of 1:25 000 and 1:50 000 mangroves can only be realistically separated into tall dense, low dense and open classes (Blasco *et al.* 1998).

Summary of remote sensing methods

Phinn *et al.* (2000) provides a framework for determining the best remote sensing data to use for mapping and managing coastal environments, depending on the desired outcome. The temporal and spatial scale of the data, as well as costs and time constraints, are important factors in the process. While remote sensing does initially appear an expensive means of mapping and managing coastal resources, as far as overall map accuracy is concerned, it has been found to be more cost-effective than traditional field-survey methods (Mumby *et al.* 1999; Dekker *et al.* 2004). This is the case despite the need for field survey data for training and error analysis of the remote sensing imagery. Remote sensing is also able to capture an entire area, rather than relying on spatial interpolation of point source field measurements, which can lead to mapping errors and can become subjective (Dekker *et al.* 2004).

Even if the quantitative values are not entirely correct, remote sensing provides relative spatial information (Malthus & Mumby 2003), which is prohibitive to capture at the same level of detail through field measurements alone (Dekker *et al.* 2004). For example, the quantitative mapping of seagrass distribution that requires diver survey (Zhang 1998), or terrestrial vegetation surveys (Lamb & O'Donnell 1996; Norris *et al.* 1997), traditionally requires data collected using quadrat and transect-based methods (Dekker *et al.* 2004).

Mumby *et al.* (1999) recommends SPOT XS or Landsat for coarse-scale regional analysis; however, for detailed habitat mapping, they recommend digital airborne scanners (such as CASI) or aerial photography. Alternatively, high-resolution imagery could potentially be used for detailed mapping analysis to establish a baseline, and then lower-resolution imagery with a higher temporal frequency could be used for monitoring changes (Blasco *et al.* 1998). In particular, if the cost of aerial photography and airborne scanners is similar, Mumby *et al.* (1999) recommend using the scanner since it is likely to be more accurate. There is still a need, however, for further testing of high-resolution remote sensing data for mangrove discrimination and coastal degradation analysis (Blasco *et al.* 1998). To date, most remote sensing studies on the coastal zone concentrate on either the land or water component, even though the functions of these ecosystems are interconnected. Hence it would be beneficial to utilise the spatial capabilities of remote sensing to map the land and water as an integrated ecosystem.

Mapping supratidal and intertidal vegetation in near-pristine estuaries using remote sensing: A case study of the Daintree River system

Introduction

A major component of the current project was to map the sedimentary habitats of selected near-pristine estuaries[2] at a national scale using aerial photography. The following investigation aimed to assist this mapping by assessing the capacity of a selection of remote sensing technologies for mapping the dominant intertidal and supratidal vegetation types surrounding near-pristine estuaries. The focus was on remote sensing's potential for mapping estuarine vegetation using a standardised and automated approach.

This study examined the remote sensing datasets covering the Daintree River estuary since this area is representative of the wetland vegetation typically surrounding estuaries in tropical and subtropical northern Australia. This area also has the most imagery available as well as an existing detailed vegetation map. The two near-pristine estuaries selected to be mapped as part of the project, Noah Creek and Cooper Creek, lie to the north of the Daintree River and are included in all but one (CASI) of the remote sensing datasets described below.

Researchers involved in mapping estuarine habitats for the National Land and Water Resources Audit (NLWRA 2002) noted that distinguishing stands of melaleuca from mangrove was difficult using some aerial photography interpretation (David Ryan, Greening Australia, pers. comm. 2004). This study aimed to address this issue by investigating the ability to accurately map the dominant vegetation cover in an estuarine environment using some of the commonly used forms of commercially available image data, including: airborne hyperspectral (CASI), satellite hyperspectral (Hyperion), satellite multispectral (Landsat 7 ETM), and airborne polarimetric imaging radar (AIRSAR). It then produced a land-cover map of the Daintree River estuary, as well as Noah Creek and Cooper Creek, using the Hyperion dataset since it was the most successful in distinguishing vegetation types. The classification method was then transferred to Landsat data and compared to the near-pristine estuary maps produced using aerial photo interpretation by Geoscience Australia. A glossary is provided on the following pages for describing the remote sensing terminology used here.

[2] The 'near-pristine' estuaries referred to in this study are those which were classified as such by the National Land and Water Resources Audit (NLWRA 2002).

Le Cussan (1991) created the vegetation map used for interpreting the land cover and assessing the accuracy of the remote sensing classifications produced in this study. It was derived from high resolution aerial photography validated by extensive field sampling of the major mapping units resulting in a 1:15 000 scale map. Although this map is significantly older than the remote sensing acquisitions, this was the best field information available and was found to be adequate by a field visit during an airborne data acquisition campaign in 1996. Even though Le Cussan's map provides detailed mangrove zonations and vegetation communities, these vegetation types were combined into six suitable dominant estuarine vegetation classes for this investigation: mangrove (separated into dense and open), melaleuca/eucalypts, saltflats, rainforest and sand dune vegetation.

The remote sensing datasets date from 1996 to 2001 (Figure 3.1); hence there is potential for changes in vegetation cover to have occurred between acquisitions when comparing the classification maps. However, based on other analysis of the region, this change was assumed to be minimal, and sites used for comparison were selected such that they were not on the edge of a vegetation zone.

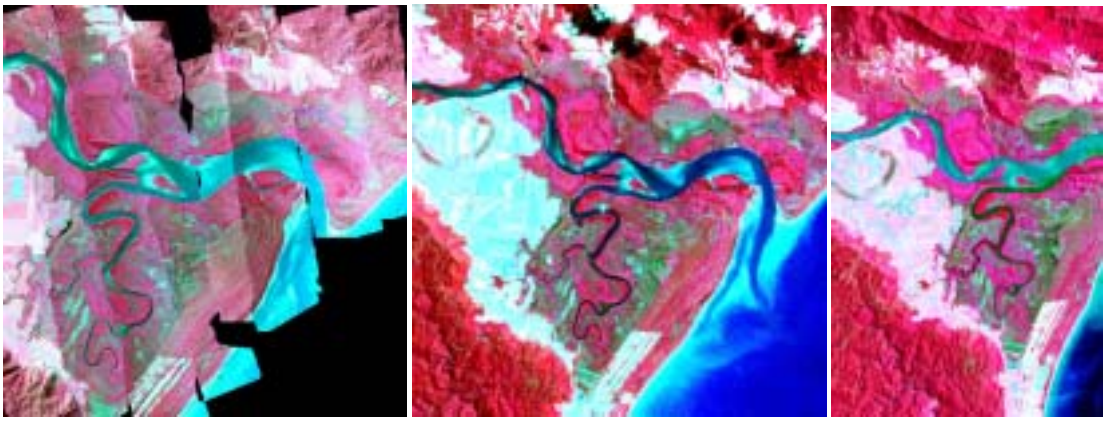

Figure 3.1. False colour images of the optical remote sensing imagery for the Daintree River

Red colour = near infrared, green = red, blue = green. *Left:* May 1996 CASI image*, Middle:* September 1999 Landsat image*; Right:* March 2001 Hyperion image.

Glossary

Term	Description
Adaptive filter	An image filter which generally preserves image sharpness and detail while suppressing noise
AIRSAR	Airborne synthetic aperture radar—An airborne imaging radar instrument developed and operated by NASA
ANOVA	Analysis of variance—A test of the statistical significance of the differences of two or more groups for one or more variables
Atmospheric correction	Image processing approach used to remove scattering and absorption effects from image data so the signal used is that emanating from the air–water interface or land surface, not the top of the atmosphere
Backscattering coefficient	A measure of the proportion of light at specific wavelengths that will be backscattered; dependent on particle size and form in water
Bandwidth	The difference between the highest and lowest wavelengths representing a band; often expressed in nanometres
Byte format	The pixel has a brightness range of 256 digital numbers
CASI	Compact airborne spectrographic imager—An airborne sensor operating in the visible and near infrared wavelengths
Chlorophyll well	The well-shaped dip occurring around the red wavelength (680 nm) of a vegetation reflectance spectrum due to chlorophyll
Confusion matrix	A table that compares the location and class of each ‘ground truth’ pixel with its corresponding location and class in the classification image
Coastal environments	Mangrove wetlands, intertidal and subtidal sections of a coastal embayment
Decision tree classification	A classifier which performs a multilevel classification based on binary decisions for placing pixels into a class
EO-1	NASA satellite; experimental platform for Hyperion and Advanced Land Imager
Geometric correction or georeferencing	The process of converting an image into a form where each pixel has a projection, datum and coordinate, enabling it to be integrated with other spatial data
Hyperion	Experimental satellite-borne hyperspectral imaging systems with 30 m pixels and 196 bands on the EO-1 platform
Hyperspectral	A device is hyperspectral if it records reflected or emitted light using more than 10 narrow spectral bandwidths (cf. multispectral)

Term	Description
Image corrections	Image processing operations designed to remove geometric and atmospheric distortions in an image data set
Image pixel	Smallest spatial sampling unit used by an imaging sensor to measure reflected or emitted energy from the surface of the earth
Integer format	The pixel has a brightness range of 65 535 digital numbers
Landsat Thematic Mapper (TM) Enhanced Thematic Mapper (ETM)	General purpose multispectral, moderate spatial resolution imaging satellite sensors that have operate since the mid 1980s (TM) and April 1999 (ETM)
Kappa coefficient	A measure of classification accuracy which also acknowledges the likelihood of chance
Maximum likelihood classification	A common remote sensing classification method which assigns pixels to a class based on its highest probability by assuming a normal distribution in the statistics of the land-cover classes
Minimum noise fraction transform	A statistical analysis designed to capture the variance and reduce the dimensionality (i.e. number of bands) in a dataset through the creation of uncorrelated bands, including the estimation of noise
Multispectral	An image data collection system where reflected or emitted energy is measured in less than 10 broad spectral bands
Multi-temporal	Data that has been collected for the same area over a series of successive dates
Near infrared (NIR)	The non-visible 700–1000 nm portion of the EMR spectrum
Normalised difference vegetation index	A normalised ratio transformation using the red and NIR pixel values, which is sensitive to vegetation cover
Occurrence texture filter	Calculation of statistical measures (e.g. mean and variance) within a processing window based on the occurrence of each brightness range
Planimetric projection	A map projection where each map element is at its true location on the ground (cf. aerial photography and some satellite images which have a perspective projection)
Polarimetry	When an imaging radar transmits and receives horizontally and vertically polarised waves
Principle component analysis	A statistical analysis designed to capture the variance and reduce the dimensionality (i.e. number of bands) in a dataset through the creation of uncorrelated bands
Radar interferometry	A technique for producing terrain models by analysing the returned radar signal from two radar receiving antennae
Radiometric correction	Conversion of image pixel digital numbers from a relative scale to an absolute physical units scale, e.g. radiance
Radiometric resolution	Smallest difference in reflected light able to be detected by a sensor and its dynamic range

Term	Description
Reflectance or spectral signature / profile	Ratio of upwelling radiance to downwelling irradiance on a target, i.e. its characteristic absorption/reflectance response
Region of interest	A selection of pixels in an image to represent a land-cover type
Spatial resolution	A measure of the scale of the smallest feature able to be detected on an image
Spectral angle mapping	An image classification approach used to group pixels with similar reflectance signature
Spectral derivative	A measure of reflectance change with respect to wavelength
Spot XS	Commercially operated high-moderate spatial resolution (20 m) multispectral and panchromatic (5 m) satellite imaging sensor
Supervised classification	Image processing approach used to group pixels with a similar spectral signature as these are assumed to be the same land-cover class
Training	The generation of (statistical) information for each land-cover class which is then used to produce a classification

Mapping estuarine vegetation using optical and radar sensors

CASI

The CASI (compact airborne spectrographic imager) data was acquired in May 1996, at 2.5 m pixel size and 14 spectral bands ranging from a wavelength of 440 to 900 nm (nanometres). Unfortunately the weather conditions were not ideal, leaving significant brightness variation between flightlines (Figure 3.2). This was originally corrected to ‘true reflectance’ (method unknown) which reduced the flightline variations; however, inspection of the spectral profiles did show unusual spectrum shape for some of the vegetation, so it was discarded from this analysis and the raw data was used instead. Since the CASI data does not cover any of the selected near-pristine estuaries chosen for mapping by the Coastal CRC, its intentional use was for identifying different vegetation cover types due to its high resolution, as well as for a preliminary assessment of vegetation discrimination. For these reasons, no classification map of dominant estuarine vegetation was completed using CASI.

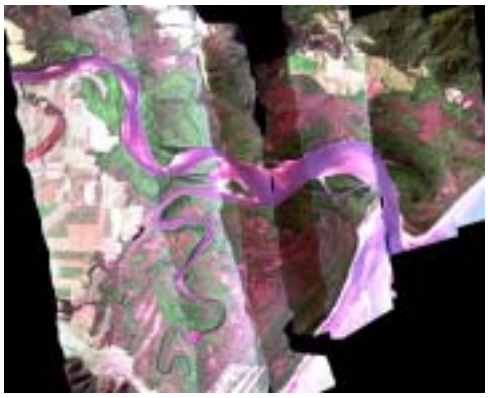

Figure 3.2. Raw CASI image over the Daintree River mangrove system

To overcome the spectral variation between flightlines for this preliminary analysis, the vegetation types were collected for each flightline and treated separately. Visual inspection of the vegetation cover types showed some apparent differences. As can be seen at this high spectral and spatial resolution (Figure 3.3), a combination of spectral and textural information may allow discrimination between the dominant vegetation types. In particular, textural information could be used for discriminating melaleuca from dense mangrove for this mangrove ecosystem, as was utilised in Held *et al.* (2003) for separating into dominant mangrove and surrounding vegetation types for this region.

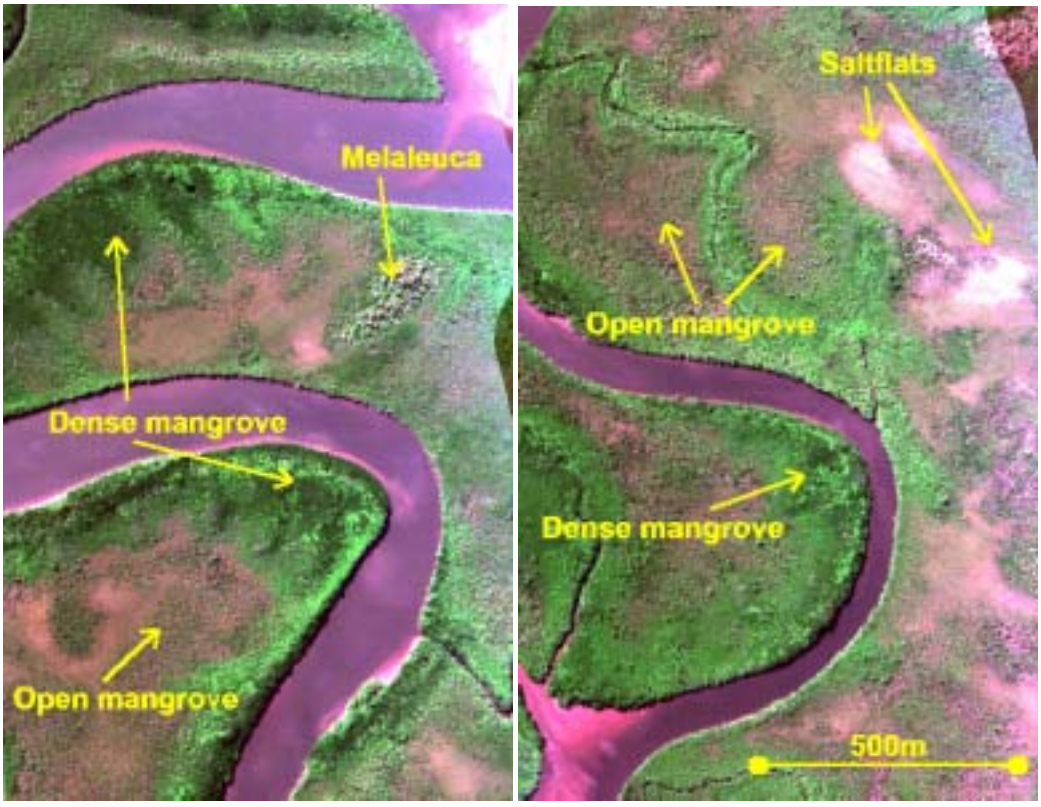

Figure 3.3. True colour CASI imagery of the Daintree River mangroves highlighting some of the dominant vegetation types

Regions of interest (ROIs) were selected along each flightline for the six different vegetation types (dense mangrove, open mangrove, melaleuca, rainforest, sand dune vegetation, saltflat). Not all of the vegetation types were available for each CASI flightline strip; however, all that were available were extracted. For each flightline, the ROIs were tested for their separability using the Jeffries-Matusita separability measure (Richards & Jai 1999) available in the remote sensing software package ENVI ®. The Jeffries-Matusita distance measure is a commonly used statistical tool in the initial assessment on how separable the classes are based on their signatures. It is used before a standard classification to assist in establishing realistic classes that are likely to be separated. This index ranges from 0 to 2.0 with numbers above 1.9 indicating good separability and values below 1.0 poor separability. The separability values from the five flightlines selected for analysis are shown in Tables 3.1 to 3.5. All 14 bands were used in the calculations. Values highlighted in red indicate classes having a very poor separability (less than 1.0), while those in yellow indicate a poor separability (1.0 to 1.9) (as described in the ENVI user manual).

The melaleuca and sand dune vegetation have the greatest confusion, with Jeffries-Matusita values below 1.0 in two cases (Tables 3.1 to 3.5). Overall, the separability between melaleuca, sand dune vegetation and rainforest was quite poor in all strips. This was understandable since these forest types all have a reasonably open canopy in the CASI imagery, as indicated by canopy shadow. This increases the standard deviation of pixel values for each ROI for these classes. Some confusion also exists between mangroves and the more open canopy types. In these situations, texture measures may be able to help in their discrimination.

Table 3.1. Jeffries-Matusita separability measure between dominant vegetation types selected for flightline 1 in the CASI image

Pair separation for strip 1 (from lowest to highest separability)		
Vegetation type 1	**Vegetation type 2**	**Jeffries-Matusita separability**
Melaleuca	Sand dune vegetation	0.6534
Rainforest	Sand dune vegetation	1.5431
Melaleuca	Rainforest	1.5991
Dense mangrove	Sand dune vegetation	1.9367
Melaleuca	Dense mangrove	1.9387
Dense mangrove	Rainforest	1.9831
Open mangrove	Saltflats	1.9855
Open mangrove	Sand dune vegetation	1.9977
Saltflats	Sand dune vegetation	1.9981
Melaleuca	Open mangrove	1.9992
Melaleuca	Saltflats	1.9998
Open mangrove	Rainforest	1.9999
Saltflats	Rainforest	1.9999
Dense mangrove	Saltflats	2.0000
Dense mangrove	Open mangrove	2.0000

Red highlights very poor separability (<1,0); yellow highlights poor separability (1.0–1.9)

Table 3.2 Jeffries-Matusita separability measure between dominant vegetation types selected for flightline 2 in the *CASI* image

Pair separation for strip 2 (from lowest to highest separability)		
Vegetation type 1	**Vegetation type 2**	**Jeffries-Matusita separability**
Melaleuca	Open mangrove	1.3962
Melaleuca	Dense mangrove	1.7958
Dense mangrove	Open mangrove	1.8449

Yellow highlights poor separability (1.0–1.9)

Table 3.3. Jeffries-Matusita separability measure between dominant vegetation types selected for flightline 3 in the *CASI* image

Pair separation for strip 3 (from lowest to highest separability)		
Vegetation type 1	**Vegetation type 2**	**Jeffries-Matusita separability**
Rainforest	Sand dune vegetation	1.0561
Melaleuca	Rainforest	1.0688
Melaleuca	Sand dune vegetation	1.1937
Dense mangrove	Rainforest	1.9527
Melaleuca	Dense mangrove	1.9609
Dense mangrove	Sand dune vegetation	1.9624
Dense mangrove	Open mangrove	1.9955
Melaleuca	Open mangrove	1.9956
Open mangrove	Sand dune vegetation	1.9961
Open mangrove	Rainforest	1.9973
Open mangrove	Saltflats	1.9983
Saltflats	Sand dune vegetation	1.9998
Saltflats	Rainforest	1.9999
Melaleuca	Saltflats	1.9999
Dense mangrove	Saltflats	2.0000

Yellow highlights poor separability (1.0–1.9)

Table 3.4. Jeffries-Matusita separability measure between dominant vegetation types selected for flightline 4 in the *CASI* image.

Pair separation for strip 4 (from lowest to highest separability)		
Vegetation type 1	**Vegetation type 2**	**Jeffries-Matusita separability**
Melaleuca	Dense mangrove	1.3615
Melaleuca	Sand dune vegetation	1.4307
Rainforest	Sand dune vegetation	1.4864
Dense mangrove	Sand dune vegetation	1.5195
Dense mangrove	Rainforest	1.7793
Melaleuca	Rainforest	1.8456
Open mangrove	Sand dune vegetation	1.8941
Melaleuca	Open mangrove	1.9838
Dense mangrove	Open mangrove	1.9890
Open mangrove	Saltflats	1.9932
Open mangrove	Rainforest	1.9957
Saltflats	Sand dune vegetation	1.9998
Saltflats	Rainforest	1.9999
Melaleuca	Saltflats	1.9999
Dense mangrove	Saltflats	1.9999

Yellow highlights poor separability (1.0–1.9)

Table 3.5. Jeffries-Matusita separability measure between dominant vegetation types selected for flightline 5 in the *CASI* image

Pair separation for strip 5 (from lowest to highest separability)		
Vegetation type 1	**Vegetation type 2**	**Jeffries-Matusita separability**
Melaleuca	Sand dune vegetation	0.9208
Sand dune vegetation	Open mangrove	1.7281
Melaleuca	Open mangrove	1.7931
Dense mangrove	Sand dune vegetation	1.9389
Melaleuca	Dense mangrove	1.9615
Dense mangrove	Open mangrove	1.9919

Red highlights very poor separability (<1,0); yellow highlights poor separability (1.0–1.9)

Texture analysis, using an occurrence texture filter (Anys *et al.* 1994) was tested to see if it improved the separation of mangroves from non-mangroves. Texture information was only briefly assessed since the other remote sensing datasets have a lower spatial resolution than the CASI so would not be of great benefit to the other datasets being assessed. The minimum noise fraction transform (in ENVI) was applied to the 14 CASI bands to reduce the correlation between bands, and an occurrence texture filter was applied to the first MNF band. This 11x11 pixel filter (in ENVI) calculated the occurrence of data range, mean and variance values. These three bands were included with the 14 CASI bands and the ROI separability calculated again for the same flightlines and ROIs (Tables 3.6 to 3.10).

The separability between vegetation classes greatly improves when the texture bands were added to the original CASI data (Tables 3.6 to 3.10). The lowest separability measure increased from 0.6 to 1.6 with most confusion between melaleuca and sand dune vegetation. These two vegetation types had similar canopy texture in the CASI imagery, which explains why inclusion of the texture bands does not completely distinguish them.

Table 3.6. Jeffries-Matusita separability measure between dominant vegetation types selected for flightline 1 in the *CASI* image using the *CASI* spectra and texture bands

Pair separation for strip 1 (from lowest to highest separability)		
Vegetation type 1	**Vegetation type 2**	**Jeffries-Matusita separability**
Melaleuca	Sand dune vegetation	1.6286
Melaleuca	Rainforest	1.9824
Rainforest	Sand dune vegetation	1.9949
Melaleuca	Dense mangrove	1.9998
Dense mangrove	Sand dune vegetation	1.9999
Open mangrove	Sand dune vegetation	2.0000
Saltflats	Sand dune vegetation	2.0000
Dense mangrove	Rainforest	2.0000
Saltflats	Rainforest	2.0000
Open mangrove	Saltflats	2.0000
Melaleuca	Open mangrove	2.0000
Dense mangrove	Rainforest	2.0000
Dense mangrove	Saltflats	2.0000
Dense mangrove	Saltflats	2.0000
Dense mangrove	Open mangrove	2.0000

Yellow highlights poor separability (1.0–1.9)

Table 3.7. Jeffries-Matusita separability measure between dominant vegetation types selected for flightline 2 in the *CASI* image using the *CASI* spectra and texture bands

Pair separation for strip 2 (from lowest to highest separability)		
Vegetation type 1	**Vegetation type 2**	**Jeffries-Matusita separability**
Dense mangrove	Open mangrove	1.9677
Melaleuca	Open mangrove	1.9677
Melaleuca	Dense mangrove	1.9980

Table 3.8. Jeffries-Matusita separability measure between dominant vegetation types selected for flightline 3 in the *CASI* image using the *CASI* spectra and texture bands

Pair separation for strip 3 (from lowest to highest separability)		
Vegetation type 1	**Vegetation type 2**	**Jeffries-Matusita separability**
Rainforest	Sand dune vegetation	1.7471
Melaleuca	Sand dune vegetation	1.9532
Melaleuca	Rainforest	1.9633
Dense mangrove	Sand dune vegetation	1.9993
Melaleuca	Dense mangrove	1.9998
Dense mangrove	Rainforest	1.9999
Saltflats	Sand dune vegetation	1.9999
Open mangrove	Saltflats	2.0000
Dense mangrove	Saltflats	2.0000
Saltflats	Rainforest	2.0000
Melaleuca	Saltflats	2.0000
Open mangrove	Sand dune vegetation	2.0000
Dense mangrove	Open mangrove	2.0000
Open mangrove	Rainforest	2.0000
Melaleuca	Open mangrove	2.0000

Yellow highlights poor separability (1.0–1.9)

Table 3.9. Jeffries-Matusita separability measure between dominant vegetation types selected for flightline 4 in the *CASI* image using the *CASI* spectra and texture bands

Pair separation for strip 4 (from lowest to highest separability)		
Vegetation type 1	**Vegetation type 2**	**Jeffries-Matusita separability**
Dense mangrove	Sand dune vegetation	1.8594
Melaleuca	Dense mangrove	1.9226
Rainforest	Sand dune vegetation	1.9727
Melaleuca	Sand dune vegetation	1.9747
Dense mangrove	Rainforest	1.9975
Melaleuca	Rainforest	1.9997
Melaleuca	Saltflats	1.9999
Open mangrove	Rainforest	2.0000
Open mangrove	Sand dune vegetation	2.0000
Melaleuca	Open mangrove	2.0000
Saltflats	Sand dune vegetation	2.0000
Dense mangrove	Saltflats	2.0000
Saltflats	Rainforest	2.0000
Open mangrove	Saltflats	2.0000
Dense mangrove	Open mangrove	2.0000

Yellow highlights poor separability (1.0–1.9)

Table 3.10. Jeffries-Matusita separability measure between dominant vegetation types selected for flightline 5in the *CASI* image using the *CASI* spectra and texture bands

Pair separation for strip 5 (from lowest to highest separability)		
Vegetation type 1	**Vegetation type 2**	**Jeffries-Matusita separability**
Melaleuca	Sand dune vegetation	1.6643
Melaleuca	Open mangrove	1.9851
Dense mangrove	Sand dune vegetation	1.9915
Sand dune vegetation	Open mangrove	1.9958
Melaleuca	Dense mangrove	1.9972
Dense mangrove	Open mangrove	1.9992

Yellow highlights poor separability (1.0–1.9)

Hyperion

The Hyperion data used for this analysis was acquired in March 2001. The space-borne Hyperion sensor consists of 196 bands at 30 m pixel size ranging from 437 nm up to 2400 nm. Its spectral range is much greater than the CASI, since it includes the short wave infrared region (SWIR) from 900 nm upwards. The infrared wavelengths have a reduced reflectance from water, so they are useful for distinguishing wet from dry land. The Hyperion data was cleaned and atmospherically corrected using a similar process to that described in Datt and Jupp (2002). This involved applying a destreaking algorithm to reduce the vertical striping inherent in many Hyperion bands, followed by correcting for the spatial offset between the visible/near-infrared detector and the shortwave-infrared detector. The atmospheric correction program ACORN (Atmospheric CORrection Now) was then used to atmospherically correct the data.

The same vegetation areas used in the CASI image were selected to create ROIs in the Hyperion image, with the exception of those that fell outside the Hyperion coverage since its swath did not extend as far east as the CASI data. Many of the vegetation areas were of small extent resulting in ROIs containing only 3–4 pixels. Due to the high dimensionality of the data, and many of the bands being correlated, a principal component analysis (PCA) was applied to the full image. This statistical process is designed to capture the variability in the data while reducing the number of bands. The best six bands were selected (based on noise-free appearance) and used for computing the Jeffries-Matusita separability for each vegetation ROI. Unlike the CASI, there were no flightline variations in the Hyperion imagery so the ROIs were combined such that one ROI represented a single vegetation type. These results are shown in Table 3.11.

Table 3.11. Jeffries-Matusita separability measure between dominant vegetation types selected for the Hyperion PCA image

Pair separation for Hyperion (from lowest to highest separability)		
Vegetation type 1	**Vegetation type 2**	**Jeffries-Matusita separability**
Rainforest	Sand dune vegetation	1.4598
Melaleuca	Sand dune vegetation	1.9618
Melaleuca	Rainforest	1.9820
Melaleuca	Dense mangrove	1.9834
Open mangrove	Saltflats	1.9959
Melaleuca	Open mangrove	1.9995
Dense mangrove	Rainforest	1.9999
Dense mangrove	Sand dune vegetation	2.0000
Open mangrove	Rainforest	2.0000
Dense mangrove	Open mangrove	2.0000
Dense mangrove	Saltflats	2.0000
Saltflats	Sand dune vegetation	2.0000
Melaleuca	Saltflats	2.0000
Rainforest	Saltflats	2.0000
Open mangrove	Sand dune vegetation	2.0000

Yellow highlights poor separability (1.0–1.9)

When using the best six Hyperion PCA bands, the vegetation classes appeared to be separable apart from some confusion between rainforest and sand dune vegetation (Table 3.11). Figure 3.4 is an image of the first three PCA bands. The dense mangrove shows up as deep red/brown, agriculture/pasture is bright green, rainforest/sand dune vegetation/melaleuca is bright blue, open mangrove is a red-cyan, while saltflats are bright cyan.

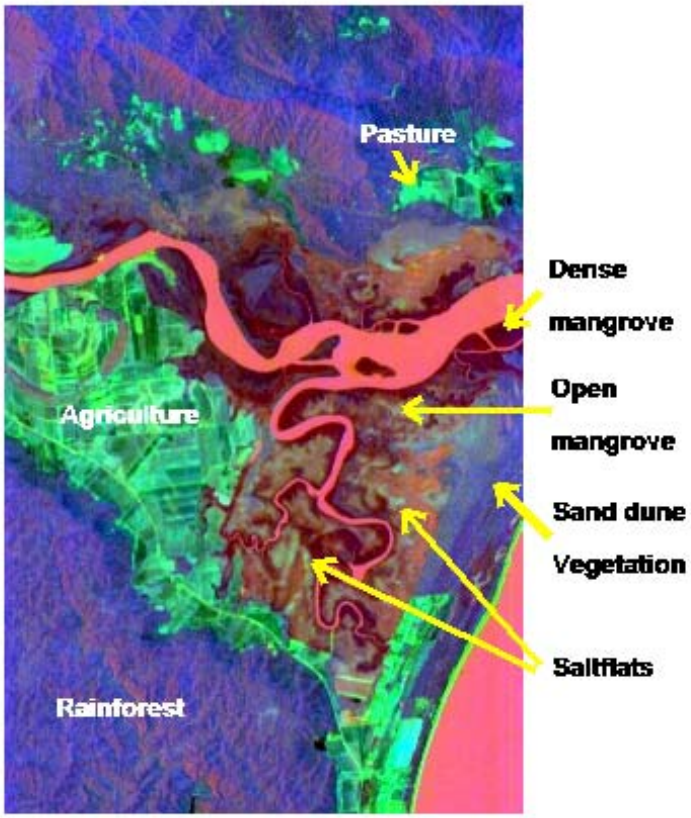

Figure 3.4. The first three principal component analysis bands for the Hyperion image

Note that melaleuca sites are not indicated here because of their small extent. The dense mangrove shows as deep red/brown, agriculture/pasture as bright green, rainforest/sand dune vegetation/melaleuca as bright blue, open mangrove as red-cyan, and saltflats as bright cyan.

A more detailed spectral analysis was also performed to exploit the spectral information that Hyperion offers. Each Hyperion band was visually examined, and those with a high level of noise were removed, leaving 135 bands. Figure 3.5 shows the reflectance spectra for the dominant vegetation types from this cleaned dataset. Despite considerable overlap between the different classes for many parts of the spectrum, some sections showed potential for discrimination. In particular, saltflats do not have the chlorophyll well around the wavelength of 680 nm that the vegetated covers do. They also have a higher reflectance around 2000–2500 nm. Open mangrove and saltflats have much lower near infrared values around 800–1100 nm due to less vegetation cover. The rainforest, melaleuca and sand dune vegetation have similar spectra; however, the melaleuca does appear separable around the 800–900 nm wavelength region and possibly the 1200–1300 nm region. The dense and open mangrove spectra may be separable from other vegetation types around the 1500–1700 nm region due to the moist soil background.

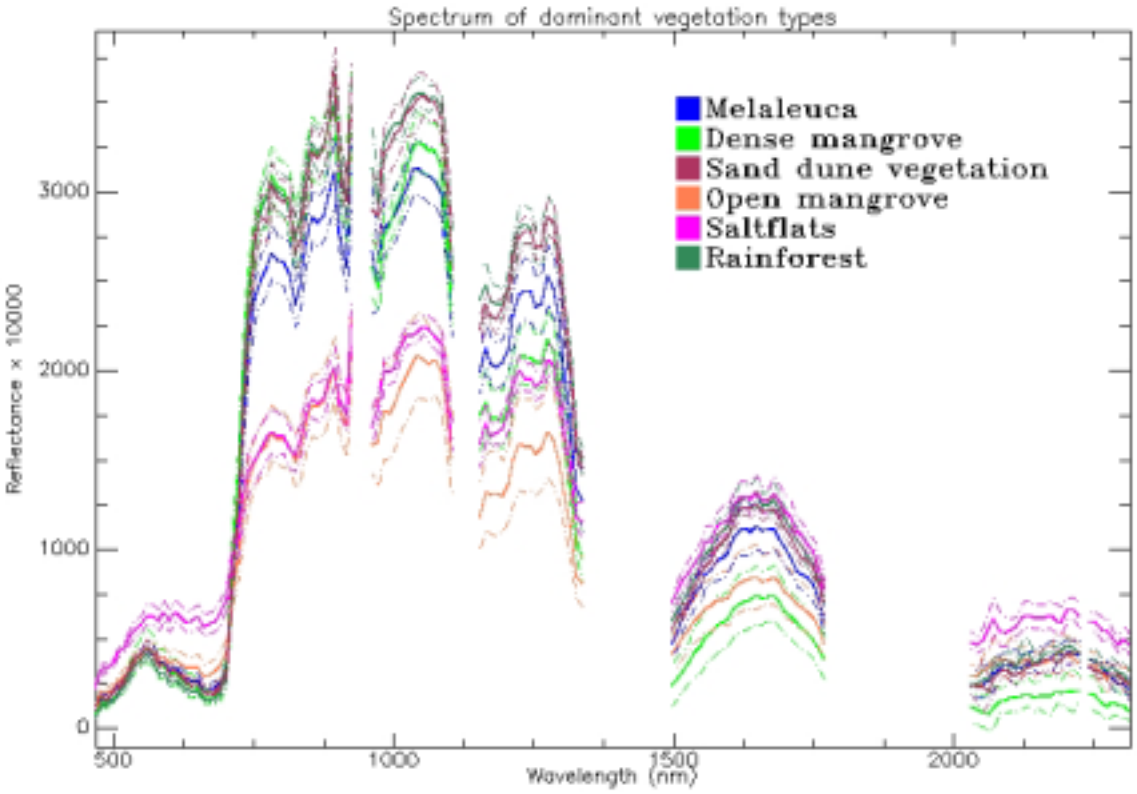

Figure 3.5. Hyperion spectra of dominant vegetation types for the Daintree River mangrove system. The thick line is the mean spectrum, while the dotted lines indicate their standard deviations

The cleaned Hyperion image, with 135 bands, was fed into a spectral angle mapper (SAM) classifier using the single ROIs for each land cover to train the data (Figure 3.6). The SAM classifier was used since it utilises the full spectral range. An additional ROI was also added to include the agriculture/pasture land cover. A digital elevation model (DEM), generated from radar interferometry at an original pixel size of 10 metres was used to eliminate heights above 30 m so only the floodplains and lowland rainforest remained. The SAM classification is shown below. Inspection of this image showed confusion between sand dune vegetation, melaleuca and rainforest. Further validation of this classification is discussed in a following section.

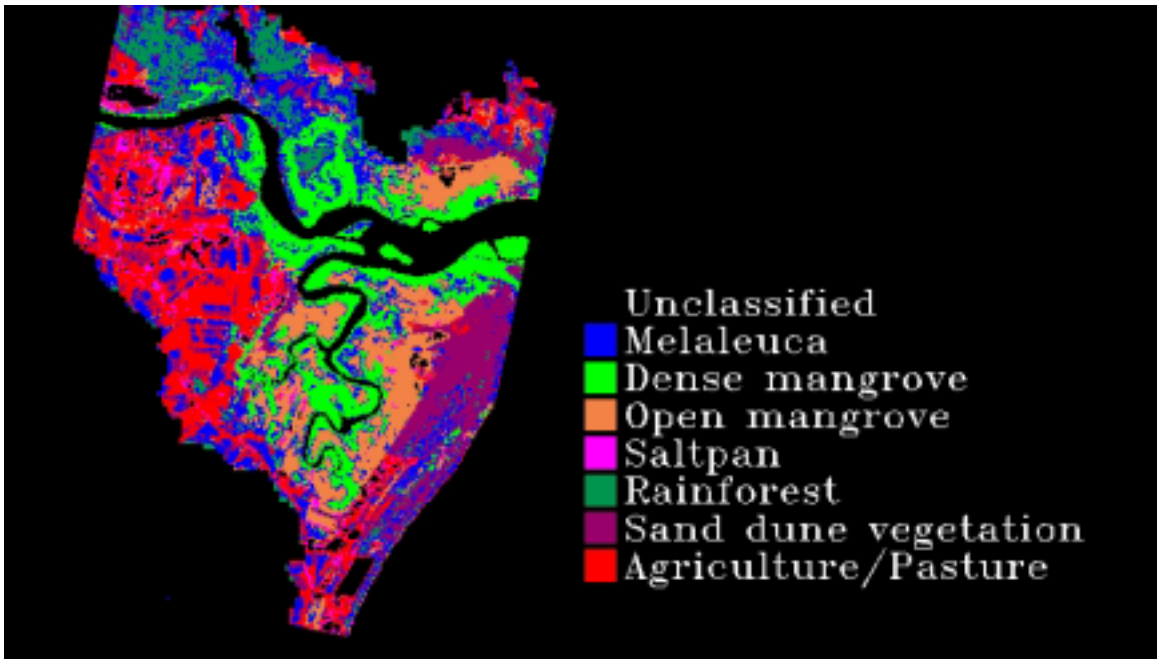

Figure 3.6. Spectral angle mapper classification of dominant vegetation types from the Hyperion data for the Daintree mangrove system

Landsat 7 Enhanced Thematic Mapper

A Landsat ETM7+ (Enhanced Thematic Mapper) image was acquired on September 1999, consisting of six broad bands (0.45–0.52 µm, 0.52–0.60 µm, 0.63–0.69 µm, 0.76–0.90 µm, 1.55–1.75 µm and 2.08–2.35 µm) with a pixel size of 25 m. The data were atmospherically corrected using ACORN. ROIs were selected for the dominant vegetation classes over the same regions as those used in the Hyperion data. Since there were no flightline variations, the ROIs for each vegetation class were combined and the Jeffries-Matusita separability was computed for these dominant vegetation classes (Table 3.12). For the Landsat bands, the melaleuca and sand dune vegetation appeared the least separable, while the others had separability values above 1.9.

The spectral profiles are shown in Figure 3.7. Visual inspection of these spectra confirms the confusion between melaleuca (shown in blue) and sand dune vegetation (maroon). The Hyperion showed better separability between these two classes in the NIR region (700–800 nm), which was not apparent in the Landsat spectral profiles. Like the Hyperion, the Landsat bands showed that the saltflats class can be separated from the vegetation classes since it has no chlorophyll well (i.e. the high absorption around 680 nm).

Table 3.12. Jeffries-Matusita separability measure between dominant vegetation types selected for Landsat ETM

Pair separation for Landsat ETM7+ (from lowest to highest separability)		
Vegetation type 1	**Vegetation type 2**	**Jeffries-Matusita separability**
Melaleuca	Sand dune vegetation	1.6153
Open mangrove	Saltflats	1.9025
Rainforest	Sand dune vegetation	1.9115
Melaleuca	Rainforest	1.9697
Melaleuca	Dense mangrove	1.9841
Dense mangrove	Rainforest	1.9999
Dense mangrove	Sand dune vegetation	1.9999
Dense mangrove	Open mangrove	2.0000
Open mangrove	Sand dune vegetation	2.0000
Melaleuca	Open mangrove	2.0000
Dense mangrove	Saltflats	2.0000
Rainforest	Saltflats	2.0000
Saltflats	Sand dune vegetation	2.0000
Melaleuca	Saltflats	2.0000
Open mangrove	Rainforest	2.0000

Yellow highlights poor separability (1.0–1.9)

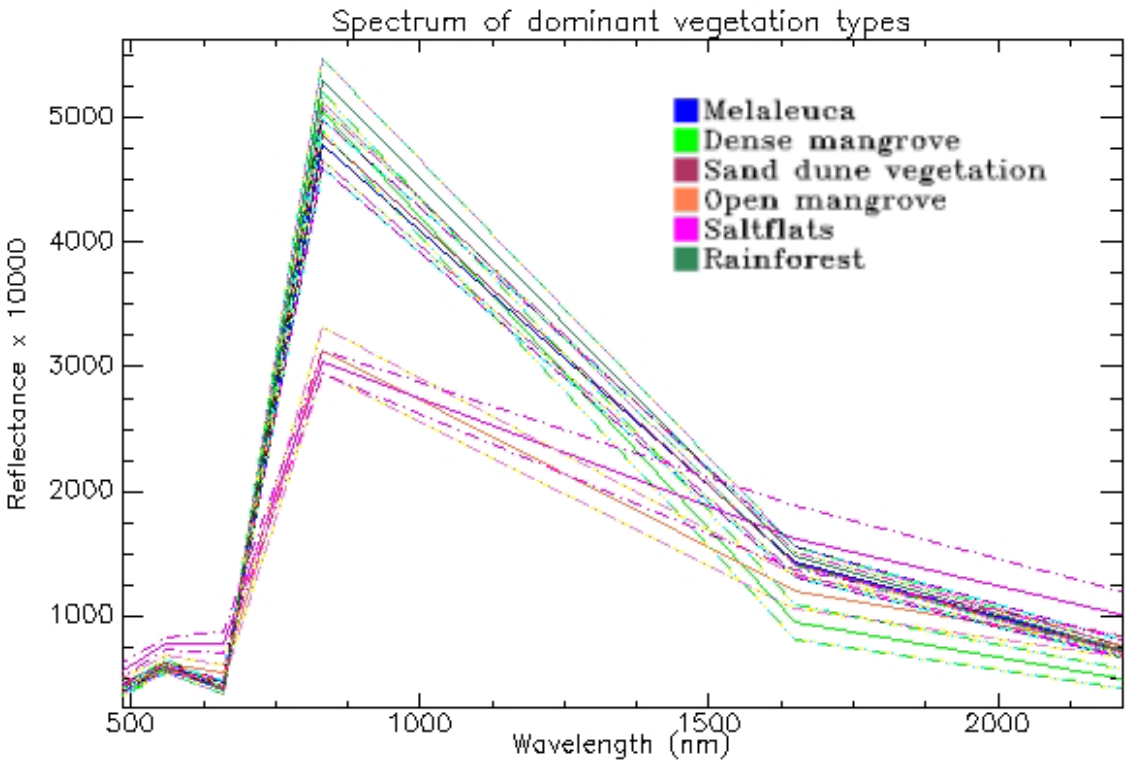

Figure 3.7. Landsat ETM7+ spectra of dominant vegetation types for the Daintree River mangrove system. The thick line is the mean spectrum, while the dotted lines indicate their standard deviations

A maximum likelihood classification (MLC) was applied to the Landsat image using the combined ROIs for each class. The ROIs for each vegetation type needed to be combined due to the size restrictions for training an MLC classification (where each training ROI must contain at least the number of bands+1 pixels). As the classification showed (Figure 3.8) there was considerable confusion between the sand dune vegetation class and melaleuca. For comparison, the SAM classification technique was also applied using the single ROIs for each class which were then combined after classification (Figure 3.9). Single ROIs are used in preference to the combined ROIs to help capture any spectral variability within the classes.

Both classification methods showed considerable confusion between melaleuca, rainforest and sand dune vegetation. The SAM classification had less confusion between melaleuca and mangrove.

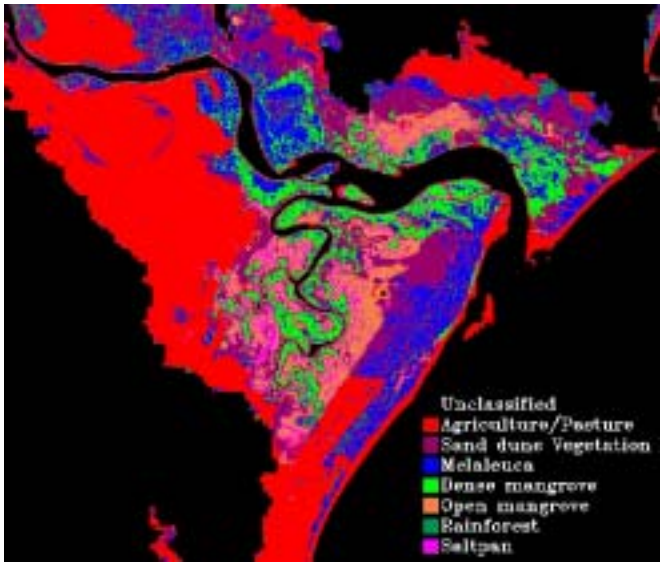

Figure 3.8. Maximum likelihood classification of dominant vegetation types from the Landsat data for the Daintree mangrove system

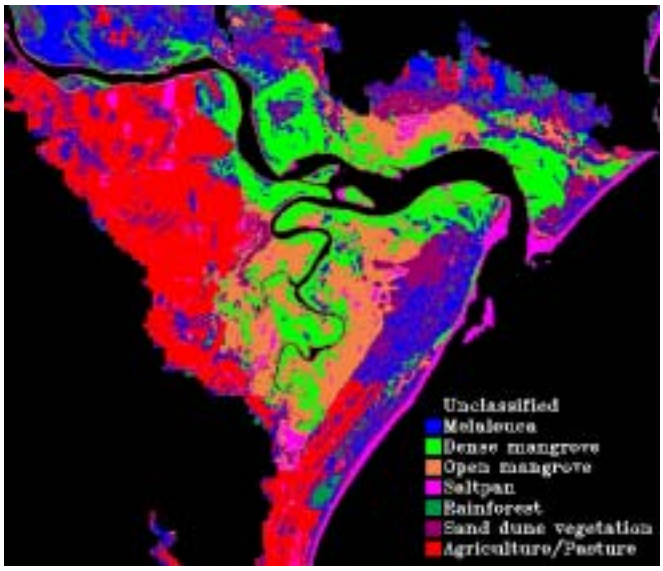

Figure 3.9. Spectral angle mapper classification of dominant vegetation types from the Landsat data for the Daintree mangrove system

AIRSAR

Airborne synthetic aperture radar (AIRSAR) data was acquired in November 1996 in TOPSAR mode, where L- (~23 cm wavelength) and P-bands (~64 cm wavelength) were in polarimetric mode and C-band (~6 cm wavelength) was in interferometric mode. Polarimetric mode means there are three bands, HH, VV and HV, where H and V stand for a horizontally and vertically polarised wave respectively, and the first term refers to the transmitted polarisation while the second term refers to the received polarisation. Interferomeric mode results in a VV band as well as a digital surface model. The pixel size was 10 metres. The data was also smoothed using an adaptive filter (5x5 gamma filter) available in ENVI to help reduce the speckle that is common in radar images.

ROIs were selected to cover the same regions as used for the Hyperion and Landsat, and the Jeffries-Matusita separability calculated for each dominant vegetation type (Table 3.13). Similarly to the Landsat and Hyperion datasets, there was confusion between the rainforest, sand dune vegetation and melaleuca vegetation classes. The AIRSAR bands also showed poor separation between the open mangrove and saltflats classes. With respect to radar backscatter, this would be dependent on how dense the vegetation cover was in the open mangrove areas, and how open the saline regions were, since any open vegetation will have a strong double bounce effect in the radar data.

Table 3.13. Jeffries-Matusita separability measure between dominant vegetation types selected for AIRSAR

Pair separation for AIRSAR (from lowest to highest separability)		
Vegetation type 1	**Vegetation type 2**	**Jeffries-Matusita separability**
Melaleuca	Rainforest	1.0529
Melaleuca	Sand dune vegetation	1.2214
Open mangrove	Saltflats	1.3148
Rainforest	Sand dune vegetation	1.4682
Dense mangrove	Rainforest	1.9463
Melaleuca	Dense mangrove	1.9790
Open mangrove	Rainforest	1.9914
Melaleuca	Open mangrove	1.9955
Dense mangrove	Sand dune vegetation	1.9972
Open mangrove	Sand dune vegetation	1.9981
Melaleuca	Saltflats	1.9985
Rainforest	Saltflats	1.9995
Dense mangrove	Open mangrove	1.9997
Saltflats	Sand dune vegetation	1.9999
Dense mangrove	Saltflats	2.0000

Yellow highlights poor separability (1.0–1.9)

Figure 3.10 shows the profiles of the different vegetation classes and uses the same colour scheme as the Hyperion and Landsat graphs. Dense mangrove (in bright green) had a lower backscatter than the other vegetation types for L- and P-bands, whereas the melaleuca had similar backscatter characteristics to rainforest.

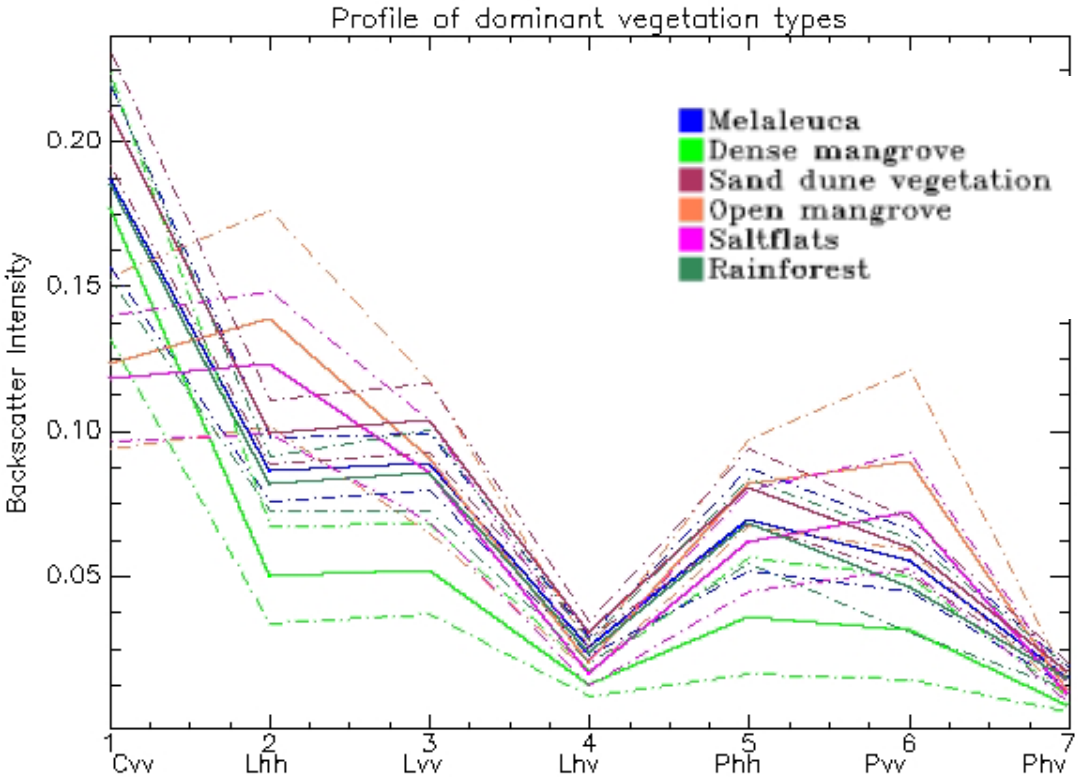

Figure 3.10. AIRSAR band profiles of dominant vegetation types for the Daintree River mangrove system. The thick line is the mean radar backscatter, while the dotted lines indicate their standard deviations

A maximum likelihood classification was performed on the AIRSAR bands using the single ROIs for the dominant vegetation classes. The agriculture/pasture land cover was not classified here since the radar had a high variability in backscatter related to the different range in biomass for the surrounding sugarcane. The classification (Figure 3.11) showed how the radar performed well on the sand dune vegetation, although there was considerable confusion between the mangrove and rainforest classes. There also appeared to be an overclassification of melaleuca as well as confusion between the melaleuca and the mangrove classes. Like the CASI, texture bands are often useful when analysing radar data; however, since the pixel size of the radar is relatively large compared to the vegetation patterns, it was not useful here. Segmentation algorithms such those available in the eCognition™ software may prove useful for this purpose.

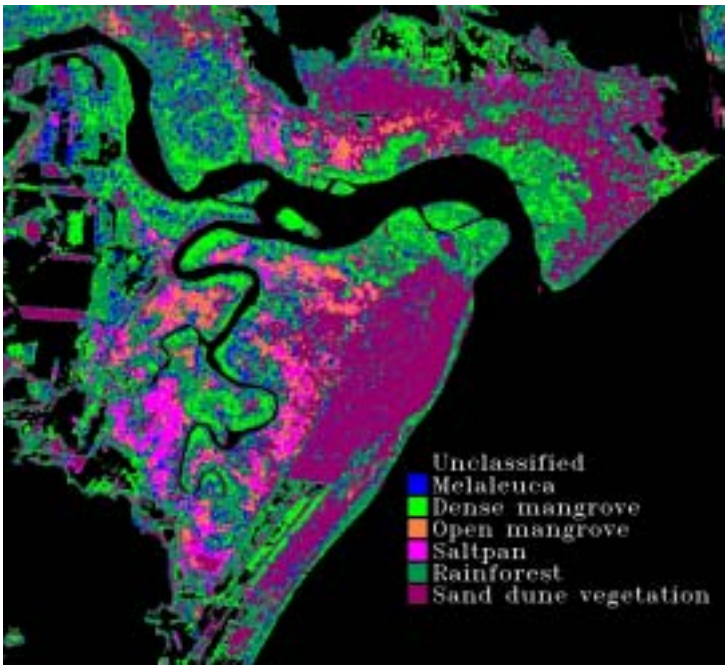

Figure 3.11. Maximum likelihood classification of dominant vegetation types from the AIRSAR data for the Daintree mangrove system

Detailed analysis and comparison with aerial photography

Hyperion

The Hyperion data was chosen for further investigation because it showed the greatest discrimination capacity, particularly for separating melaleuca from mangroves. As before, the vegetation map of Le Cussan (1991) was used for interpreting the imagery and collecting spectra for developing the classifications. To allow for more control and an understanding of the environmental and physiological factors determining the separation of classes, spectra were examined in detail to determine where in the spectral range the best separation occurred, and a classification was formed on a hierarchical basis using threshold values. The analysis was based on visual inspection of the spectra accompanied by knowledge of where the separation was likely, as well as statistical analysis. Due to the higher noise levels in the longer wavelengths, above 2000 nm, these regions were avoided where possible. PCA bands from the previous Hyperion section were not used here since one of the goals was to develop a method of classification that was not site dependent.

Firstly, water was masked out due to its very low reflectance in the infrared region of the spectrum. The agriculture and pasture regions tended to have a high reflectance in the shortwave infrared region, particularly above 1500 nm, which was relatively independent of the level of vegetation cover in the cropping areas.

As before, the DEM was used to remove the upland rainforest to leave only the floodplain and lowland vegetation.

The rainforest, sand dune vegetation and melaleuca classes were combined in order to create a more robust separation from mangroves. An ANOVA (ANalysis Of VAriance) analysis was then performed to determine what spectral region(s) provided a statistically significant separation. This was done using ROIs from the original rainforest/sand dune vegetation/melaleuca and open/dense mangrove classes as well as additional ROIs collected in the melaleuca and mangrove regions where the Hyperion classification in Figure 3.6 showed there was confusion. The ANOVA results are shown in the Figure 3.12. The red/orange tones are spectra from dense and open mangrove and blue tones are from rainforest, sand dune vegetation and melaleuca. The dark green line shows where the separation between mangroves and rainforest/sand dune vegetation/melaleuca was statistically significant at the 99% confidence level.

To investigate where the best separation occurred, the minimum value from the rainforest/sand dune vegetation/melaleuca class was subtracted from the maximum value from the mangrove class and is shown in Figure 3.12 by the light green line. This was indicative of where the least overlap existed, and the 1660 nm band was chosen on this basis. This region of the spectrum distinguishes underlying moisture reasonably well. While separation of melaleuca from rainforest and sand dune vegetation was desirable, and Figure 3.5 indicated it may have been possible, particularly around 800 nm, a simple threshold value could not be found when these bands were inspected.

The threshold used to separate mangroves from rainforest/sand dune vegetation/melaleuca also included saltflats due to the high reflectance of the saltflat regions in the infrared section of the spectrum. The 1053 nm wavelength was then used to isolate saltflats since that point was where the greatest separation occurred (Figure 3.13). For the mangrove vegetation, open and dense mangrove were separated utilising the lower near-infrared response of the open mangrove due to its sparse canopy cover. The 793 nm band was chosen as this was in the region of greatest separability (Figure 3.5).

These threshold results were then combined into a decision tree for classification. The decision tree and classification are shown in Figures 3.14 and 3.15 respectively.

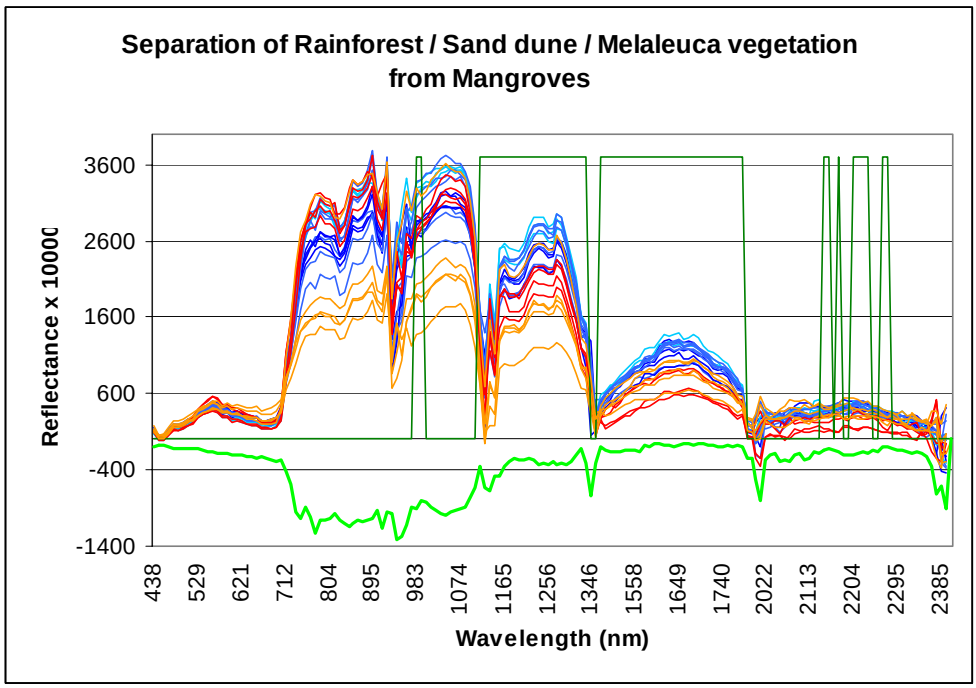

Figure 3.12. Spectrum of rainforest, sand dune vegetation, melaleuca (blue tones) and dense, open mangrove (orange tones) from the Hyperion data

The dark green line shows where the rainforest/sand dune vegetation/melaleuca vegetation is significantly different to the mangroves. The light green line shows the minimum value from the rainforest/sand dune vegetation/melaleuca class subtracted from the maximum value from the mangrove class.

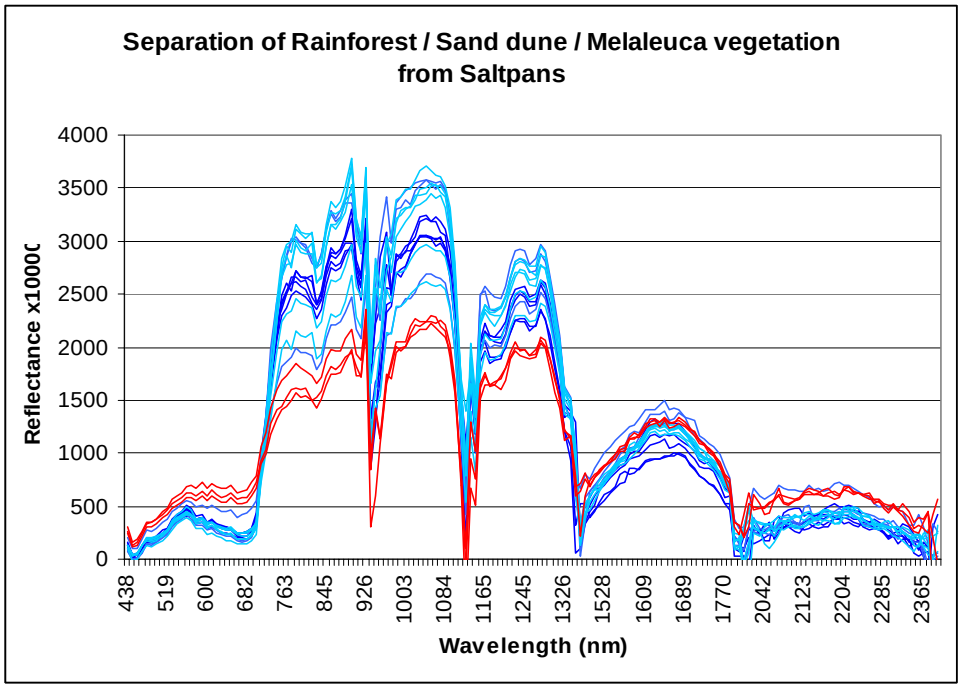

Figure 3.13. Spectrum of rainforest, sand dune vegetation, melaleuca (blue tones) and saltflat (orange tones) from the Hyperion data

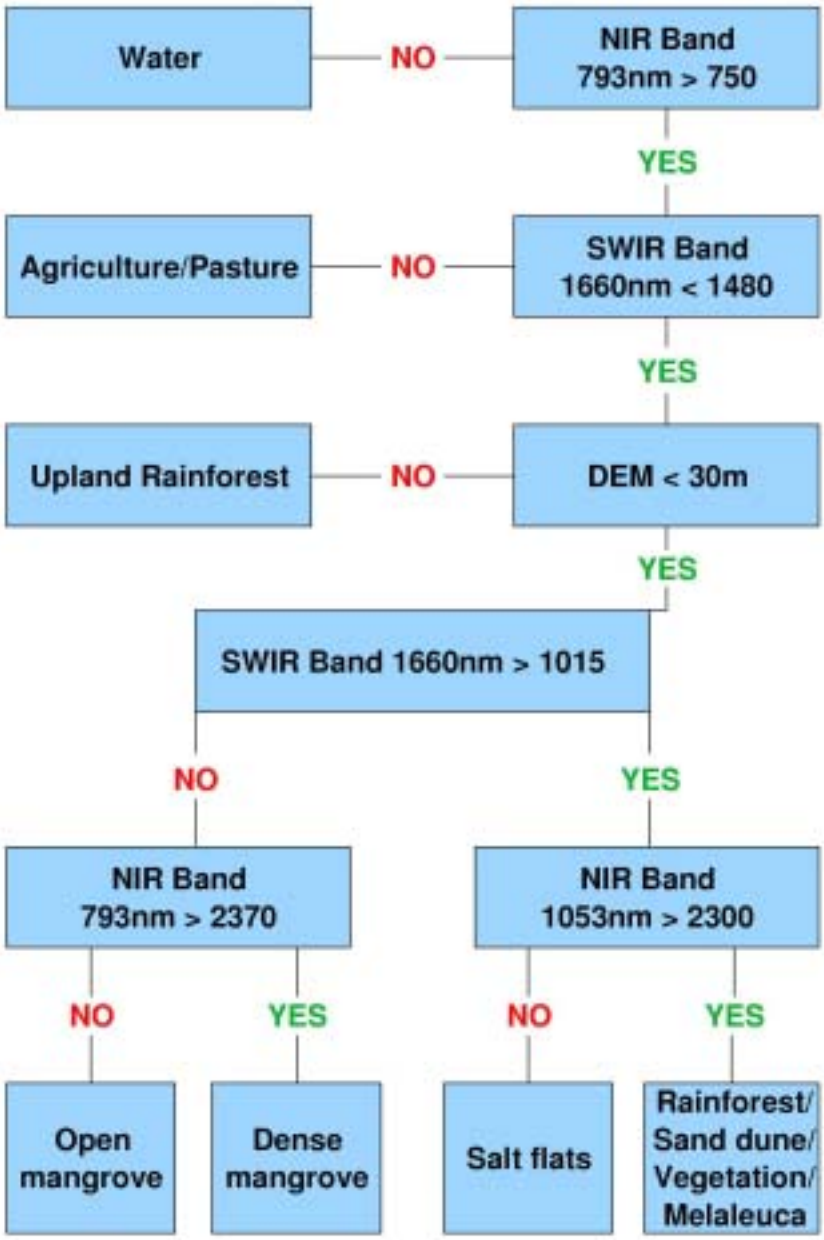

Figure 3.14. Decision tree used to classify the Hyperion data and create the map shown in Figure 3.15. The threshold bands used are shown in nanometres and the threshold value is shown in reflectance x 10000

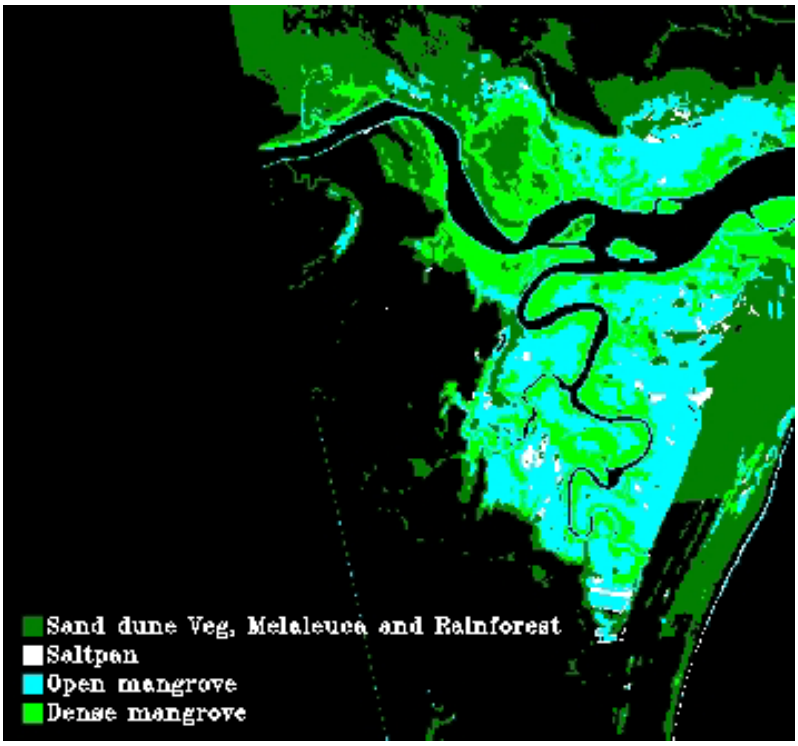

Figure 3.15. Decision tree classification of dominant vegetation types (using threshold values shown in Figure 3.14) from the Hyperion data for the Daintree mangrove system

To assess how well the decision tree classification performed, validation regions were selected again using the map by Le Cussan (1991). Due to the small areas of some vegetation types, particularly Melaleuca, only 342 pixels were collected for validation. The confusion matrix is shown in Table 3.14. Based on Le Cussan's map, the overall accuracy of the Hyperion classification was 92.1%, with a Kappa coefficient of 0.85. The greatest confusion appeared to be between the saltflats and rainforest/sand dune vegetation/melaleuca vegetation. Inspection of the CASI image for this region showed there was some scattered vegetation amongst the saline regions, so this confusion may be due to the relatively large pixel size of the Hyperion data.

To investigate how well the melaleuca sites were distinguished from mangrove sites, the validation ROIs over the melaleuca vegetation were examined on a site-by-site, rather than individual pixel, basis. Six melaleuca sites were selected and of these, five were successfully classified as rainforest/sand dune vegetation/ melaleuca vegetation. The other site was confused with dense mangrove. This classification technique performed better than the SAM classification shown in Figure 3.6. Using the same validation ROIs, the SAM classification had an accuracy of 87.7% with a Kappa coefficient of 0.77. Its confusion matrix (Table 3.15) revealed there was a lot more confusion between the rainforest/ sand dune vegetation/melaleuca and open mangrove classes.

Table 3.14. Confusion matrix from the validation ROIs for the decision tree classification of the Hyperion data into dominant vegetation types

	Ground truth				
Class	**RF/ SD/ Mel**	**Saltflats**	**Open mangrove**	**Dense mangrove**	**Total**
Unclassified	1	0	0	0	1
RF/ SD/ Mel	206	12	0	4	222
Saltflats	0	11	0	0	11
Open mangrove	1	0	42	0	43
Dense mangrove	5	0	4	56	64
Total	213	23	46	60	342

Table 3.15. Confusion matrix from the validation ROIs for the spectral angle mapper classification (Figure 3.6) of the Hyperion data into dominant vegetation types

	Ground truth				
Class	**RF/ SD/ Mel**	**Saltflats**	**Open mangrove**	**Dense mangrove**	**Total**
Unclassified	1	0	0	0	2
RF/ SD/ Mel	201	0	16	2	219
Saltflats	3	14	0	0	17
Open mangrove	7	9	27	0	43
Dense mangrove	1	0	3	58	95
Total	213	23	46	60	342

The decision tree classification, which appeared to perform best, was used to classify the Hyperion data for the Noah Creek and Cooper Creek near-pristine estuaries (Figure 3.16). Although this classification cannot be validated, vegetation patterns appear realistic based on past field visits to these sites.

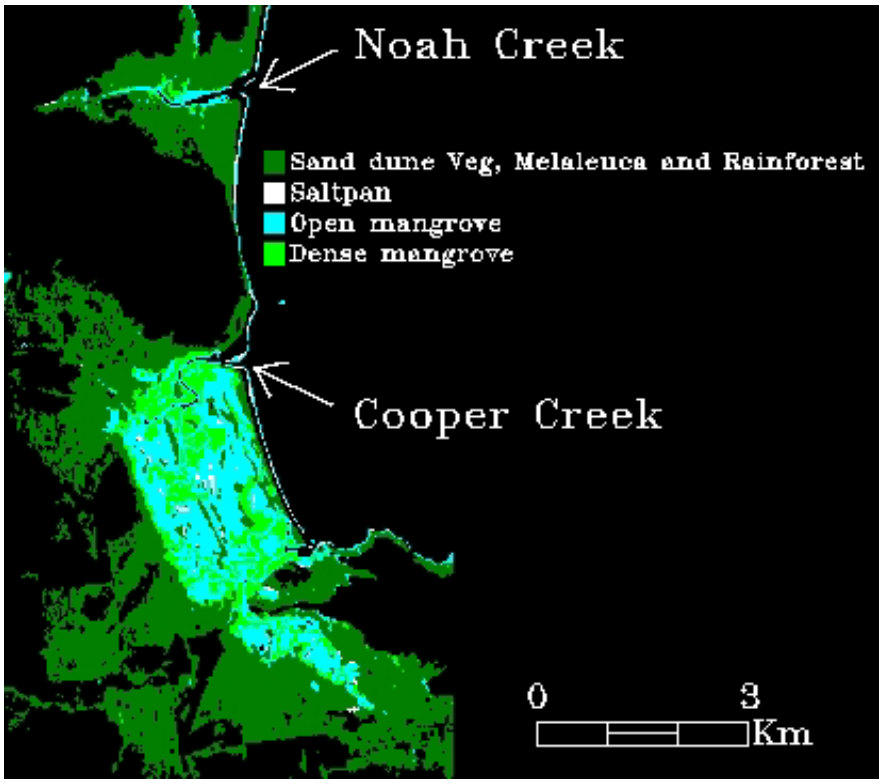

Figure 3.16. Decision tree classification of dominant vegetation types (using threshold values shown in Figure 3.14) from the Hyperion data for the Noah and Cooper Creeks

Landsat ETM7+

Landsat data is more readily available and covers a greater extent than Hyperion (which has a swath width of only 7 km), making Landsat more suitable for continental scale mapping. For this reason a similar decision tree to that of Hyperion was developed for Landsat bands. It is important to note however that the narrower bandwidths, larger brightness range and greater selection of bands from Hyperion allow for greater separability between vegetation types than is possible with Landsat.

The same method as used for Hyperion was used to develop a classification tree for the Landsat bands, with the exception that there was no band around the 1053 nm wavelength so the 830 nm band was used instead. The decision tree is shown in Figure 3.17. Note that even though the images were atmospherically corrected, there was a difference in the reflectance magnitude between the Landsat and Hyperion images. Reasons for this could not be resolved; however, the relative reflectances between the different vegetation types are similar within the images.

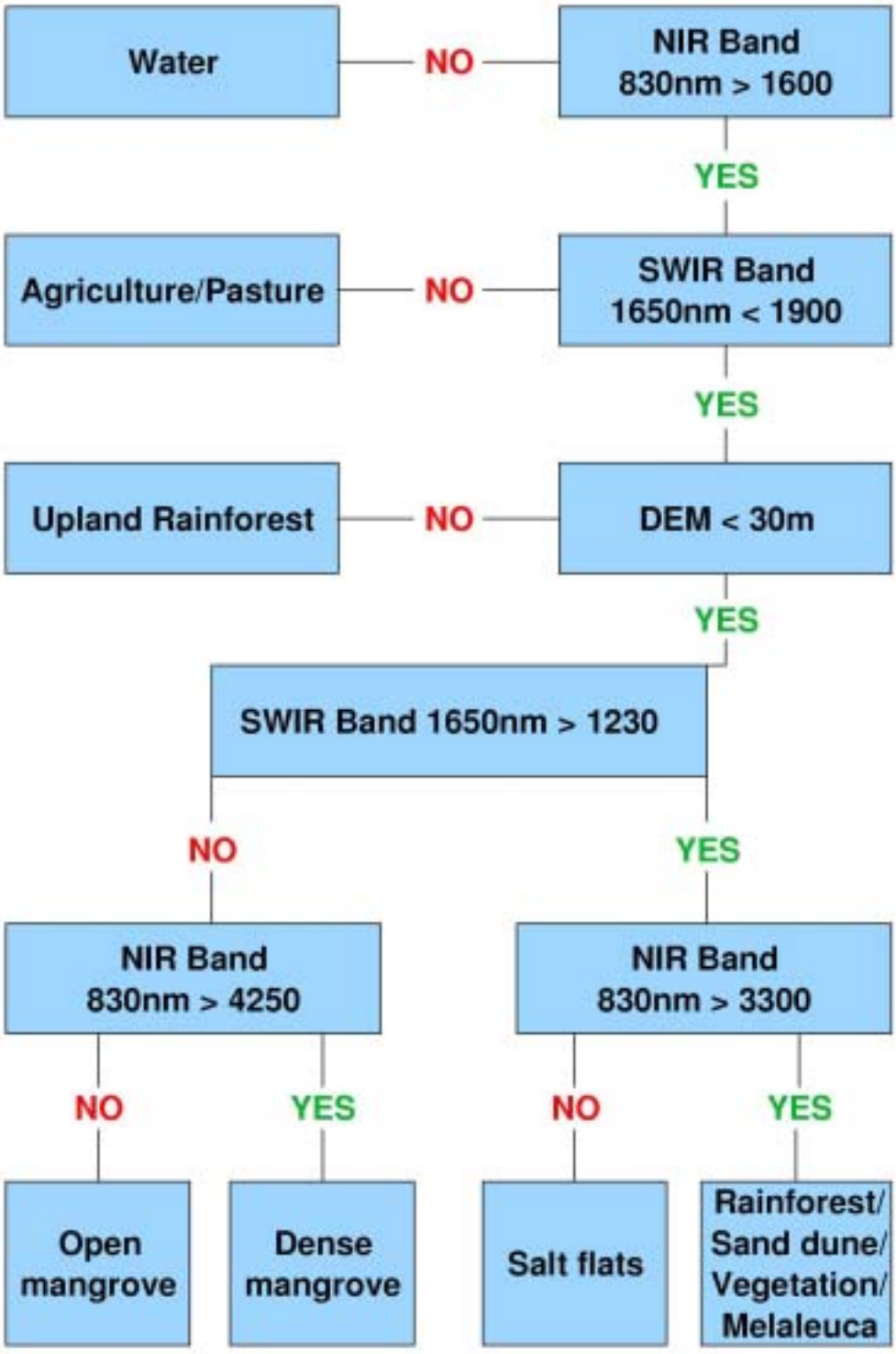

Figure 3.17. Decision tree used to classify the Landsat data and create the map shown in Figure 3.18. The threshold bands used are shown in nanometres and the threshold value is shown in reflectance x 10000

Using the same validation sites from Le Cussan's map, the Landsat classification (Figure 3.18) was very similar to the Hyperion classification with an accuracy of 93.2% (and Kappa coefficient of 0.87), compared to 92.1% from Hyperion. However there were some areas where the classification differed. There were four areas where this discrepancy was most noticeable, so ROIs (consisting of nine pixels) were selected for these sites and an accuracy assessment made (Table 3.16). The main confusion appeared to be open mangrove being mistakenly classified as saltflats in the Landsat data, which was correctly classified in the Hyperion. The other area was a dense mangrove site which was classified as sand dune vegetation/rainforest/melaleuca in the Hyperion data, but six of the nine pixels in the Landsat classification were correctly classified.

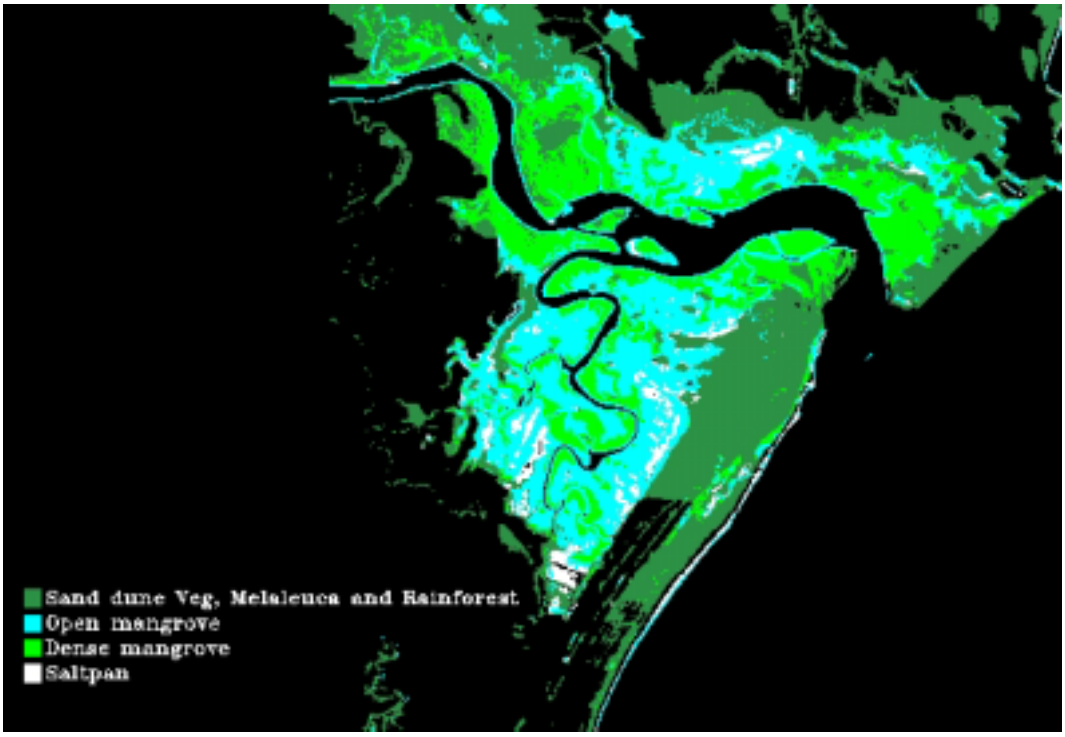

Figure 3.18. Decision tree classification of dominant vegetation types (using threshold values shown in Figure 3.17) from the Landsat data for the Daintree mangrove system

Table 3.16. Comparison of Hyperion and Landsat classification accuracy in regions of discrepancy

Site and vegetation type	Hyperion	Landsat
1 – Open mangrove	Open mangrove	Saltflats
2 – Open mangrove	Open mangrove	Saltflats
3 – Open mangrove	Open mangrove	Saltflats
4 – Dense mangrove	RF/SD/Mel	66% dense mangrove, 33% RF/SD/Mel

Columns 1, 2 and 3 represent vegetation cover for the site, classification of site by Hyperion decision tree, and classification of site by Landsat decision tree, respectively. Each site represents nine pixels.

Overall, it appeared the Hyperion data was performing better than the Landsat; however, this was to be expected due to the greater choice of bands, narrower bandwidths and larger brightness range of the Hyperion data (Hyperion is in integer format rather than byte format). Despite this, the wider availability of Landsat data warranted trialling a classification of the Noah Creek and Cooper Creek Landsat datasets (Figure 3.19).

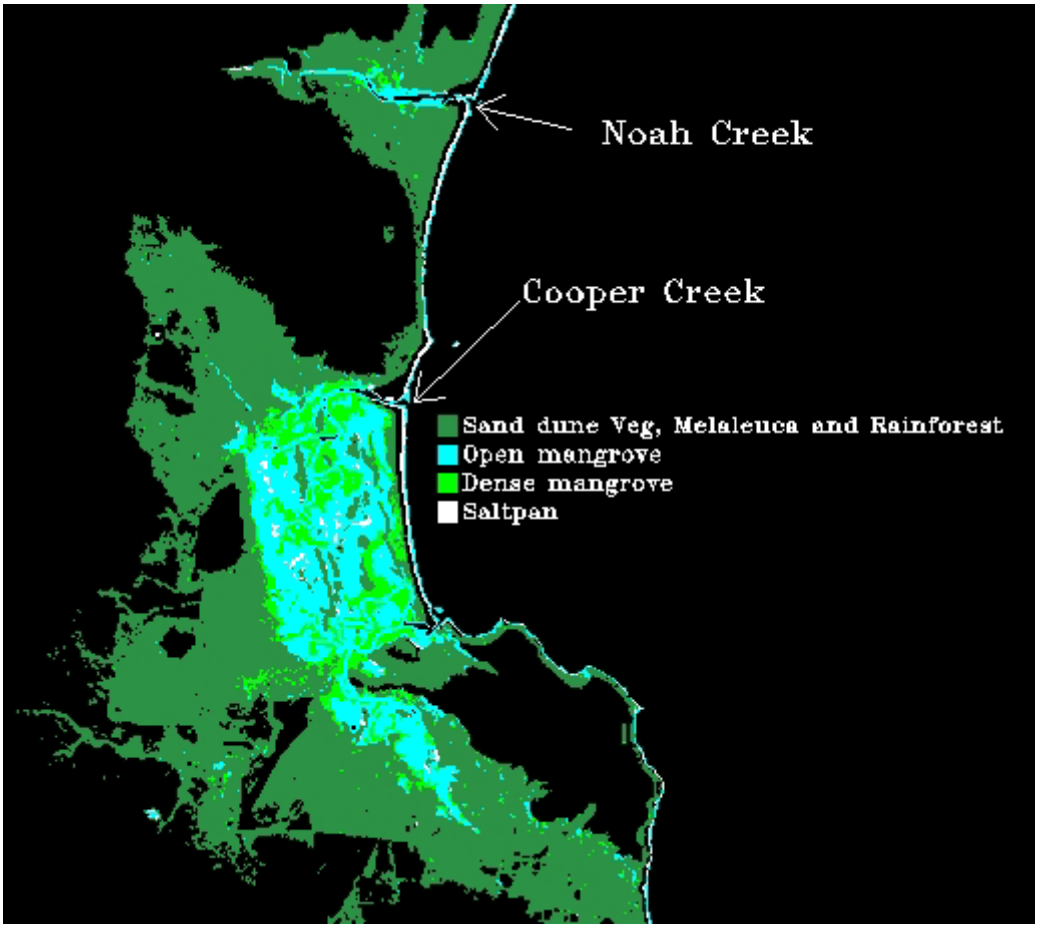

Figure 3.19. Decision tree classification of dominant vegetation types (using threshold values shown in Figure 3.17) from the Landsat data for the Noah and Cooper Creeks

The Landsat classification of Noah and Cooper creeks proved to be very similar to the Hyperion classification. The main difference appeared to be where some of the dense mangrove class showed up in the rainforest on the southern section of the Landsat image. This was likely a mistake, and provides an example where the Hyperion data is superior.

One of the main problems in classifying vegetation in coastal environments is the small and linear nature of some of the vegetation types. The relatively low resolution of both the Landsat and Hyperion (around 30 m pixels) means there are a lot of mixed pixels resulting in lost detail and some misclassification

occurring along these narrow features. This was particularly noticeable where the rivers narrow inland, and the mixed pixels were classified as open mangrove.

Comparison of classifications with aerial photo interpretation

The classifications performed at Geoscience Australia using aerial photo interpretation (API) are shown draped over a grey-scale Landsat image for the Daintree River (Figure 3.20) and the Noah and Cooper Creeks (Figure 3.22). The classifications produced from the aerial photography and Landsat imagery were still comparable, although the remote sensing classifications have not classified water in this instance. The saltmarsh/saltflats class in the API classification appeared as a mixture of the open mangrove and saltflats classes in the Landsat classification. The dense mangrove class from the Landsat classification followed a similar spatial distribution and pattern to the API map.

The main discrepancy appeared in the centre of the image (the 'X' in Figure 3.20) which was classified in the API as saltmarsh/saltflats, but was classified as the higher biomass sand dune vegetation/melaleuca/rainforest class using Landsat data. According to Le Cussan's vegetation map, this area is acacia vine thicket. Using the digital terrain model produced from radar interferometry (the 'X' in Figure 3.21), it can be seen that this vegetation is of medium height, falling in between the low saline regions of little to no vegetation cover (blue), and the tall vegetation (yellow).

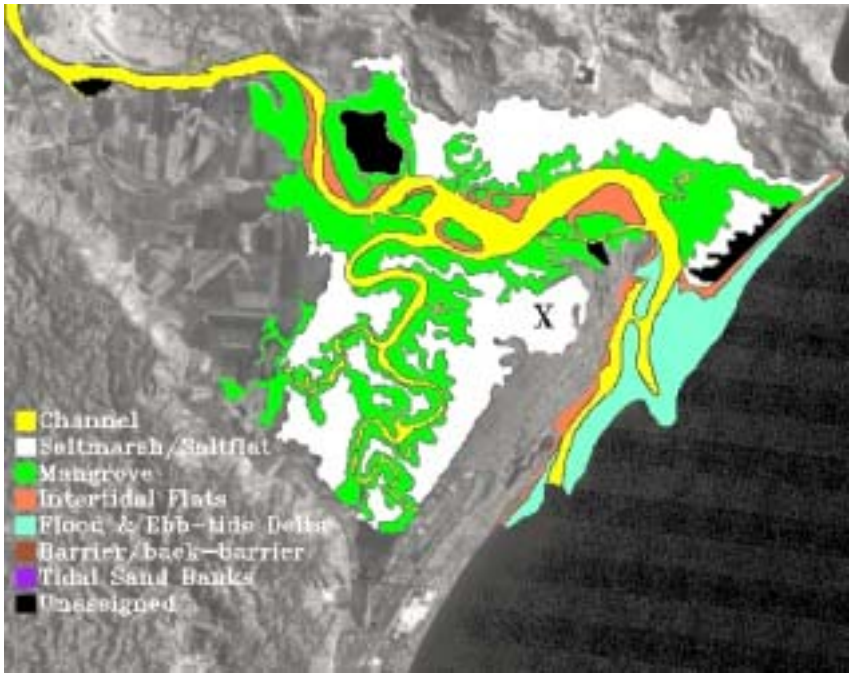

Figure 3.20. Aerial photo interpretation of the dominant land-cover types, draped over a grey-scale Landsat band for the Daintree River estuary. The 'X' indicates the region of discrepancy between the API and Landsat classifications

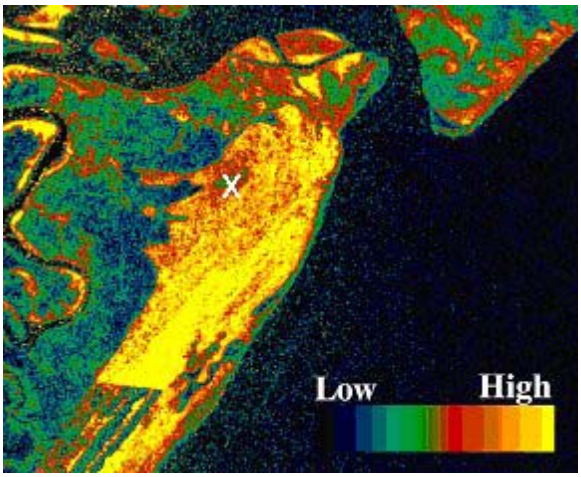

Figure 3.21. Digital terrain model of the Daintree River, produced from radar interferometry data. The 'X' indicates the region of discrepancy between the API and Landsat classifications

The Noah and Cooper Creek classifications (Figure 3.22) were also similar from API and Landsat. Again the combined open mangrove and saltflats classes in the Landsat classification were comparable with the API map. Due to the larger pixel size of the Landsat imagery, the detail was not as sharp as the API images, hence the narrow waterways tended to be classified as open mangrove since they were mixed pixels. For both Noah and Cooper Creeks, the area classified as tidal sand banks in the API image (purple) was unclassified in the Landsat image. This was because its bright reflectance meant it was masked from further classifications along with the agricultural regions.

The three small 'unassigned' classes in the API were identified and classified as sand dune vegetation/ melaleuca/rainforest in the Landsat scenes. The large 'unassigned' class in the API scene running along the coast appeared as a mixture of vegetation cover types in the Landsat classification. When this was compared to the radar interferometry digital terrain model (the white outline in Figure 3.23), it can be seen that the land cover here contained a mixture of high and low vegetation. Without field data, the exact nature of this vegetation cover cannot be verified.

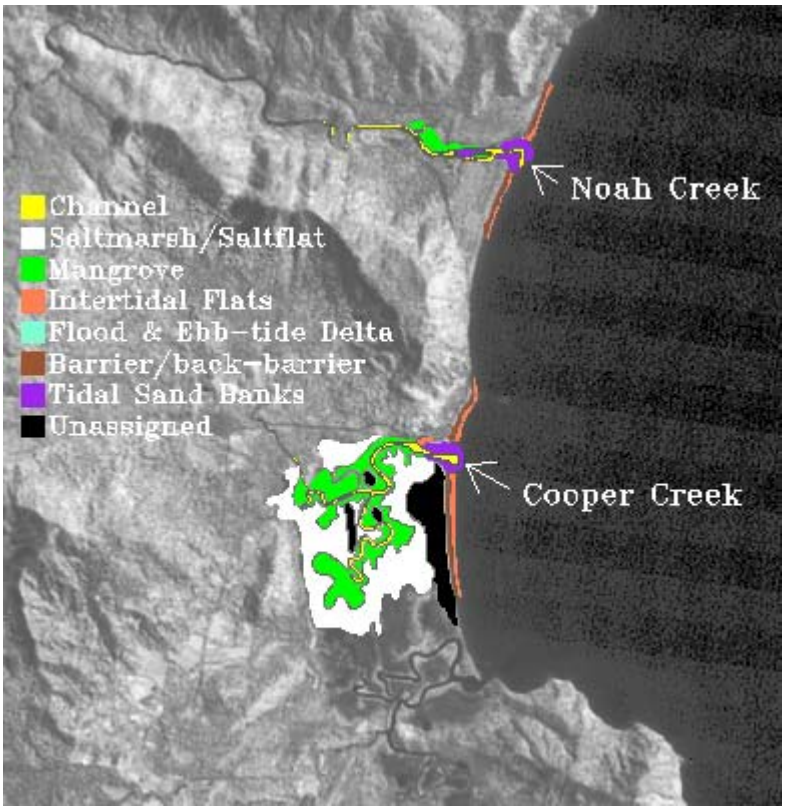

Figure 3.22. Aerial photo interpretation of the dominant land-cover types, draped over a grey-scale Landsat band for the Noah and Cooper Creek estuaries

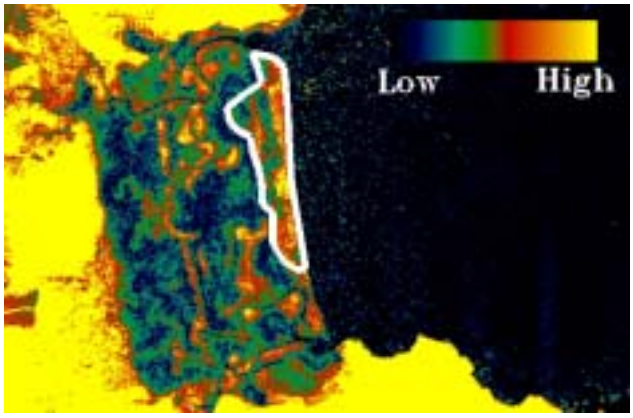

Figure 3.23. Digital terrain model of Cooper Creek, produced from radar interferometry data. The white outline indicates the region of discrepancy between the API and Landsat classifications

Although no field data was available for the near-pristine estuaries of Noah and Cooper Creeks, the similarity between the API maps and the Landsat classifications—two methods which were performed completely independent of each other—indicated these maps are of reasonable integrity.

Summary and recommendations

CASI, Hyperion, Landsat ETM7+ and AIRSAR remote sensing datasets were investigated for their ability to discriminate between dominant vegetation types in an estuarine environment. Table 3.17 summarises their advantages and disadvantages. All data types showed confusion between sand dune vegetation, rainforest and melaleuca vegetation types. The Hyperion data had the greatest potential for separating most of the dominant vegetation, so was therefore investigated further using a fully automated user-defined decision tree classification. Validation of this classification showed an accuracy of 92.1%; however, the rainforest, sand dune vegetation and melaleuca were combined into one class. The decision-tree classification approach was also tested on Landsat ETM data, as Landsat data are more readily available at a national scale, and have much greater coverage than Hyperion. Apart from some discrepancies between the saltflats and open mangrove vegetation, the two classifications were comparable.

The Landsat ETM classifications from the Daintree River, Cooper Creek and Noah Creek were compared to the aerial photo interpretations performed at Geoscience Australia. Although slightly different land-cover types were used, the results were comparable for the common classes. The advantage in using Landsat data in an automatic classification routine over API is that it is fast and can cover large regions. The disadvantage is that user knowledge and experience cannot be applied at the same level of detail. This study was performed on the Daintree River mangrove ecosystem, and hence the results are specific to this estuarine environment. Further investigation could adapt these methods to other estuary locations and forms.

Table 3.17. Advantages and disadvantages of the different remote sensing datasets used in this investigation

Characteristic	**Aerial photography**	**Airborne hyperspectral CASI**	**Satellite hyperspectral Hyperion**	**Airborne polarimetric radar AIRSAR**	**Satellite multispectral Landsat ETM**
Resolution (*with respect to vegetation patterns)*	Very good	Good	Average	Average	Average
Extent (*swath width, ability to obtain national coverage*)	Poor	Very poor	Poor	Poor	Good
Spectral bands (*more bands usually gives better discrimination power*)	Poor	Good	Very good	Average	Poor
Brightness sensitivity range	Poor	Good	Good	Good	Poor
Weather independent	Poor	Poor	Poor	Good	Poor
Ease of acquisition (*airborne systems require deployment*)	Low	Low	Good	Low	Good

Improvement of the automatic remote sensing classifications, including further discrimination of the land-cover types, may benefit from investigating the following approaches:

- The use of spectral derivatives and vegetation indices from the Hyperion data may help. However, ratios can become very noisy in the Hyperion data so further cleaning would be required to maintain spatial sensitivity.
- Benefits have been found in combining different remote sensing data. In particular, radar backscatter and optical reflectance can complement each other (e.g. Blasco *et al.* 1998; Held *et al.* 2003). There may be benefit in combining the AIRSAR and optical datasets (either Hyperion or Landsat) to improve the vegetation discrimination.
- Due to the small size and/or narrow width of some of the vegetation distributions, an automatic segmentation routine, such as that available in eCognition™, would greatly assist in the classification process (this is highlighted in the following chapter). Segmentation would allow statistics and texture to be extracted and used in discriminating different vegetation types. This could be particularly useful in radar imagery where speckle is inherent, but also in the optical datasets where mixed pixels were apparent.
- Smaller pixel size would help identify and classify particularly small and linear land-cover types. Instruments such as the SPOT sensor now have a pixel size as small as 2.5 m.

4. Estuary classification using eCognition™: Wildman River case study

Introduction

During the Comparative Geomorphology of Estuaries Project, there was a need to evaluate additional methodologies for classifying geomorphic habitats from remote sensing data. This case study provides an example of geomorphic habitat classification (Wildman River estuary, Northern Territory, Australia, Figure 4.1) using an image segmentation and spatial rule(s) based approach. The majority of the classification work was carried out in the eCognition™ software package.

The aim of the case study was primarily a general evaluation of an image segmentation classification approach using eCognition™ software, with a view to completing the classification work in the future. Specifically, the results of classifying mangroves using eCognition™ was compared to the manual interpretation outlined in Chapter 2.

Methods

Scene selection/study site

A tide-dominated estuary was chosen for classification using segmentation methodology because this type of estuary is common in the remote areas of northern Australia and offers a complexity of habitats. Further sites should be considered before using this methodology for continent-wide approach.

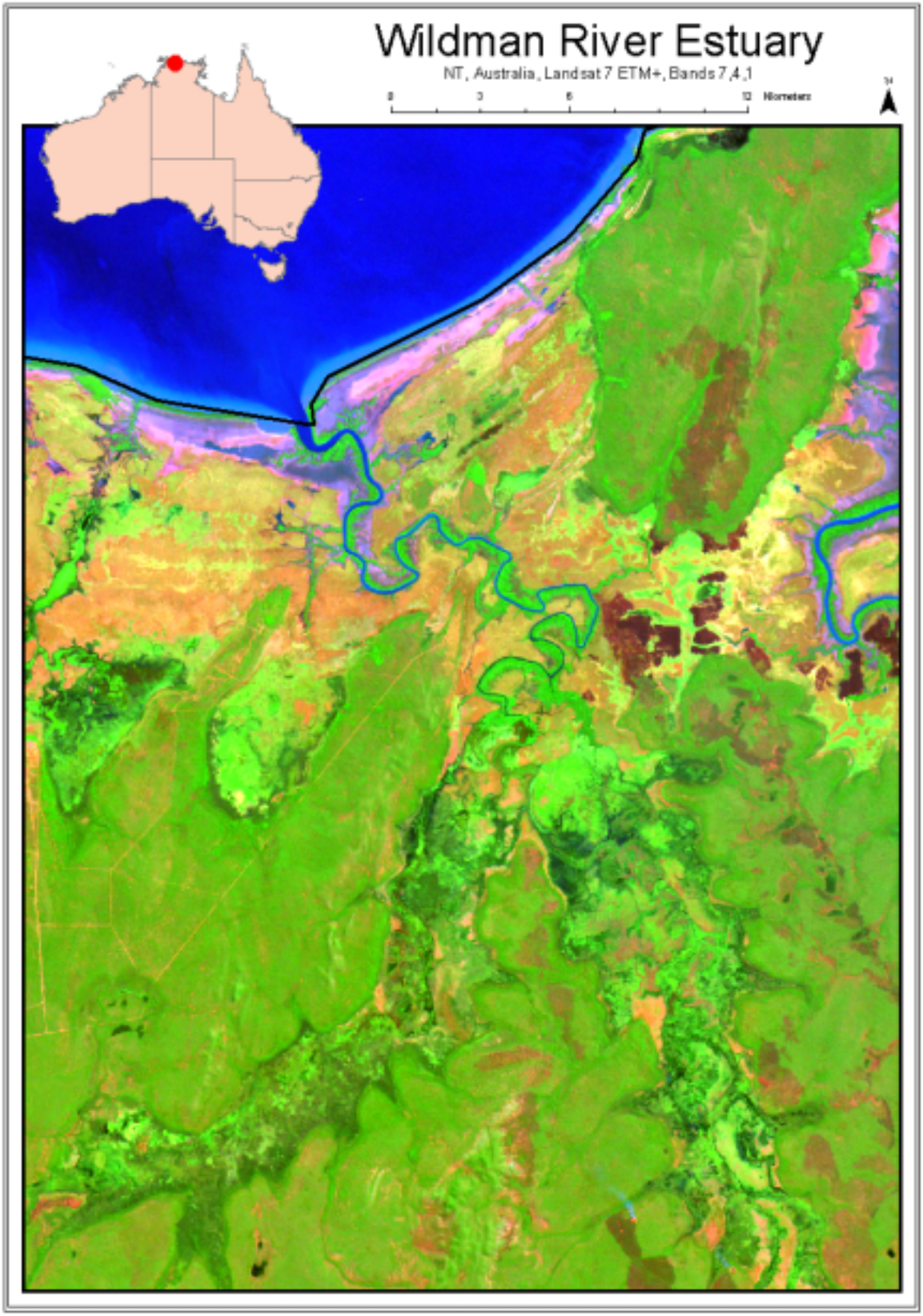

Figure 4.1. Wildman River estuary context map

A 40 x 55 km subset of a Landsat 7 triple scene collected on 27 May 2003 was the primary dataset used for feature classification. The subset was centred on the Wildman River estuary and a matching subset of the SRTM (Shuttle Radar Topography Mission) data for Australia provided elevation data (Figure 4.1). The panchromatic and thermal bands were not included in the input files for the image classification; the panchromatic band did not provide any additional useful spectral information to enhance class separability and the thermal bands were of too coarse a resolution to be of benefit to the classification.

The data for the case study was obtained from the ACRES catalogue, and the publicly available SRTM 3 second dataset for Australia.

Figure 4.2 illustrates the basic methodology used to achieve the results detailed at the end of the report, and a textual description of the processes follows.

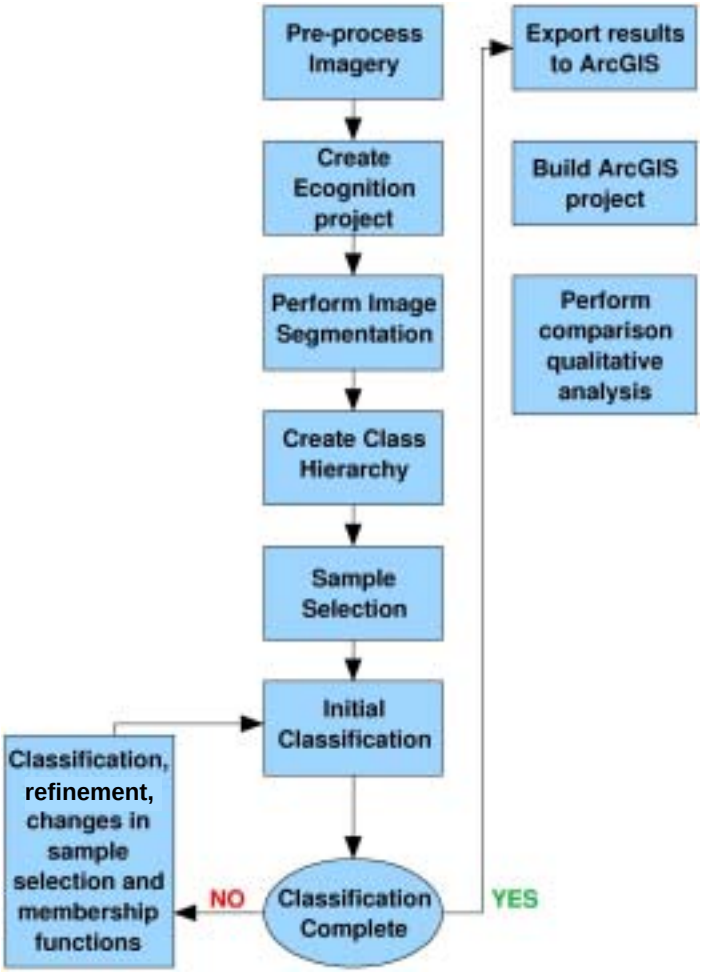

Figure 4.2. Process flowchart for Wildman River case study

Image pre-processing

Although eCognition™ 4.0 Professional software (Definiens AG) has the capability to import numerous remote sensing image formats, this case study had difficulties with the supported projections. The Landsat and SRTM data were both natively in Geographic project and Geocentric Datum of Australia 1994; however eCognition™ did not appear to support degrees as a unit for pixel size, therefore the input data were reprojected to UTM Zone MGA94 and metres. Once reprojected the images were clipped to an area covering the Wildman River estuary. No additional corrections were applied to the input data, apart from the generation of the products below, that is, no atmospheric or illumination correction was applied.

Two additional images were added to the project to evaluate the use of principal preclassified analysis data in the eCognition™ classification engine. The layers were selected from output of running the 'spectral hourglass wizard' under Envi 4.2 (Research Systems Inc.) using default settings. The wizard performs the following operations on the data:

- Minimum noise fraction calculation (~principal component processing)
- Pixel purity index and automated end member extraction
- Running of matched filter, spectral angle mapper (SAM), and linear un-mixing algorithms
- Creation of output files.

(For more details please consult the Envi user documentation.)

Of the resultant 'unmixed' classes, two layers were sent to eCognition™. The end members represented in the imagery broadly represented mangroves and saltmarsh, although the algorithms were not able to definitively spectrally isolate mangroves and saltmarsh from background vegetation classes; such classification would require greater spectral detail in the imagery. Figures 4.3 and 4.4 show the unmixed layers imported into eCognition™.

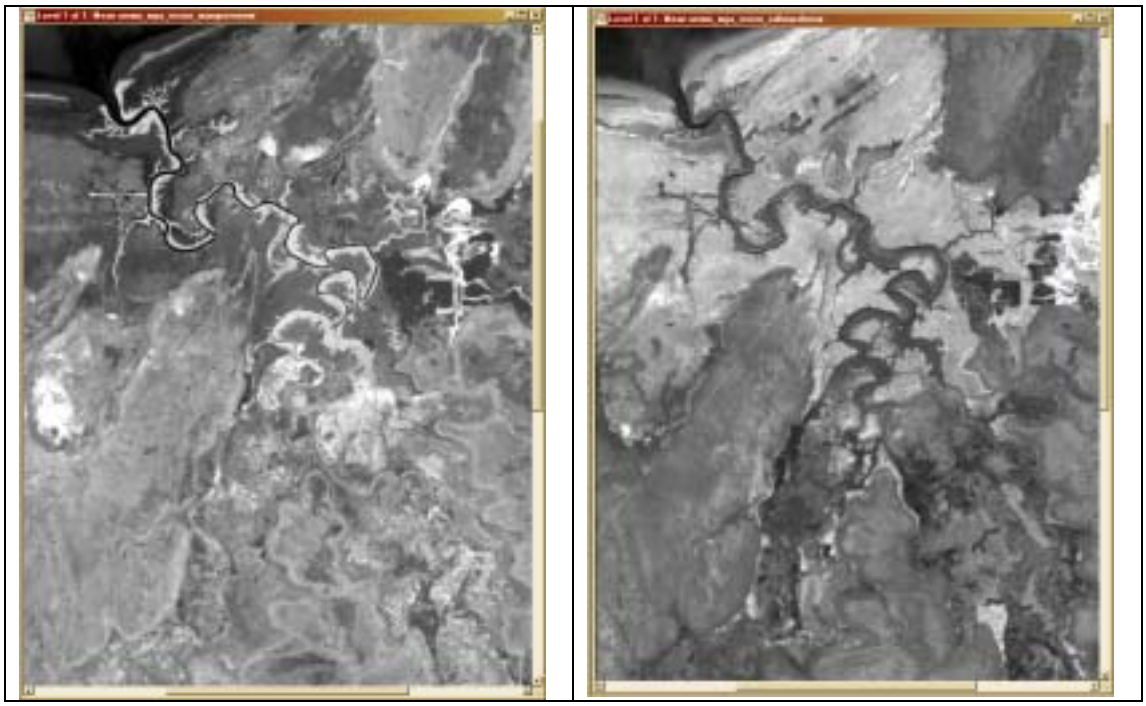

Figures 4.3 and 4.4. Linear unmixing results from Envi; the left image highlights green vegetation including mangrove; the right image highlights the drier saltmarsh areas. Brighter pixels correspond to higher probability of being that specific end member

eCognition™ project creation

All image layers, SRTM included, were imported into eCognition™ at their native resolution; eCognition™ resamples all image layers to the highest resolution of the input layers, and hence the SRTM data was resampled to the resolution of the Landsat data (~ 25 m).

Image segmentation

The image segmentation routine in eCognition™ breaks the image up into primary objects based on three primary factors:

- Shape
- Spectral response (colour)
- Scale factor.

Object creation is weighted (depending on user input) to homogeneity of object shape with respect to other objects or homogeneity of colour (spectral response) of a group of pixels. The weighting of colour and shape sum to unity, for example, a weighting of 0.9 for colour would mean a weighting of 0.1 for shape.

The scale factor determines the mean size of the object created. The scale factor was set such that the objects created were capturing relevant information about features, that is, objects were created small enough so that they would contain spectrally homogeneous pixels.

The primary object (segment) creation process is iterative; to maximise the spectral information in the scene as a means of classification, the primary objects were created as spectrally homogeneous as possible. For this project a scale factor of 8 and a shape factor of 0.1 (colour factor of 0.9) were determined to provide the best segmentation results for capturing features of interest. These factors were determined through running the segmentation routine multiple times and examination of the resultant image objects. Figure 4.5 shows a subset of the study area with the polygon outlines for the image objects.

The SRTM dataset was not used in the segmentation of the scene; it was employed with membership functions later in the process, which place elevation thresholds on vegetation distribution.

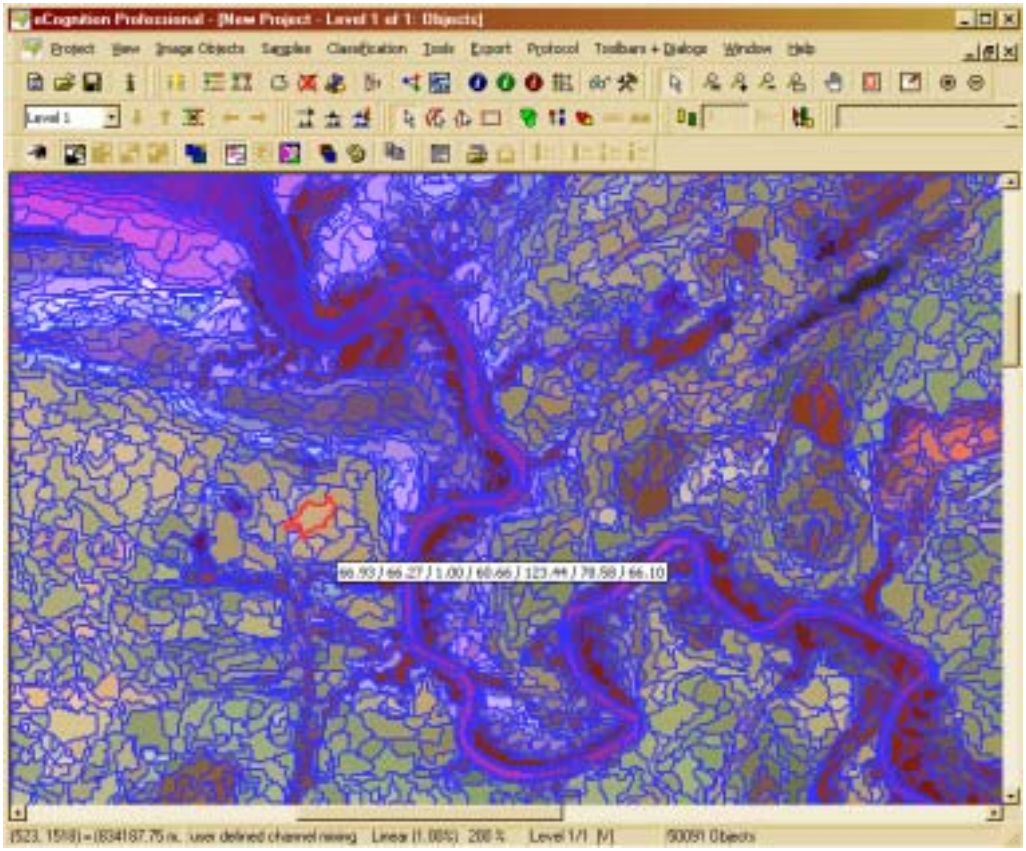

Figure 4.5. Primary objects (segments) created in eCognition™

Creation of class hierarchy

For ease of comparison with the manual interpretation, the class labels from that classification were used.

The applicable classes established for this classification are as follows:

- Intertidal (2 classes)
- Mangrove
- Saltflat
- Saltmarsh
- Water.

Additional classes were added to the classification list to aid in the classification. The additional classes were necessary as a means of training the classifier to identify what was not a feature of interest. During the manual interpretation/classification these additional land-cover types were visually excluded; however, since eCognition™ performs a full scene classification the following additional land-cover types needed to be classified as not mangrove:

- Dry vegetation
- Green vegetation 1
- Green vegetation 2
- Green vegetation 3
- Burn scar.

The use of thematic boundaries from the manual interpretation was investigated as a means of masking areas of the imagery that were considered outside the estuary, and reducing the classification complexity. Figure 4.6 illustrates the use of the thematic boundary for the Wildman River estuary (imported from the manual interpretation). The grey coloured area is classed as non-estuary while the full colour section was classed as estuary in the manual classification.

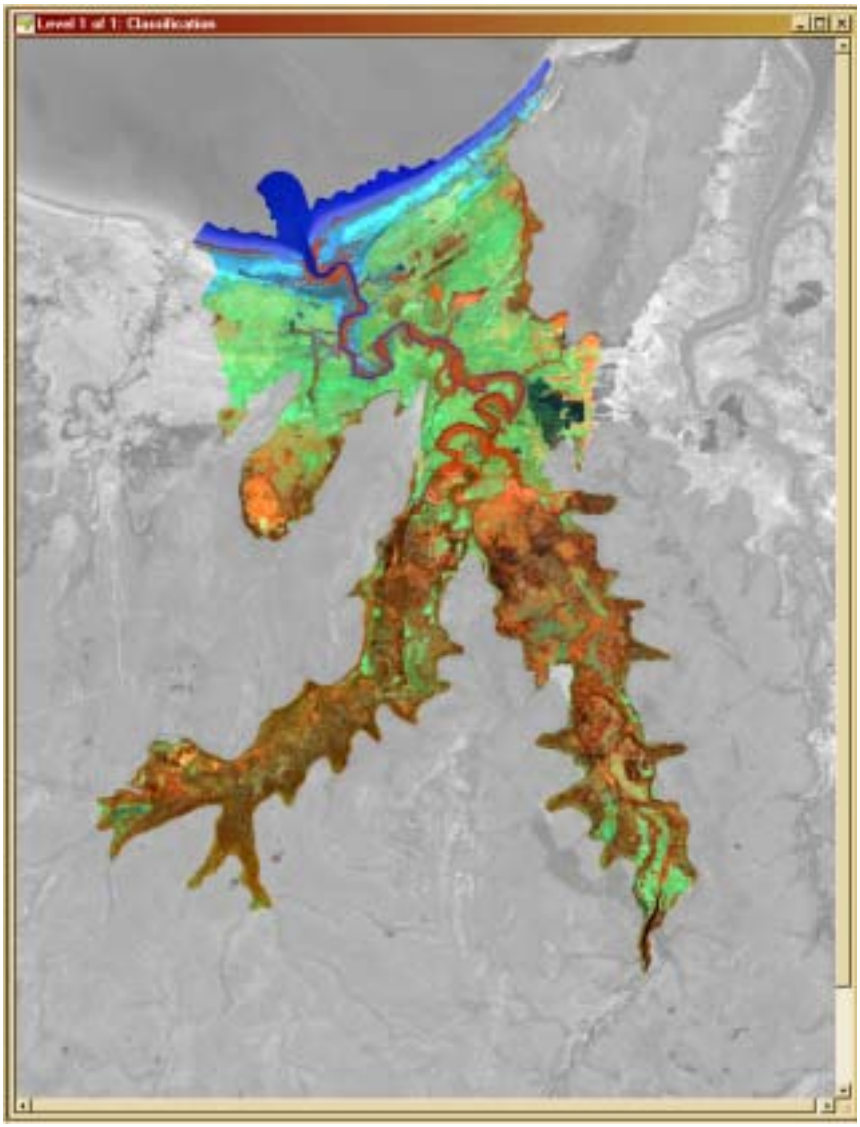

Figure 4.6. Thematic boundaries from manual interpretation as mask in eCognition™

eCognition™ supports import of shape file for use as a thematic layer for use in the classification. During the import processed the vector layer is rasterised, but due to issues with the import engine it was necessary to convert the vector to raster format prior to import into the project. The masking effect is achieved by creating an 'abstract' class in eCognition™, which acts as a pass through filter, all classes defined below the abstract class 'inherit' the data defined by that class, in this case all the data in colour in Figure 4.6.

Figure 4.7 illustrates the dialog of a class created under the abstract class ‘estuary’. The thematic layer has a value of one inside the estuary boundary and zero outside the boundary, making for a simple binary mask.

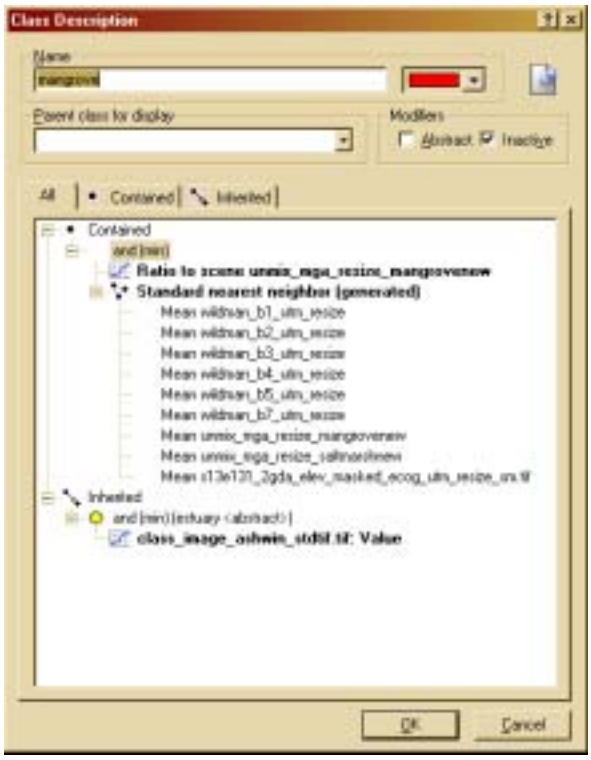

Figure 4.7. Mangrove class ‘inherits’ data classified by the ‘abstract’ estuary class

The additional unmixing layers generated in Envi and shown in Figures 4.3 and 4.4 were also evaluated as a means of masking and filtering data. The images were thresholded in eCognition™; areas above the threshold were passed through for further classification using the nearest neighbour classifier, while data below the threshold was excluded for consideration as mangrove or saltflat. In essence, the layers were used to constrain the area available to be considered as mangrove or saltmarsh.

In practice, however, the resulting class hierarchy and classification was not improved over the results achieved using the nearest neighbour classification of the full scene and membership functions to control the distribution of classes.

Sample selection

eCognition™ requires you to select representative samples of all your classes in order for its nearest neighbour classifier to work. The nearest neighbour classifier is typically the first step in the classification process, and was the first step for this case study. Membership functions as discussed above could be used to reduce the scene complexity; however, in this case there was no significant reduction in scene complexity since the areas of vegetation causing the most misclassification problems were included inside the estuary boundaries illustrated in Figure 4.6.

The attributes that can be used to classify data are grouped into:

Object features

- Layer values; including layer means, ratios, standard deviation, minimum and maximum pixel values, proximity to neighbours exhibiting one of the above
- Shape
- Texture
- Hierarchy

Class-related features

- Relations to neighbour objects
- Relations to sub-objects
- Relations to super-objects
- Membership to…
- Classified as…
- Classification value of…

Global features

- Scene-related
- Class-related.

Each of the bullet points above has a drop-down list with five or more operators that can be used as a rule to drive the classification of the primary objects, allowing for intricate classification routines and decision trees. The use of these feature sets and membership functions may be a viable method to reduce the dependence on sample selection in the future and therefore reduce the operator input required to select representative samples. A simple example is the ability to separate data based in normalised difference vegetation index (NVDI) response.

For the purposes of this case study the land-cover types to be classified were sufficiently distinguishable by eye that adequate representative samples could be selected.

Initial classification

The initial classification process (nearest neighbour) is started once the class hierarchy has been completed and the samples for each class have been selected. The classification was run with the default nearest neighbour settings.

Classification refinement and the addition of membership function rules

The initial results will almost always need refining and this process is completed in two steps:

- Training the nearest neighbour classifier
- Classification refinement using membership function rules.

eCognition™ has inbuilt tools for displaying the statistics for any particular sample class in relation to any other sample class, and identifying what are called ‘critical’ samples, that is, sample(s) in a class that overlap, in spectral (feature) space, with the domain of another class.

Figure 4.8 demonstrates the use of a scatter plot to display the relative locations of class samples. The scatter plot shows the standard deviation of band 1 against the mean of band 5. The different colour points belong to four separate classes (after initial classification) that have been displayed (mangrove – red; wet vegetation – green; dry vegetation – yellow; saltflat – grey), the larger coloured circles representing samples. A sample navigation function allows the operator to click on any of the circles and the software will zoom to that sample in the image display window (not shown here). (This step is usually used for troubleshooting critical samples.)

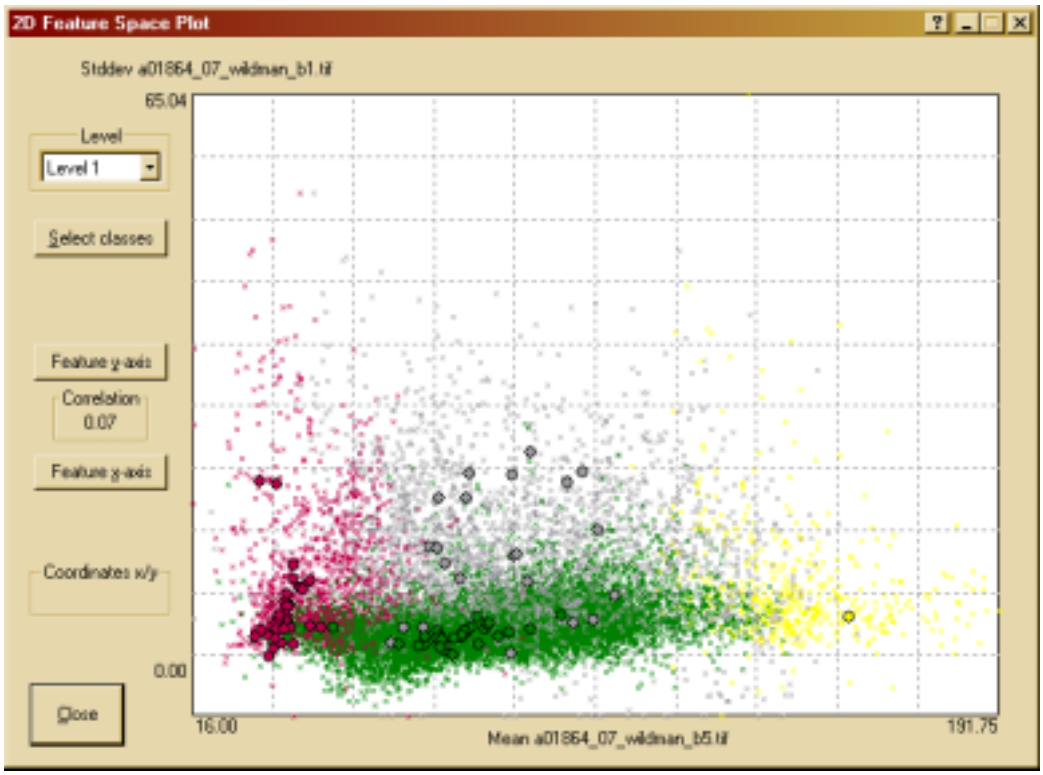

Figure 4.8. Scatter plot showing class samples on standard deviation of band 1 against mean of band 5

The refinement process may take several classification iterations, until the operator believes that the result is the best that can be achieved using the nearest neighbour classifier. To aid in this assessment eCognition™ has two types of accuracy assessment tools, one set which assesses classification stability and the second that compares the accuracy of the classification against ground truth or operator-selected samples (alternate samples to those used to drive the classification). The comparison against ground truth or alternate samples was not used as a validation tool in eCognition™ as its results were exported to ArcGIS for comparison against the manual interpretation work. The classification stability assessment was used to aid in the refinement of the nearest neighbour classification.

Figure 4.9 illustrates the final stability of the classification after all refinement was completed. Because of the fuzzy logic employed by eCognition™ to compute the membership of a specific object to a class, objects can have membership (to a lesser degree) to classes other than the class to which they were finally assigned. Dark green in the image shows low level of ambiguity in the classification and red shows high levels of ambiguity. The main the areas of saltmarsh, saltflat and mangrove show low levels of ambiguity, demonstrating the ease of separation from other land-cover types. Areas of high ambiguity (red) were predominantly associated with the green vegetation types.

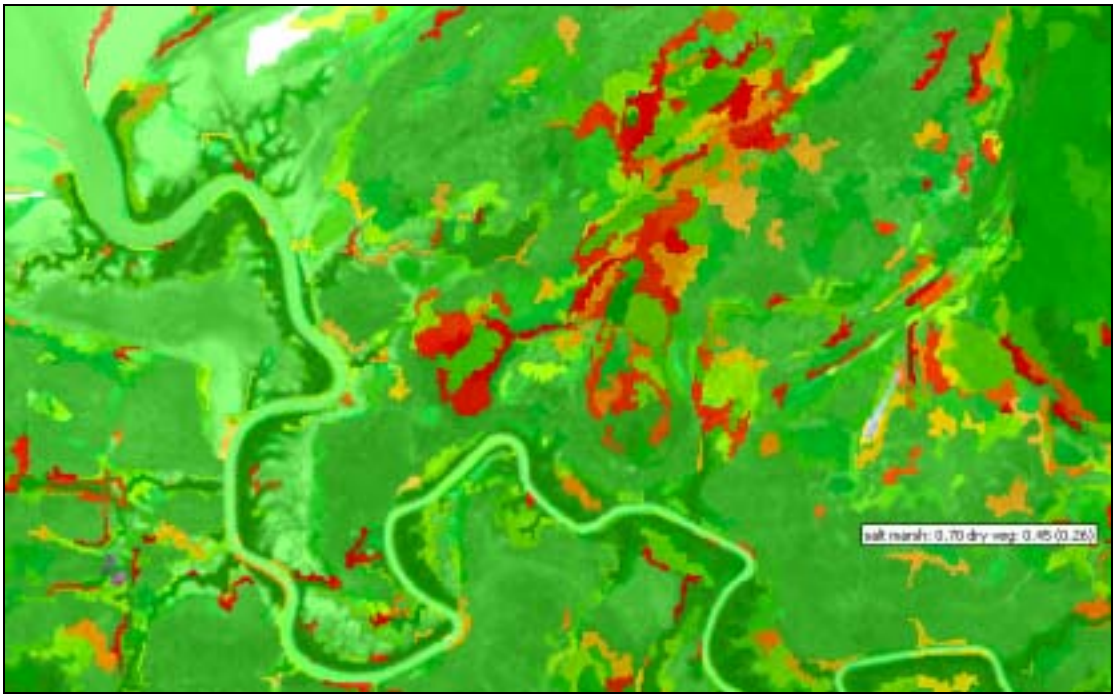

Figure 4.9. Classification stability for Wildman River eCognition™ case study

The small white inset is typical of the information provided by eCognition™ when the mouse pointer is held over a particular object, when viewing the classification stability data spatially; it shows a membership value of 0.7 out of 1.0 for saltmarsh and 0.45 for the next closest membership value, dry vegetation. This tool was particularly useful when determining how the addition and subtraction of individual samples for each class were affecting the domain of the class or which other classes it may be confused with.

In some cases it was impossible to achieve the right classification of certain objects because of their spectral similarity with other classes; the addition of membership function rules was an effective method in reducing the classification confusion. The membership function rules added were based on the SRTM elevation dataset and on class-related features.

Table 4.1 details the membership function rules that were applied to each class to control their classification.

Table 4.1. Membership function rules used for eCognition™ classification of Wildman River dataset

Class	Rule	Rule
Green vegetation 2	No water or saltflat neighbours	Not within 31 m of water
Green vegetation 1	No water or saltflat neighbours	
Saltmarsh	Not above 6 m	
Saltflat	Not above 6 m	
Mangrove	Not above 6.5 m	Must be within 50 m of water
Water	N/A	
Dry vegetation	N/A	

Two examples of the rule dialog in eCognition™ are shown in Figures 4.10 and 4.11, which illustrate the dialog for configuring the membership functions for a particular class. The main features of the membership function are (1) the shape of the function, selectable at the top, (2) the border of the function and (3) the maximum membership value attributable through the function. Figure 4.10 shows the distance from water allowable for an object still to be classified as mangrove, and there is a narrow range for the fuzzy membership function to work within, creating a firm boundary. Figure 4.11 demonstrates a simple binary rule, that there are no green vegetation 2 objects allowed next to saltflat objects.

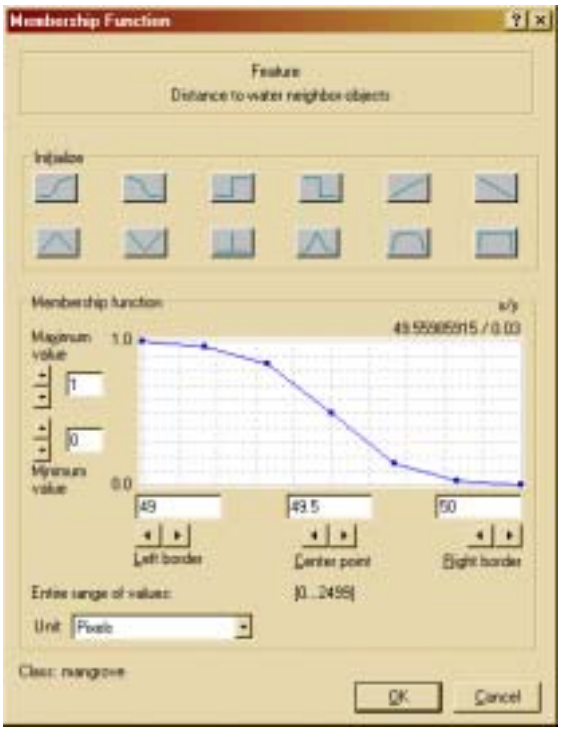

Figure 4.10. Setting the distance rule – no mangrove class more than 50 m away from water

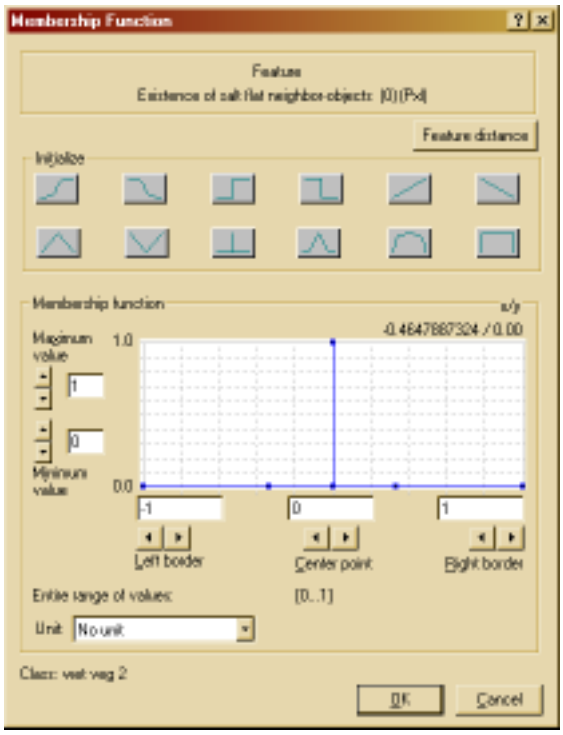

Figure 4.11. Membership function rule setting – no green vegetation 2 class neighbouring a saltflat object

Export results to ArcGIS

Once completed the classification was exported to shape file format. eCognition™ gives several options, including export as a tif, but for the purposes of this case study it was necessary to retain as much information as possible in a vector format for comparison against manual interpretation effort.

Results

The shape file exported from eCognition™ contains all the primary objects created during the image segmentation procedure. For the purposes of analysis this data needed manipulation to make it comparable to the dataset produced by manual interpretation.

The decision was made to compare only the mangrove class from each classification because it is a discrete class and can be readily identified in the manual interpretation, enabling the discussion of the relative merits of each approach by providing a baseline by which to compare them.

The following steps were performed on the eCognition™ dataset:

- Dissolve all primary objects adjacent to other primary objects of the same class – resulting in fewer larger polygons.
- Clip the dataset to the extents provided by the interpreted dataset.

In order to compare the relative extents of the mangrove class across classification techniques, the datasets were then processed in the following way:

- Select for specific class from the eCognition™ dataset – save as layer file.
- Select for specific class from the interpreted dataset – save as layer file.
- 'Union' the new layers to produce a combined dataset.
- Select for polygons where eCognition™ and interpreted dataset agree – save as layer file.
- Select for polygons where classified as interpreted only – save as layer file.
- Select for polygons where classified as eCognition™ only – save as layer file.
- Generate area statistics on layer files.

The results generated from these procedures are described on the following pages.

Table 4.2 details the relative area of mangroves as classified by eCognition™ and the manual interpretation method. The manual classification method covers an area larger than that from the eCognition™ method.

Table 4.2. Areas of polygons, comparing eCognition™ classification to interpreted classification for mangroves

Class name	Area (ha)
Mangrove interpreted total	1781.9
Mangrove eCognition™ total	1203.4
Mangrove eCognition/interpreted agreement	1186.7 (66.6%)
Mangrove eCognition only	16.7
Mangrove interpreted only	595.2

The comparative results of the other classes will not be presented here as the results are such that a numeric comparison is not warranted; instead the results are best explored visually.

Figures 4.12 and 4.13 are the Wildman River classification produced by eCognition™ and manual interpretation, respectively. The classifications appear similar at the beginning of the estuary closest to the ocean, but diverge significantly after the last of the classified mangrove. The eCognition™ classification changes from predominantly saltmarsh to a mixture of green vegetation class and a minor amount of the saltmarsh class. In contrast, the manual classification extends the saltmarsh/saltflat class much further inland.

By looking at the SRTM dataset (Figure 4.14) overlaid with the manual classification, it appears that the manual classification follows the contours down the valleys and low-lying areas. Encouragingly, the mangrove classification ‘appears’ similar in its distribution, if not in overall area as detailed in Table 4.2.

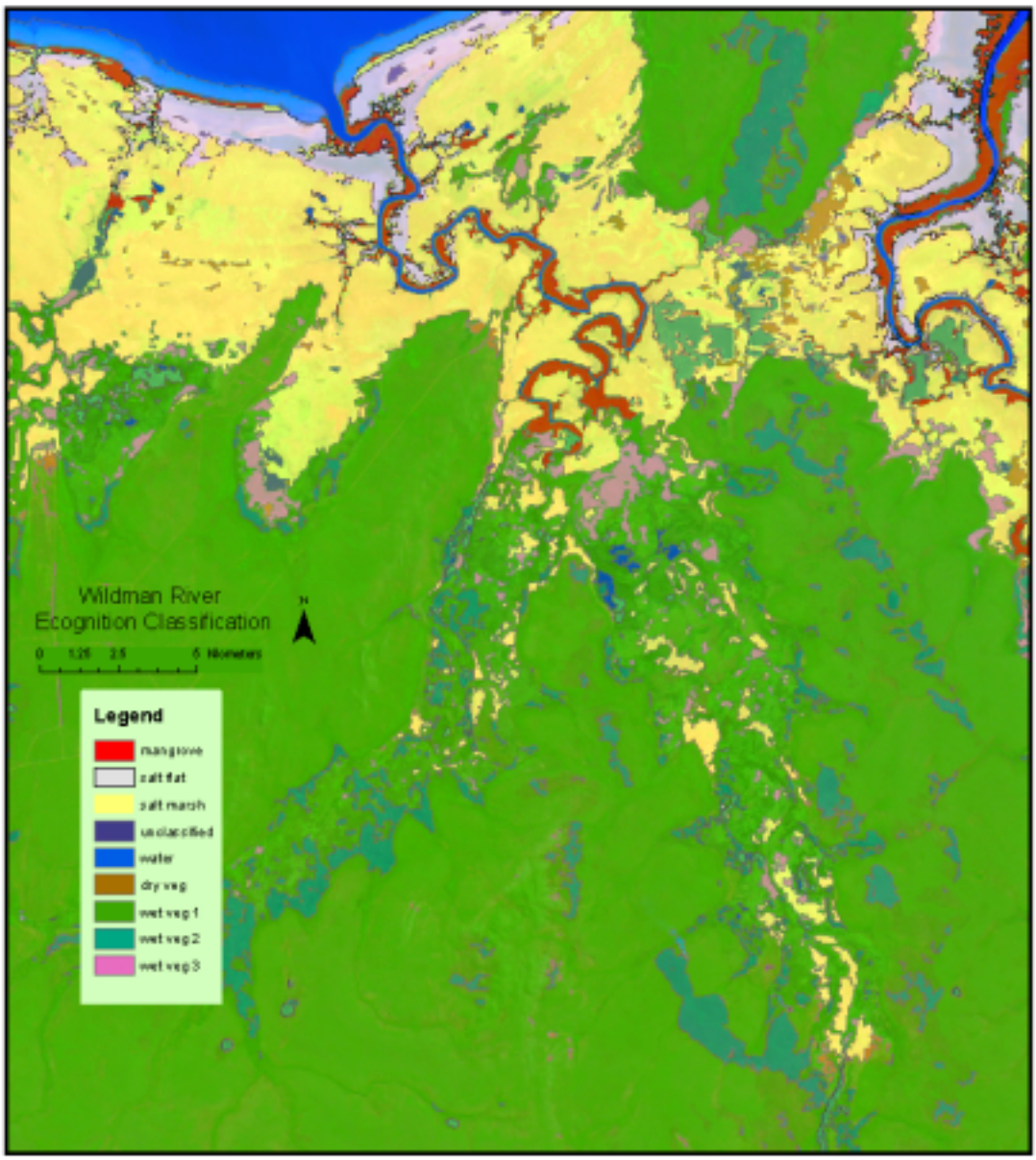

Figure 4.12. Wildman River eCognition™ classification

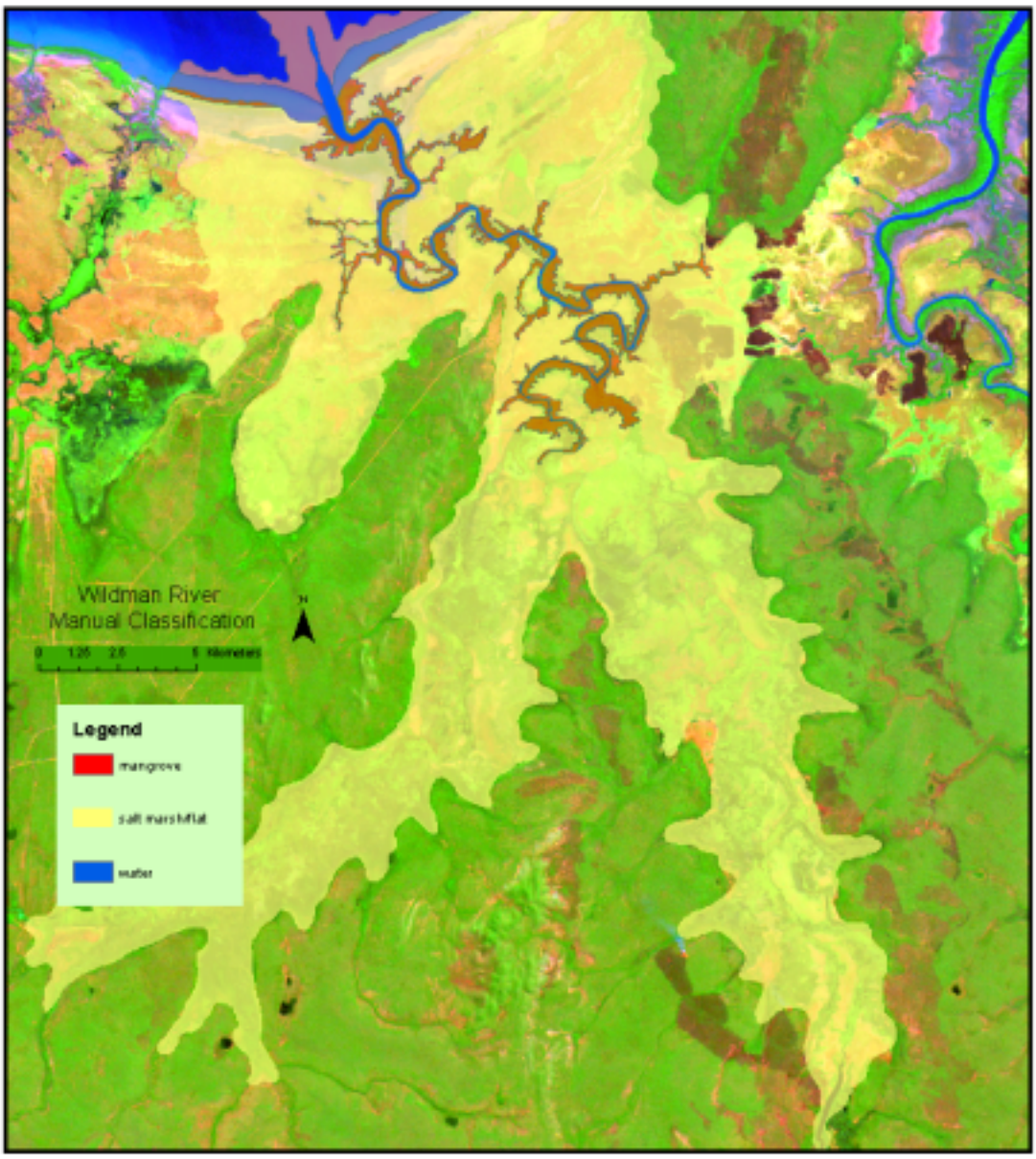

Figure 4.13. Wildman River manual interpretation classification

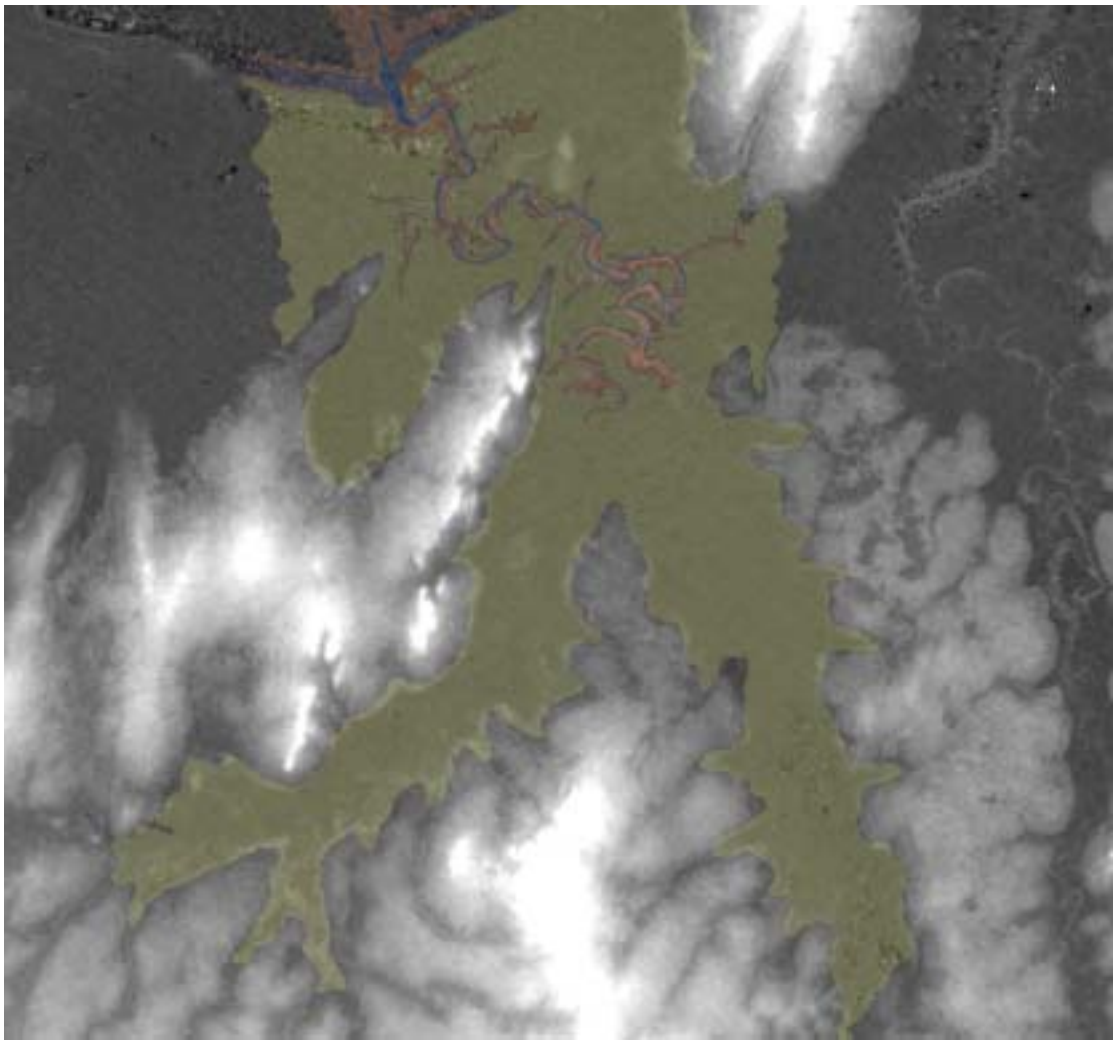

Figure 4.14. SRTM dataset for Wildman River; white high and dark low

Discussion

A primary aim of this study was to evaluate segmentation and rule-based (expert) classification as a method for generating classifications of near-pristine estuaries. To that end an assessment needs to be made as to its performance in this function with respect to the baseline established by manual classification work.

The difference in area between the manual classification of mangrove and that produced by eCognition™ can be accounted for by the following factors:

1. eCognition™ misclassified some mangrove pixels, mainly due to the resolution of the imagery.
2. The manual interpretation method appears to have some non-systematic offsets in the spatial distribution of its mangrove class – that is, it does not line up in some areas with the Landsat imagery and consequently with the eCognition™ classification.
3. The manual interpretation method appears, because of smooth line work, to capture more pixels as mangrove than is actually the case.

Figures 4.15–4.18 illustrate some of the issues regarding the performance of the manual and eCognition™ classification methods, as detailed above. They also provide reasonable explanation for the differences in area of mangroves from each method. In all figures, the area classified as mangrove is shown by the polygon outline and the polygons are displayed with 70% transparency to allow the Landsat image to remain visible beneath it; mangrove pixels show up as green.

Figures 4.15 and 4.16 show the mouth of the Wildman River Estuary and illustrate the problems with the overgeneralising by the manual method (Figure 4.15) and with misclassification by eCognition™ (Figure 4.16). Examination of Figure 4.15 shows that the vector describing the mangrove (green areas) is too general, caused by generalising the mangrove stand(s) to such an extent as to include areas of saltflat (showing as pink within the bounds of the classified mangrove polygon). Figure 4.16 demonstrates that the eCognition™ mangrove classification is better constrained just to the mangrove pixels (green in these images) but in some cases fails to classify the outer limits of the stand correctly (these pixels are classified as saltmarsh when viewing the full scene classification). eCognition™ also fails to identify some of the ‘fingers’ in the mangrove stands, which are captured—if a little haphazardly—by the manual method. This failure is a product of image resolution and not the eCognition™ classification engine; a higher resolution image would allow for better delineation of these features.

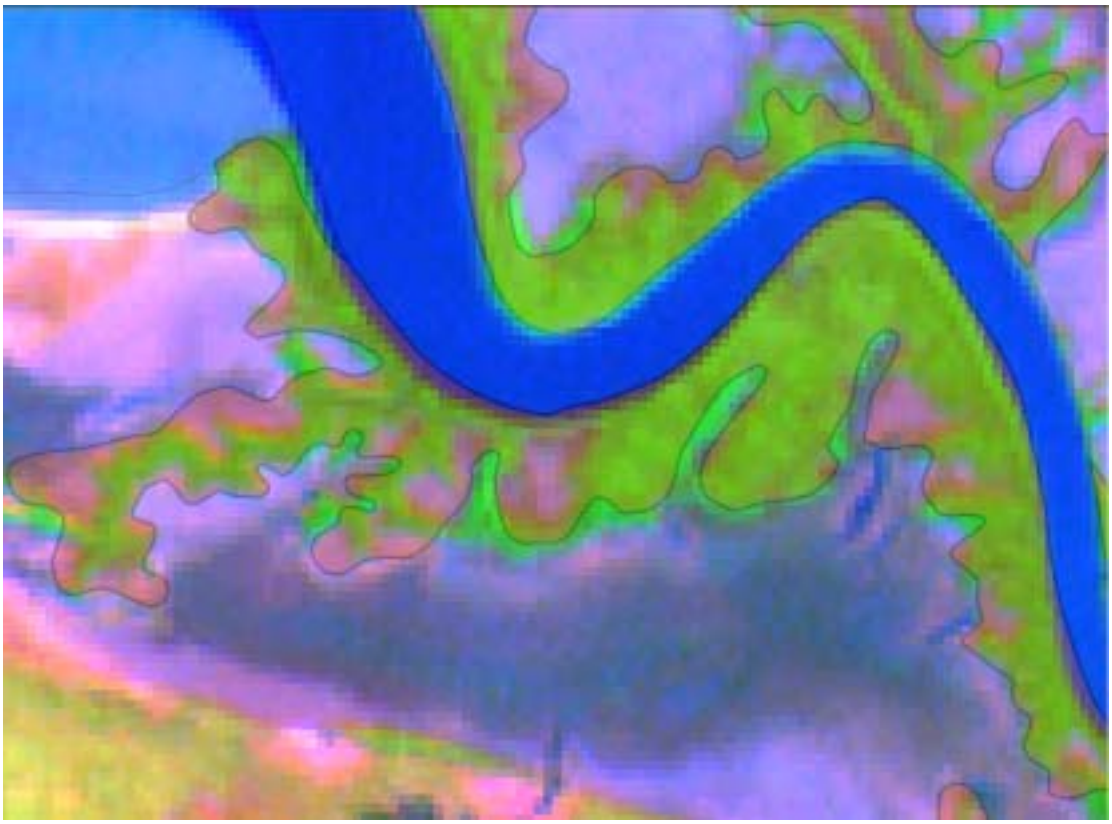

Figure 4.15. Manual classification at the mouth of the Wildman River estuary

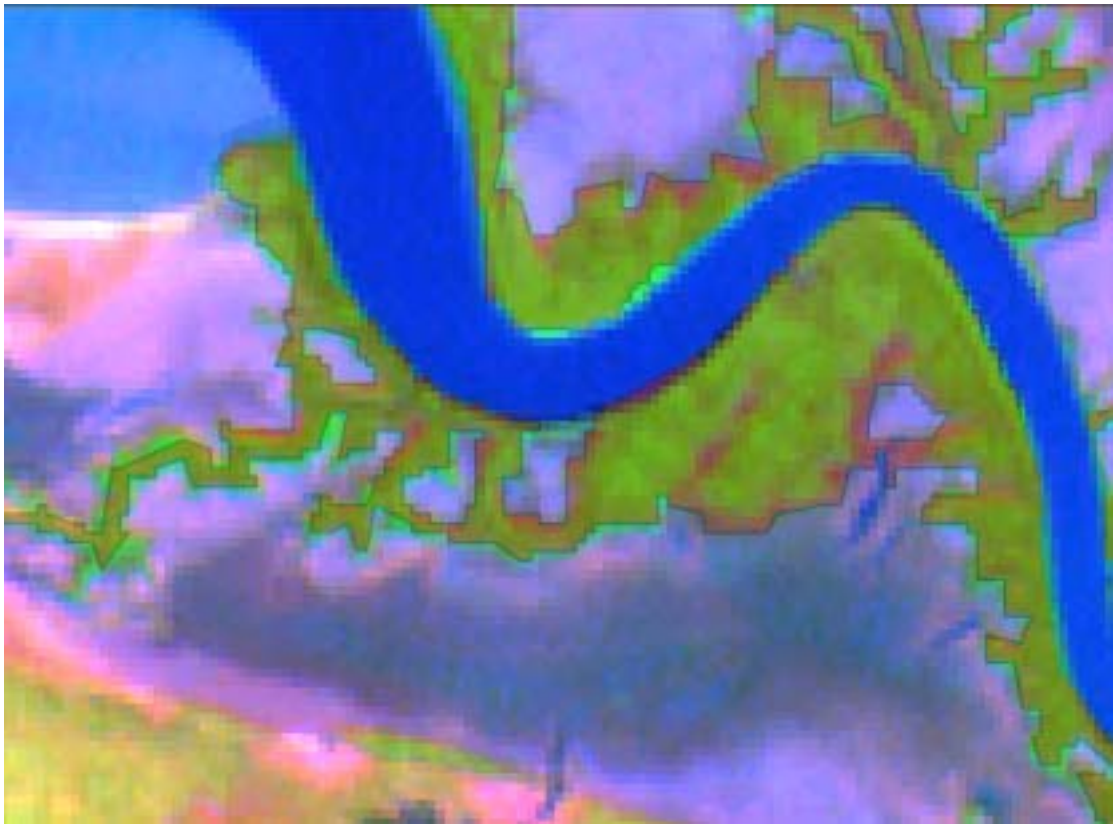

Figure 4.16. eCognition™ classification at the mouth of the Wildman River estuary

Figures 4.16 and 4.17 were included to illustrate an offset problem in the manual classification vectors. In Figure 4.16 it is apparent that the vector boundaries from the manual classification method are offset from the Landsat image underneath. Examination of the rest of the dataset shows that this offset is non-uniform, and indeed no further offsets of this magnitude were visible. This would seem to rule out any issues related to datum or projection that would introduce a systematic offset or block shift. A more likely reason(s) for the offset are errors introduced during the digitising and scanning process. eCognition™ is immune from such errors since the classification vectors are derived directly from the imagery during the segmentation process. (See Figure 4.18 for results over the same area from eCognition™.)

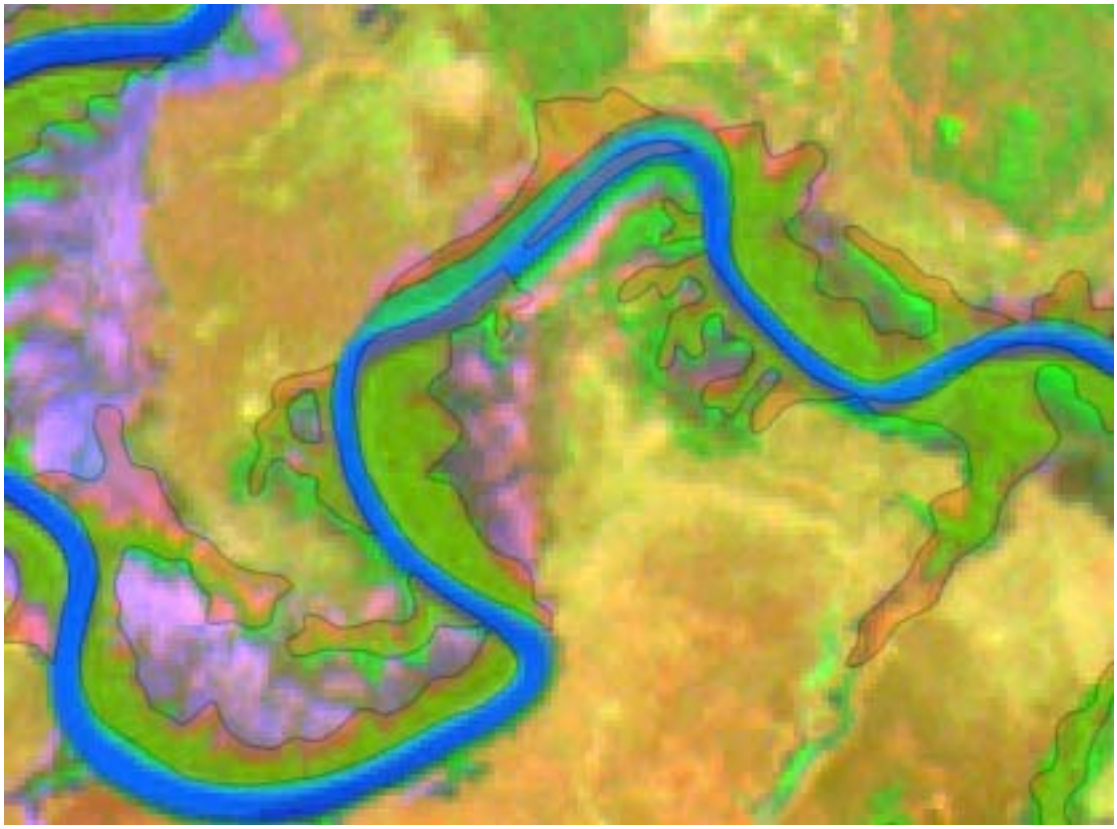

Figure 4.17. Manual classification, showing offset on river bend in Wildman River estuary

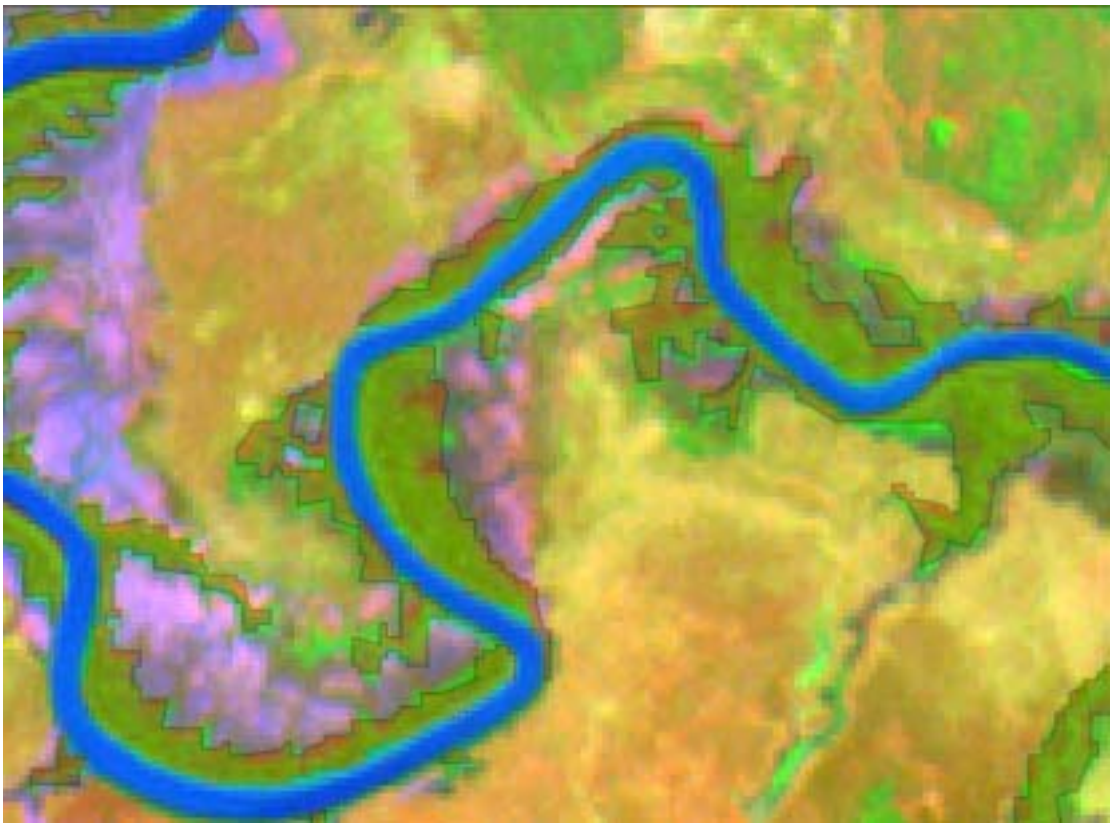

Figure 4.18. eCognition™ classification in same location as Figure 4.17

From all the examples shown in the above figures it is apparent that the vectors derived from the vector imagery (eCognition™ results) appear blocky compared with the much smoother vector outlines of the manual interpretation effort. The vectors are generated during the image segmentation process in eCognition™; they are designed to capture pixel groups based on colour and shape, and hence the vectors follow the outline of pixels. Therefore, the blocky appearance of the vectors from the eCognition™ results is a direct result of the resolution of the input imagery and the scale at which it is viewed. To achieve smoother vectors using the eCognition™ process, higher-resolution imagery would be required. Higher-resolution imagery would also allow eCognition™ to resolve some of the finer 'finger' like features of the mangrove stands. Options to smooth the vector output from eCognition™ were ineffective with imagery at this scale. (See Figures 4.14 and 4.15: manual interpretation captures the fingers and eCognition™ does not.)

The absolute accuracy of the expert classification versus that done manually is difficult to determine without accurate ground truthing information for the study site. At the time of writing the only mapping available for the site was contained in the manual interpretation classification, which as evidenced by the discussion above suffers from its own inaccuracies. Qualitatively, by examining the

classification, the expert method appears to successfully capture the different class types at least as well as the manual interpretation method.

This project experimented with the use of additional layers to help constrain the classification work within eCognition™, and while they proved of no significant value here, the same cannot be said for future potential projects. It is conceivable that thematic layers could be used to (1) constrain the area for classification, potentially reducing the classification complexity and (2) further improve classification results through the input of layers such as those generated in Envi through the application of specialist algorithms.

Systematically constraining the areas to be classified should improve throughput in the classification process by focussing operator efforts on the classification of only the area of interest, decreasing scene complexity and providing a boundary for all further monitoring work.

Additional corrections to the input dataset not considered in this study include atmospheric correction and illumination correction (i.e. BRDF) that would improve the quality of the data and provide a solid basis for temporal analysis.

Comparative outcomes

From the results and discussion above it is obvious that expert classification and manual interpretation both have their advantages and disadvantages. In the context of evaluating expert classification techniques as an alternative to manual methods, the following advantages and disadvantages are apparent.

Advantages for expert classification

- Classification vectors are derived directly from image layers resulting in an improvement over the manual method in that there are no offsets introduced via errors in digitising and scanning.
- Classification is better constrained by the values of the pixels in a measurable fashion, and statistics can be generated as to its reliability, which can be expected to be repeatable across scenes and projects.
- Reduction in operator bias should increase the value of classification in a temporal monitoring framework.

Disadvantages for expert classification

- Expert classification does not remove operator bias completely, since it still relies on operators to select representative samples for each class.
- Levels of accuracy are in part dependent on the amount of time dedicated to refinement of the classification schemes.
- Expert classification may require a larger investment in training and software than manual classification methods for a project the size of the near-pristine estuaries mapping project.

Conclusions and recommendations

The Wildman River Case study demonstrates that expert classification is a viable alternative to interpreting information by hand. The expert classification produced using eCognition™ achieved results not only comparable to the manual interpretation results but in some cases preferable. The expert classification does not eliminate operator bias in such work, but provides a framework and constraints such that consistent results should be achievable.

eCognition™ strengths are:

- It provides tools to analyse disparate (SRTM, Landsat) multi-resolution datasets in an integrated fashion.
- Segmentation and membership functions allow for the implementation of physically based landscape relationships into the classification methodology.
- Classification hierarchies are transferable from scene to scene, creating efficiencies in processing and setup times.
- It provides a framework and constraints that can produce consistent results.

Some weaknesses are:

- Operator input is still required for sample selection and classifier training.
- It is a relatively new approach and the software requires a high skill level of users for implementing solutions ‘from scratch’.

Further research into the performance of eCognition™ as a tool to perform this type of classification work is needed. Specifically, the results from eCognition™ should be compared to the results from a standard pixel-based classifier. This would enable a quantitative evaluation of the results from eCognition™. In addition, the process and methodology should be applied to additional representative scenes from the various bioregional areas of Australia’s coastline.

5. References

Ackleson, S.G. & Klemas, V. (1987) Remote-sensing of submerged aquatic vegetation in lower Chesapeake Bay – A comparison of Landsat MSS to TM Imagery. *Remote Sensing of Environment* 22(2), 235–248.

Anys, H., Bannari, A., He, D.C. & Morin, D. (1994) Texture analysis for the mapping of urban areas using airborne MEIS-II images. In: *Proceedings of the first international airborne remote sensing conference and exhibition*, ERIM, Strasbourg, France, 231–245.

Aschbacher, J., Ofren, R.S., Delsol, J.P., Suselo, T.B., Vibulsresth, S. & Charrupat, T. (1995) An integrated comparative approach to mangrove vegetation mapping using remote sensing and GIS technologies: preliminary results. *Hydrobiologia* 295, 285–294.

Blasco, F., Guaquelin, T., Rasolofoharinoro, M. & Denis, J. (1998) Recent advances in mangrove studies using remote sensing data. *Marine and Freshwater Research* 49, 287–296.

Blasco, F., Saenger, P. & Janodet, E. (1996) Mangroves as indicators of coastal change. *Catena* 27, 167–178.

Boegh, E., Soegaard, H., Broge, N., Hasager, C.B., Jensen, N.O., Schelde, K. & Thomsen, A. (2002) Airborne multispectral data for quantifying leaf area index, nitrogen concentration, and photosynthetic efficiency in agriculture. *Remote Sensing of Environment* 81, 179–193.

Boyd, R., Dalrymple, R. & Zaitlin, B.A. (1992) Classification of clastic coastal depositional environments. *Sedimentary Geology* 80, 139–150.

Brando, V.E. & Dekker A.G. (2003) Satellite hyperspectral remote sensing for estimating estuarine and coastal water quality. *IEEE Transactions on Geoscience and Remote Sensing* 41(6), 1378–1387.

Brando, V.E., Dekker, A.G., Phinn, S.R. & Roelfsema, C.R. (2004) Optimized mapping of inherent optical properties in coastal water bodies. *Remote Sensing of Environment* (in preparation).

Coops, N.C., Stone, C., Culvenor, D.S. & Chisholm, L. (2004) Assessment of crown condition in eucalypt vegetation by remotely sensed optical indices. *Journal of Environmental Quality* 33, 956–965.

Dahdouh-Guebas, F. (2002) The use of remote sensing and GIS in the sustainable management of tropical coastal ecosystems*. Environment, Development and Sustainability* 4, 93–112.

Dahdouh-Guebas, F., Zetterstrom, T., Ronnback, P., Troell, M., Wickramasinghe, A. & Keodam, N. (2002) Recent changes in land use in the Pambala-shilaw lagoon complex (Sri Lanka) investigated using remote sensing and GIS: Conservation of mangroves vs. development of shrimp farming. *Environment, Development and Sustainability* 4, 185–200.

Dahdouh-Guebas, F., Verheyden, A., De Genst, W., Hettiarachchi, S. & Koedam, N. (2000) Four decade vegetation dynamics in Sri Lankan mangroves as detected from sequential aerial photography: a case study in Galle. *Bulletin of Marine Science* 67(2), 741–759.

Dalrymple, R.W., Zaitlin, B.A. & Boyd, R. (1992) Estuarine facies models; conceptual basis and stratigraphic implications. *Journal of Sedimentary Petrology* 62, 1130–1146.

Datt, B. & Jupp, D.L.B. (2002) *Hyperion data processing workshop: Hands-on processing instructions.* CSIRO Earth Observation Centre, ANU, Canberra.

Davis, C.O., Lamela, G.M., Donato, T.F. & Bachmann, C.M. (2004) Coastal margins and estuaries. In *Manual of remote sensing*, 3rd edition, S. Ustin (Ed.), 4, 401–446.

Dekker, A.G., Brando, V.E. & Anstee, J.M. (2004) Retrospective seagrass change detection in a shallow coastal tidal Australian lake. Submitted to *Remote Sensing of Environment.*

Dekker, A.G., Brando, V.E., Anstee, J.M., Pinnel, N., Kutser, T., Hoogenboom, H.J., Peters, S.W.M., Pasterkamp, R., Vos, R.J., Olbert, C., & Malthus, T.J. (2001) Imaging spectrometry of water. In *Imaging Spectrometry: Basic principles and prospective applications*, IV, pp. 307–359. Kluwer Academic Publishers, Dordrecht.

De Vries, C., Danaher, K.F & Dunning, M.C. (2002) Assessing and monitoring Queensland's fish habitats using Landsat TM and ETM+ imagery. In *Proceedings of the 11th Australasian remote sensing and photogrammetry conference, Brisbane, Queensland, 2–6 September*. CD ROM, Causal Publications.

D'Iorio, M. (2003) *Mangroves and shoreline change on Molokai, Hawaii: Assessing the role of introduced Rhizophora mangle in sediment dynamics and coastal change using remote sensing and GIS*. PhD dissertation, University of California, Santa Cruz, June 2003.

Drake, J.B., Dubayah, R.O., Knox, R.G., Clark, D.B. & Blair, J.B. (2002) Sensitivity of large-footprint lidar to canopy structure and biomass in a neotropical rainforest. *Remote Sensing of Environment* 81, 378–392.

Foster-Smith, R.L. & Sotheran, I.S. (2003) Mapping marine benthic biotopes using acoustic ground discrimination systems. *International Journal of Remote Sensing* 24(13), 2761–2784.

Green, E.P., Clark, C.D., Mumby, P.J., Edwards, A.J. & Ellis, A.C. (1998a) Remote sensing techniques for mangrove mapping. *International Journal of Remote Sensing* 19(5), 935–956.

Green, E.P., Mumby, P.J., Edwards, A.J., Clark, C.D. & Ellis, A.C. (1998b) The assessment of mangrove areas using high resolution multispectral airborne imagery. *Journal of Coastal Research* 14(2), 433–443.

Hardman-Mountford, N.J. & McGlade, J.M. (2003) Seasonal and interannual variability of oceanographic processes in the Gulf of Guinea: an investigation using AVHRR sea surface temperature data. *International Journal of Remote Sensing* 24(16), 3247–3268.

Harris, P.T., Heap, A.D., Bryce, S.M. Porter-Smith, R., Ryan, D.A. & Heggie, D.T. (2002) Classification of Australian coastal depositional environments based upon a quantitative analysis of wave, tidal and fluvial power. *Journal of Sedimentary Research* 72(6), 858–870.

Heap, A., Bryce, S., Ryan, D., Radke, L., Smith, C., Harris, P. & Heggie, D. (2001) *Australian estuaries and coastal waterways: A geoscience perspective for improved and integrated resource management.* A report to the National Land and Water Resources Audit, Theme 7: Ecosystem Health. Australian Geological Survey Organisation Record. 2001/07.

Held, A., Ticehurst, C., Lymburner, L. & Williams, N. (2003) High resolution mapping of tropical mangrove ecosystems using hyperspectral and radar remote sensing. *International Journal of Remote Sensing* 24(13), 2739–2759.

Jayatissa, L.P., Guero, M.-C., Hettiarachchi, S. & Koedam, N. (2002) Changes in vegetation cover and socio-economic transitions in a coastal lagoon (Kalametiya, Sri Lanka), as observed by teledetection and ground truthing, can be attributed to an upstream irrigation scheme. *Environment, Development and Sustainability* 4, 167–183.

Jensen, J.R., Rutchey, K., Koch, M.S. & Narumalani, S. (1995) Inland wetland change detection in the Everglades Water Conservation Area 2a, using a time-series of normalized remotely-sensed data. *Photogrammetric Engineering and Remote Sensing* 61(2), 199–209.

Kairo, J.G., Kivyatu, B. & Koedam, N. (2002) Application of remote sensing and GIS in the management of mangrove forests within and adjacent to Kiunga marine protected area, Lamu, Kenya. *Environment, Development and Sustainability* 4, 153–166.

Keith, D.J., Walker, H.A. & Paul, J.F. (2002) Terrestrial vegetation greenness of the Lower Galveston Bay watershed from satellite remote sensing and its relation to water use and the salinity regime of the Galveston Bay Estuary (USA). *International Journal of Remote Sensing* 23(5), 905–916.

Lamb, D. & O'Donnell, J. (1996) Airborne video for assessment of water quality in Australian inland rivers. *Australian Journal of Soil and Water Conservation* 9(1), 14–20.

Leckie, D.G., Gougeon, F.A., Walsworth, N. & Paradine, D. (2003) Stand delineation and composition estimation using semi-automated individual tree crown analysis. *Remote Sensing of Environment* 85, 355–369.

Le Cussan, J. (1991) *A report on the intertidal vegetation of the Daintree, Endeavour and Russell/Mulgrave Rivers.* Unpublished report, Queensland National Parks and Wildlife Service, 139 pp.

Levesque, J. & King, D.J. (2003) Spatial analysis of radiometric fractions from high-resolution multispectral imagery for modelling individual tree crown and forest canopy structure and health. *Remote Sensing of Environment* 84, 589–602.

Liceaga-Correa, M.A. & Euan-Avila, J.I. (2002) Assessment of coral reef bathymetric mapping using visible Landsat Thematic Mapper data. *International Journal of Remote Sensing* 23(1), 3–14.

Lim, K., Treitz, P., Baldwin, K., Morrison, I. & Green, J. (2003) Lidar remote sensing of biophysical properties of tolerant northern hardwood forests. *Canadian Journal of Remote Sensing* 29(5), 658–678.

Lubin, D., Li, W., Dustan, P., Mazel, C. & Stamnes, K. (2001) Spectral signatures of coral reefs: features from space. *Remote Sensing of Environment* 75, 127–137.

Lucas, R.M., Mitchell, A.L., Rosenqvist, A., Proisy, C., Melius, A. & Ticehurst, C. (2005) The potential of L-band SAR for quantifying mangrove characteristics and change: Case studies from the tropics. Submitted to special edition of *Aquatic Conservation: Marine and Freshwater Ecosystems*.

Lucas, R.M., Mitchell, A.L. & Saatchi, S. (2004) Remote sensing of mangroves: A review. *Progress in Physical Geography* (in preparation).

Lucas, R.M., Ellison, J.C., Mitchell, A., Donnelly, B., Finlayson, M. & Milne, A.K. (2002) Use of stereo aerial photography for quantifying changes in the extent and height of mangroves in tropical Australia. *Wetlands Ecology and Management* 10, 161–175.

Macleod, R.D. & Congalton, R.G. (1998) A quantitative comparison of change-detection algorithms for monitoring eelgrass from remote sensing data, *Photogrammetric Engineering and Remote Sensing* 64(3), 207–216.

Malthus, T.J. & Karpouzli, E. (2003) Integrating field and high spatial resolution satellite-based methods for monitoring shallow submersed aquatic habitats in the Sound of Eriskay, Scotland, UK. *International Journal of Remote Sensing* 24(13), 2585–2593.

Malthus, T.J. & Mumby, P.J. (2003) Remote sensing of the coastal zone: an overview and priorities for future research. *International Journal of Remote Sensing* 24(13), 2805–2815.

Mougin, E., Proisy, C., Marty, G., Fromard, F., Puig, H., Betoulle, J.L. & Rudant, J.P. (1999) Multifrequency and multipolarisation radar backscattering from mangrove forests. *IEEE Transactions on Geoscience and Remote Sensing* 37(1), 94–102.

Mumby, P.J., Skirving, W., Strong, A.E., Hardy, J.T., LeDrew, E.F., Hochberg, E.J., Stumpf, R.P. & David, L.T. (2003) Remote sensing of coral reefs and their physical environment. *Marine Pollution Bulletin* (in press).

Mumby, P.J. & Edwards, A.J. (2002) Mapping marine environments with IKONOS imagery: enhanced spatial resolution can deliver greater thematic accuracy. *Remote Sensing of Environment* 82, 248–257.

Mumby, P.J., Green, E.P., Edwards, A.J. & Clark, C.D. (1999) The cost-effectiveness of remote sensing for tropical coastal resources assessment and management. *Journal of Environmental Management* 55, 157–166.

Mumby, P.J., Green, E.P., Clark, C.D. & Edwards, A.J. (1998) Digital analysis of multispectral airborne imagery of coral reefs. *Coral Reefs* 17, 59–69.

Mumby, P.J., Green, E.P., Edwards, A.J., & Clarke. C.D. (1997) Coral reef habitat mapping: how much detail can remote sensing provide? *Marine Biology* 130, 193–202.

Murray, E., Radke, L., Brooke, B., Ryan, D., Moss, A., Murphy, R., Robb, M & Rissik, D. (2006) Australia's near-pristine estuaries: Current knowledge and management. Technical Report No. 63. Cooperative Research Centre for Coastal Zone, Estuary and Waterway Management, Brisbane.

NLWRA (2002) *Australian catchment, river and estuary assessment 2002*, *Volume 1*. National Land and Water Resources Audit, Commonwealth Government, Canberra.

Norris, J.G., Wyllie-Echeverria, S., Mumford, T., Bailey, A. & Turner, T. (1997) Estimating basal area coverage of subtidal seagrass beds using underwater videography. *Aquatic Botany* 58, 269–286.

Perez, A.C., Damen, M.C.J., Geneletti, C. & Hobma, T.W. (2002) Monitoring a recent delta formation in a tropical coastal wetland using remote sensing and GIS. Case study: Guapo River Delta, Laguna De Tacarigua, Venezuela. *Environment, Development and Sustainability* 4, 201–219.

Phinn, S.R., Dekker, A.G., Brando, V.E. & Roelfsema, C.M. (2004) Mapping water quality and substrate cover in optically complex coastal and reef waters: An integrated approach. Submitted to *Marine Pollution Bulletin*, special issue on 'Catchment to reef: Water quality issues in the Great Barrier Reef region'.

Phinn, S., Menges, C., Hill, G.J.E. & Stanford, M. (2000) Optimizing remotely sensed solutions for monitoring, modeling, and managing coastal environments. *Remote Sensing of Environment* 73, 117–132.

Proisy, C., Mougin, E., Fromard, F., Trichon, V. & Karam, M.A. (2002) On the influence of canopy structure on the radar backscattering of mangrove forests. *International Journal of Remote Sensing* 23(20), 4197–4210.

Radke, L., Brooke, B., Ticehurst, C. & Murray E. (2006a) *Major achievements of the Comparative Geomorphology of Estuaries Project*. Technical Report No. 65. Cooperative Research Centre for Coastal Zone, Estuary and Waterway Management, Brisbane.

Radke, L., Brooke, B., Ryan, D. Lahtinen, A. & Heap, A. (2006b) *An initial assessment of estuarine geomorphic indicators of coastal waterway health – Final report.* Technical Report No. 66. Cooperative Research Centre for Coastal Zone, Estuary and Waterway Management, Brisbane.

Rasolofoharinoro, M., Blasco, F., Bellan, M.F, Aizpuru, M., Guaquelin, T. & Denis, J. (1998) A remote sensing based methodology for mangrove studies in Madagascar. *International Journal of Remote Sensing* 19, 1873–1886.

Richards, J. & Jai, X. (1999) *Remote sensing digital images analysis: An introduction*. 3rd edition. Berlin, Germany: Springer-Verlag.

Ryan, D.A., Heap, A.D., Radke, L., & Heggie, D.T. (2003) *Conceptual models of Australia's estuaries and coastal waterways: applications for coastal resource management*. Geoscience Australia, Record 2003/09, 127pp.

Saintilan, N. & Williams, R.J. (1998) Mangrove transgression into saltmarsh environments in south-east Australia. *Global Ecology and Biogeography* 8, 177–124.

Saintilan, N. & Wilton, K. (2001) Changes in the distribution of mangroves and saltmarshes in Jervis Bay, Australia. *Wetlands Ecology and Management* 9, 409–420.

Saito, H., Bellan, M.F., Al-Habshi, A., Aizpuru, M. & Blasco, F. (2003) Mangrove research and coastal ecosystem studies with SPOT-4 HRVIR and TERRA ASTER in the Arabian Gulf. *International Journal of Remote Sensing* 24(21), 4073–4092.

Simard, M., De Grandi, G., Saatchi, S. & Mayaux, P. (2002) Mapping tropical coastal vegetation using JERS-1 and ERS-1 radar data with a decision tree classifier. *International Journal of Remote Sensing* 23(7), 1461–1474.

Souza Filho, P.W.M. & Paradella, W.R. (2002) Recognition of the main geobotanical features along the Braganca mangrove coast (Brazilian Amazon Region) from Landsat TM and Radarsat-1 data. *Wetlands Ecology and Management* 10, 123–132.

Sulong, I., Mohd-Lokman, H., Mohd-Tarmizi, K. & Ismail, A. (2002) Mangrove mapping using Landsat imagery and aerial photographs: Kemaman district, Terengganu, Malaysia. *Environment, Development and Sustainability* 4, 135–152.

Ticehurst, C., Lymburner, L., Held, A., Palylyk, C., Martindale, D., Sarosa, W., Phinn, S. & Stanford, M. (2001) Mapping tree crowns using hyperspectral and high spatial resolution imagery. In *Proceedings for the third international conference on geospatial information in agriculture and forestry, Denver, Colorado, 5-7 November 2001.* (CD ROM).

Verheyden, A., Dahdouh-Guebas, F., Thomaes, K., De Genst, W., Hettiarachchi, S. & Koedam, N. (2002) High-resolution vegetation data for mangrove research as obtained from aerial photography. *Environment, Development and Sustainability* 4, 113–133.

Vrabel, J. (1996) Multispectral imagery band sharpening study. *Photogrammetric Engineering and Remote Sensing* 62(9), 1075–1083.

Wang, L., Sousa, W.P., Gong, P. & Biging, G.S. (2004) Comparison of IKONOS and QuickBird images for mapping mangrove species on the Caribbean coast of Panama. *Remote Sensing of Environment* 91, 432–440.

Ward, D.H., Markon, C.J. & Douglas, D.C. (1997) Distribution and stability of eelgrass beds at Izembek Lagoon, Alaska, *Aquatic Botany* 58, 229–240.

Welch, R. & Ahlers, W. (1987) Merging multi-resolution SPOT HRV and Landsat TM data. *Photogrammetric Engineering and Remote Sensing* 53(3), 301–303.

Wilton, K.M. & Saintilan, N. (2000) *Protocols for mangrove and saltmarsh habitat mapping*. Australian Catholic University Coastal Wetlands Unit Technical Report 2000/01.

Zainal, A.J.M., Dalby, D.H. & Robinson, I.S. (1993) Monitoring marine ecological changes on the east coast of Bahrain with Landsat TM, *Photogrammetric Engineering and Remote Sensing* 59, 415–421.

Zhang, X. (1998) On the estimation of biomass of submerged vegetation using sat thematic mapper (TM) imagery: a case study of the Honghu, PR China. *International Journal of Remote Sensing* 19(1), 11–20.